Marie Sigmundsdatter Stølen

Heat from the ground and sun

An energy-optimizing project at Mære Landbruksskole

Master's thesis

Trondheim, June 2010

Norwegian University of Science and Technology
Faculty of Engineering Science and Technology
Department of Geology and Mineral Resources Engineering

Academic supervisor: Bjørge Brattli

NTNU
Norwegian University of Science and Technology

NTNU
Norges teknisk-naturvitenskapelige universitet
Studieprogrammet Geofag og petroleumsteknologi

Fakultet for ingeniørvitenskap og teknologi

MASTEROPPGAVEN

Kandidatens navn: Marie Sigmundsdatter Stølen

Oppgavens tittel: Varme frå grunn og sola – Eit energioptimaliseringsprosjekt ved Mære Landbruksskole

English title: Heat from the ground and sun – an energy-optimizing project at Mære Landbruksskole

Utfyllende tekst: Se vedlegg

1.

2.

Studieretning: Miljø- og naturressursteknikk

Hovedprofil: Miljø- og hydrogeologi

Tidsrom: 18.01.-14.06.2010

.....

Faglærer

Prosjektbeskrivelse Masteroppgave

Varme frå grunn og sola – Eit energioptimaliseringsprosjekt ved Mære Landbruksskole

Mastergradsstudent: Marie Sigmundsdatter Stølen (NTNU)
Veiledere: Bjørge Brattli (NTNU), Heiko Liebel (NTNU), Kirsti Midttømme (NGI), Helge Skarphagen (NIVA)

Bakgrunn

Ved landbruksskolen på Mære (Nord-Trøndelag) leter man etter en mulighet til å effektivisere energiforbruket. Veksthuset fanger om sommeren mer solvarme en nødvendig og overskuddet blir pr i dag ikke brukt, men "forsvinner" gjennom luftingen. Akkurat denne varmen kan lagres i grunnen om sommeren og hentes opp om vinteren når oppvarmingsbehovet er størst. Planen er å bore flere energibrønner til dette formålet.
Høsten 2009 ble det boret en testbrønn på Mære hvor det ble installert to typer kollektorer, en vanlig og ny type, en såkalt turbo kollektor, som "dobbelt U-rør" i samme brønn. Dette gir den unike muligheten å karakterisere de fysikalske og termodynamiske forskjellene mellom de to typene. Turbo kollektoren er mer kostbart enn en vanlig kollektor. Dermed er det en viktig informasjon for brukeren om det lønner seg å investere i en dyrere borehullsvarmeveksler. Ved hjelp av en differensialtrykkmåler installert på termisk responstest-hengeren og en vibrasjonsmåler installert direkte på kollektoren er det mulig å undersøke overgangen fra laminær til turbulent strømning i kollektoren avhengig av strømningshastighet og temperatur på væsken (viskositet). For en best mulig varmeoverføring fra kollektoren til berggrunn eller omvendt er det viktig å ha en turbulent strømning i kollektoren når den er koblet til en varmepumpe og satt i drift. Hvis turbulent strømning nåes ved en lavere strømningshastighet kan man redusere energikostnadene for sirkulasjonspumpingen av kollektorvæsken. Eventuelle fordeler og ulemper av begge typene vil bli synlige. Den nye viten kommer til å bli anvendt i brønnparken på Mære og i konsulent- og bygningsbransjen generelt.

Hovedmålene med oppgaven

1. Det pedagogiske målet med masteroppgaven er at studenten skal lære å kjenne prosessene som hører til planleggingen og dimensjoneringen av et innovativt energioptimaliseringsprosjekt.
2. Det nytterelaterte målet er å få geologiske og termogeologiske data om berggrunnen på Mære og å få testet en ny type kollektortype på et vitenskapelig fundert nivå.

Prosjektinnhold

1. Innledende litteraturstudie om grunnvarme
    - Bakgrunn om forskjellige typer grunnvarmesystemer (åpne og lukkede systemer) og grunnvarme generelt
    - Hvilke prosesser er involvert i en termisk responstest
    - Fysikalsk og teknisk bakgrunn om forskjellige kollektortyper
    - Litteratursøk relatert til valgte fordypningsemne

2. Feltarbeid på Mære
    - *Geologi*: Det skal utføres en kartlegging av geologien i området. Varmeledningsevnen i bergartsprøver skal undersøkes ved laboratoriet på Norges geologiske undersøkelse (NGU). Kvartsinnholdet av bergarten skal bestemmes så fremt det er tid til dette.
    - *Termisk respons testing (TRT)*: Det skal utføres TRT i en testbrønn for å måle varmeledningsevnen både i grunnen og den termiske kontakten mellom kollektoren og brønnen/bergarten (såkalt borehullsmotstand) som er avgjørende for dimensjoneringen av den fremtidige brønnparken.
    - *Kollektortyper*: Ved siden av TRT'en i den vanlige kollektoren skal det også utføres en TRT i en såkalt turbo kollektor i samme brønn.
    - *Fysikalske egenskaper av kollektortyper*: Strømningsraten av den sirkulerende væsken i kollektoren skal bestemmes når laminær strømning går over til turbulent strømning, dersom dette viser seg å være teknisk gjennomførbart. Prosedyren skal utføres i begge kollektortypene.

3. Dataanalyse
    - *Geologi:* Forekommer sprekker? Hva forventes av eventuell grunnvanns-bevegelse? Er bergarten anisotrop med hensyn til varmelednings-egenskaper? Hvilken varmeledningsevne i brønnen kan forventes ut fra laboratoriemålingen og den geologiske kartleggingen?
    - *TRT og kollektortyper:* Beregn varmeledningsevnen og borehullsmotstand for begge typer kollektorer.
    - *Fysikalske egenskaper av kollektortyper:* Hvilken strømningsrate trengs for å nå turbulent strømning, dersom målinger kan gjennomføres? Hva har resultatene fra TRT'en og de fysikalske testene å si for dimensjoneringen av brønnparken (modellering i Earth Energy Designer, EED)?

4. Forfatte masteroppgaven.

Samandrag

Grunnvarme som ein kilde til lagring og uttak av varme kan redusere utslepp av CO_2 til atmosfæren betrakteleg og samtidig føre til økonomiske gevinster. Utfordringa ligg i å senke kostnadar til installasjon og drift av grunnvarme-systemer, auke det bærekraftige uttaket av energi frå kvart borhol og utvikle teknologi for å ta i bruk grunnvarme på nye områder. Det er difor utvikla eit forskningsprosjekt ved Mære landbruksskole i Nord-Trøndelag der eit dynamisk system skal utviklast og testast for å benytte seg av solvarme frå eit veksthus om sommaren, energibrønner og eit korttids varmelager.

Som ein del av forskningsprosjektet på Mære er det i masteroppgåva fokusert på å undersøke geologiske parametre nødvendig for dimensjonering av brønnparken. I tillegg har innstallering av to ulike typer kollektorslanger i ein testbrønn, ein vanleg og ein turbo kollektor, gjort det muleg å undersøke ulikheitar mellom desse i samme brønn. Turbo kollektoren er dyrare enn ein standard kollektor, men riller på innsiden skal gje større varmeoverføring og mindre trykktap. Ein differensialtrykkmålar innstallert på termisk responstest hengaren kombinert med vibrasjonsmålarar festa direkte på kollektoren gjorde det muleg å undersøke trykktap og vibrasjonar for kollektorane ved ulike strømningshastigheiter. Turbulent strømning gjer betre varmeoverføring men krev ein høgare strømningshastigheit og dermed større trykktap, og difor er det interessant å undersøke overgongen mellom laminær og turbulent strømning.

Det vart påvist lite grunnvannstrømning i området, men sprekker i og rundt området av brønnparken tyder på at det kan skape utfordringar ved boring. Utfallet av ein termisk responstest under ein langvaring kuldeperiode viste at det ikkje er gunstig å gjennomføre tester i kuldeperioder utan å kontrollere med temperaturloggarar plassert i brønnen under testen. Resultatet frå felttesten viste ein termisk konduktivitet på 4.0 $\mathrm{W/(m \cdot K)}$, mens laboratorieforsøk med kjerneprøver tatt i området viste verdier på 3.0 $\mathrm{W/(m \cdot K)}$. Den termiske konduktiviten var 25 % høgare målt parallelt med foalisjonen enn normalt på, mest sannsynleg på grunn av kvartsårer. Boreholsmotstanden var lik for begge kollektorer, og kalkulert som 0,07 $\mathrm{(K \cdot m)/W}$. Simulering viser at ein brønnpark med desse eigenskapane er stabil over lang tid. I tillegg viser simulering at det ikkje er tilrådeleg økonomisk å kun bruke generiske verdier ved dimensjonering av anlegg, men supplere med laboratorieforsøk eller termisk responstester. Ved Reynolds tal over 10 000 har dei to kollektorane same trykktap. Derimot viser lågare Reynolds-tal noko overraskande at standard kollektoren har lågare trykktap enn turbo kollektoren, noko som betyr at den har lågare friksjonfaktor og at pumpa bruker mindre energi. Tala for turbo kollektoren er unormalt høge, og det det er difor ikkje muleg å konkludere med kva for kollektor som viser dei beste eigenskapane. Vibrasjonsanalysa viser ikkje noko eintydig overgong mellom laminær og turbulent strømning.

Det er anbefalt å gjennomføre fleire tester på trykktap i felt med Reynolds tall under 10 000 for å verifisere eller avkrefte resultatane som viser at standard kollektoren har lågare trykktap enn turbo kollektoren. Vidare vil det vere av interesse å visualisere strømningar i ein gjennomsiktig slange med same eigenskapar som turbo kollektoren. Vibrasjonsmålingar bør gjennomførast på nytt basert på erfaringar frå denne oppgåva.

Abstract

Using the ground as a heat source or sink may significantly reduce CO_2 emissions in the atmosphere while at the same time leading to economic gain. However, the technology must be made more competitive by cost reduction, sustainable use and expansion of technology for new applications. Thus, a project at Mære Landbruksskole in Nord-Trøndelag, Norway, has been initiated to develop and test a dynamic system for using heat from the sun through a greenhouse during summer, energy wells and short-term storage of heat.

As a part of the research-project at Mære, this master's thesis focuses on investigating the geological parameters necessary to design the borehole thermal energy storage (BTES). The installation of two different borehole heat exchangers in a test-well, a standard and a turbo collector, made it possible to examine the differences between these in the same well. The turbo collector is more expensive than the standard collector, but micro fins on the inside gives a better heat transfer and lower pressure drop. A differential pressure transmitter installed on the test equipment in combination with a vibration indicator set directly on the collector, allowed an investigation of the pressure drop and vibrations for the collectors at different flow velocities. Turbulent flow gives a higher heat transfer but requires a higher flow velocity and thus a higher pressure drop. It is therefore of great interest to investigate the transition between laminar and turbulent flow.

The presence of groundwater flow was not found to be significant, but fractures in and around the field site might create challenges in drilling operations. The duration of a thermal response test in a cold period showed that it is not favorable to carry out field tests in cold periods without controlling the measurements by placing temperature loggers in the well during the test. Results from the field test revealed a thermal conductivity of 4.0 $W/(m \cdot K)$, while laboratory tests using core samples showed values of 3.0 $W/(m \cdot K)$. The thermal conductivity was 25 % higher for measurements parallel to the foliation compared with normal oriented, most likely because of quartz ores. The borehole thermal resistance was similar for both collectors, and calculated as 0.07 $(K \cdot m)/W$. Simulations show that a BTES with these properties is stable over time. Simulations also show that it is not advisable for economic reasons to only use generic value when dimensioning a system of this size, but necessary to supply with laboratory tests or thermal response tests. At Reynolds numbers above 10 000, both collectors have the same pressure drop. Quite surprisingly, lower Reynolds numbers show that the standard collector have a lower pressure drop than that of the turbo collector, thus having a lower friction factor and less need for energy from the pump. The values for the turbo collector are abnormally high, and no conclusion as to which collector is a better choice can be reached. The vibration analysis does not portray a definite transition between laminar and turbulent flow.

Further experiments regarding pressure drop should be performed with Reynolds number less than 10 000 to verify or undermine the results which show a lower pressure drop for the standard collector than the turbo collector. A visualization of flow through a transparent pipe with similar features as the turbo collector would be of great interest. It is also recommended to perform new vibration measurements with the experiments from this thesis in mind.

Preface

This report is written during the spring of 2010 as the final document of a master's thesis specializing in Environmental and Hydrogeology at the Norwegian University of Science and Technology (NTNU). The purpose and scope of the master's thesis was suggested by Heiko Liebel (NTNU) and Helge Skarphagen at the Norwegian Institute for Water Research (NIVA) as a part of a research project called "Active dynamic thermal storage for industrial processes". The project is lead by Harald Gether (NTNU) in cooperation with Jørn Stene (SINTEF and NTNU), Kai Nielsen (NTNU) and Helge Skarphagen (NIVA). Funding is provided by Nord-Trøndelag Fylkeskommune, Enova and the Norwegian Research Council.

The project team deserves gratitude for letting me take part in the project, both in terms of funding the fieldwork and letting me use available data and resources. A special thanks to Helge Skarphagen for his support when it comes to practicalities on the fieldsite and his enthusiastic approach towards my thesis.

The Geological Survey of Norway (NGU) was helpful by lending us equipment, maps, and taking part in discussions. Thanks to Bjørn Willemoes-Wissing for teaching me laboratory procedures.

Frode Haukand at the department of acoustics at SINTEF lent us equipment and contributed greatly by analyzing vibration data. Simon E. Hagen and the others at the department of infrastructure at SINTEF helped out with preparation of geological samples and DTA analysis. Torill Sørløkk and Kjell Kvam have been helpful analyzing XRD at the laboratory of the department of Geology and Mineral Resources Engineering at NTNU.

Bjørge Brattli, my supervisor, helped out with practical issues in this thesis and gave me useful input on how to write a good report. My external supervisor, Kirsti Midttømme (NGI), has been a great resource for any question regarding thermal response tests. A special thanks to Heiko Liebel for enjoyable moments during fieldwork, teaching me all about ground source heat and being a great motivator. I wish you good luck with your doctoral thesis.

Finally, I would like to thank my fellow students at "lesesalen" for discussions on geology and everything else. Also, thanks to my private supporters for proofreading, taking part in discussion and motivating me.

Trondheim, June 10th 2010

Marie S. Stølen

Contents

List of Figures

List of Tables

Aims and Scope

The scholastic goal of this master's thesis is to learn and understand the processes of planning and dimensioning an innovative research project in the field of ground source heat. This goal is pursued by:

1. *Literature study*, concerning the basics of ground source heat and different configurations of systems, the processes related to a thermal response test and different types of borehole heat exchangers and their basic properties and performance.
2. *Fieldwork*, including an investigation of the geological and thermogeological properties of the area, a thermal response test and the comparison of two different borehole heat exchangers and their physical properties with regard to different flow conditions.

The main questions to be answered in this master thesis in addition to experiences with new methods in the field are:

1. What are the basic geological and thermal properties in this area affecting how the energy scheme is dimensioned?
2. Which of the two borehole heat exchangers is most energy efficient?
3. How can one alter the flow in order to optimize the energy gain?

This master's thesis do not go into how the whole energy scheme for the project at Mære is simulated and dimensioned, but rather provides the parameters necessary to dimension the BTES. Further, the heat pump is not investigated in detail, nor is the goal to improve the plant or the technical equipment. The heat transfer properties of the borehole heat exchanger are not investigated except during the thermal response test.

Nomenclature

Symbol	*Quantity*	*Units*
λ	Thermal conductivity	$\mathrm{W/(m \cdot K)}$
$\frac{d\theta}{dx}$	Thermal gradient	K/m
$\dot{Q}_{heat}$	Heat flow	W
ϕ_q	Heat flux	$\mathrm{W/m^2}$
E_b	Energy radiated	$\mathrm{W/m^2}$
θ	Absolute temperature	K
A	Cross-sectional area of material	$\mathrm{m^2}$
u_m	Mean fluid velocity	m/s
ρ	Density	$\mathrm{kg/m^3}$
μ	Dynamic viscosity	$\mathrm{kg/(m \cdot s)}$
D	Inner pipe diameter	m
ΔP	Pressure drop	Pa
$\dot{V}$	Heat carrier fluid volumetric flow	$\mathrm{m^3/s}$
η_{pump}	Pump efficiency	
E_{pump}	Pumping power	W
ΔP_f	Pressure drop due to friction	Pa
L	Total tube length	m
A	Cross-sectional area	$\mathrm{m^2}$
α	Thermal diffusivity	$\mathrm{m^2/s}$
S_C	Specific heat capacity	$\mathrm{J/(K \cdot kg)}$
S_{VC}	Specific volumetric heat capacity	$\mathrm{J/(K \cdot m^3)}$
T_f	Fluid temperature in the collector	K
T_b	Temperature at the borehole wall	K
ΔT_{fluid}	Temperature difference from the intial temperature	K
R_b	Thermal resistance	$\mathrm{(K \cdot m)/W}$
$\Delta T(r_b, t)$	Temperature increase	K
q	Heat injection rate per unit borehole length	W/m
H	Effective borehole depth	m
r	Radius from the borehole	m
r_b	Borehole radius	m
t	Time after application of heat injection	s
Q	Injected heat power	W
T_{sur}	Undisturbed intial temperature of the ground	K
ϵ	Roughness	mm
$\Delta T(z)$	Temperature difference before and after TRT at depth z	K
$T_{after}(z)$	Temperature measured after TRT at depth z	K
$T_{ini}(z)$	Temperature measured before TRT at depth z	K

Dimensionless groups

Symbol	*Quantity*	*Expression*
Re	Reynolds number	$\frac{\mathrm{u_m}\rho\mathrm{D}}{\mu}$
γ	Euler's constant	0.5772
f	Friction factor	$\Delta\mathrm{P_f} \cdot \frac{2}{\rho\mathrm{u_m^2}} \cdot \frac{\mathrm{D}}{\mathrm{L}}$
τ	Time parameter	ln(t)

Abbreviations

Symbol	*Quantity*
BHE	Borehole Heat Exchanger
$BTES$	Borehole Thermal Energy Storage
COP	Coefficient Of Performance
DTA	Differential Thermal Analysis
$DTES$	Dynamic Thermal Energy Storage
EED	Earth Energy Designer
$GSHP$	Ground Source Heat Pump
IEA	International Energy Agency
$IPCC$	Intergovernmental Panel on Climate Change
NGU	Geological Survey of Norway
$NIVA$	Norwegian Institute for Water Research
$NTNU$	The Norwegian University of Science and Technology
PIV	Particle Image Velocimetry
TRT	Thermal Response Test
$UTES$	Underground Thermal Energy Storage
XRD	X-Ray Diffraction

Chapter 1

Introduction

On the 18th of December 2009 at the United Nations Climate Change Conference, world leaders agreed that the climate change is one of the greatest challenges of our time (UN, 2009). It was concluded that deep cuts in global green house gases is required in order to level out the increase in global temperature. The Intergovernmental Panel on Climate Change (IPCC), in their latest report from 2007, have shown that CO_2-neutral renewable energy sources should be further developed in order to increasingly replace fossil energy sources and thus reduce emissions to the atmosphere (Sims et al., 2007).

The Stern Review from 2006, concluded that the building sector accounts for 8 percent of the total greenhouse gas emissions, or 20 percent if upstream emissions associated with heat and electricity are included (Stern, 2006). From 1970-1990 the amount of direct and indirect emissions from this sector grew by 75 percent (Metz et al., 2007). According to the 2007 IPCC report, it is found that the building sector has the highest potential for reducing emissions with a net economic benefit, especially when it comes to heating and cooling (Sims et al., 2007). Thus, by using renewable energy-supply technologies like solar, wind, geothermal and biomass in the building sector, emissions can be significantly reduced.

Geothermal energy is recognized as being one of the key technologies for renewable energy-supply (Sims et al., 2007; IEA, 2006). By using energy from the ground as a heat source or sink, ground source heat pumps (GSHP's) makes it possible to use this energy directly for both heating and cooling of buildings. The general characteristics of geothermal energy that make it of significant importance to both electricity production and direct use include:

- Global distribution - available in both developing and developed countries
- Environmentally friendly - it has low emissions of greenhouse gases
- Indigenous nature - it is independent of external supply and demand effects and fluctuating exchange rates
- Independence of weather and season

High-temperature geothermal energy fields found in geodynamically active regions like in Iceland can be used for direct heating and even in binary power plants. However, within a drilling depth of 2 km these fields are rare, and so far deep geothermal projects are not cost-effective in Scandinavia (Lund, 2007). The direct application of ground source heat is therefore more applicable. The annual savings in fuel oil in this sector accounts for 170 million barrels and 24 million tonnes in carbon emissions to the atmosphere (Lund et al., 2005). As can be seen in Figure 1.1, the largest growth within the field of ground source heat include the installation and use of heat pumps, as they can be used anywhere in the world. Today GSHP's have the largest energy use and installed capacity worldwide when it comes

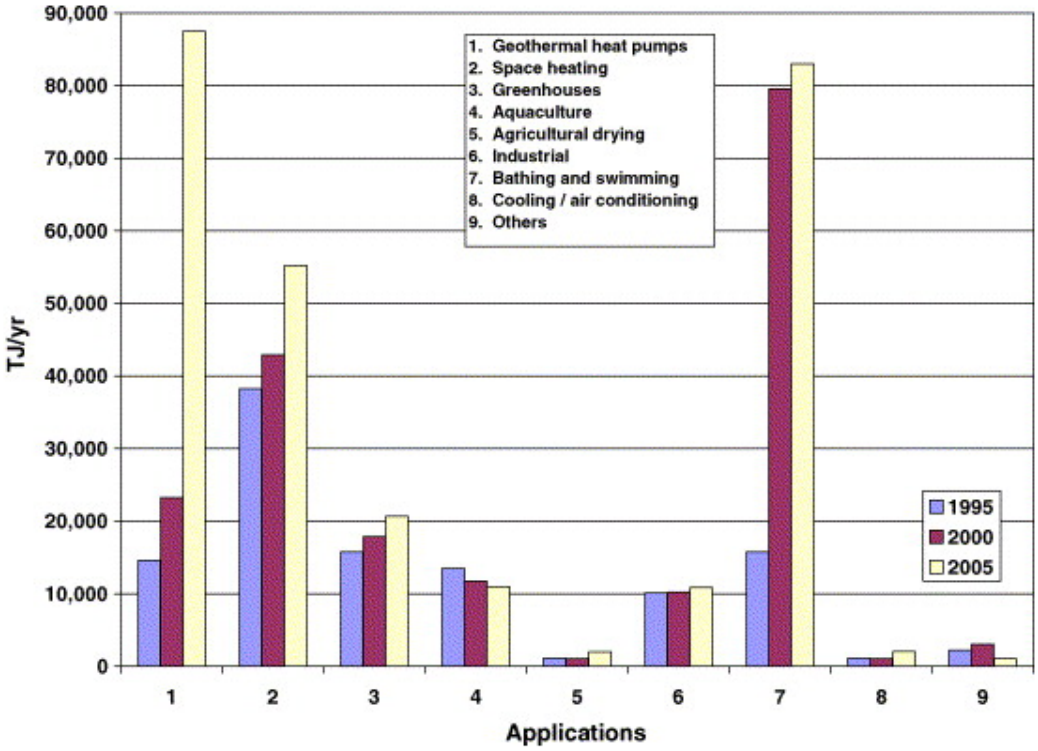

Figure 1.1: Comparison of world wide direct application of geoenergy (Lund et al., 2005). Notice the large increase in the use of heat pumps from 2000-2005

to use of geothermal energy, accounting for 54 % and 32 %, respectively. However, costs, as well as social and environmental barriers, are restricting this growth. As ground source heat is considered one of the key technologies to reduce greenhouse heating, IEA has made the utilization of this resource one of their prioritized areas of research and development for renewable energy sources (IEA, 2006).

In Norway, hydropower resources have traditionally supplied almost all domestic electricity demand. However, an increasing electricity demand has lead to energy policies focusing on a decreased dependency on electricity for heating, more flexibility in energy uses and and increased share of renewable energy other than hydropower (Midttømme, 2005). Norway is now one of the top five countries in the world when it comes to the largest increase in the use and installed capacity of geothermal energy. This is mainly due to the increased use of GSHP's (Lund et al., 2005), and today 26000 GSHP's are installed, having a capacity of 3.0 TWh (Midttømme, 2010). At present, there are no deep geothermal projects running, although an attempt was made in 1999, failing for technical reasons (Midttømme, 2005). For residential sectors the potential for GSHP's is high and it is an increasing interest in thermal energy storage. In comparison with neigbouring countries like Sweden, Norway has a vast potential of using its geothermal resources.

In order to facilitate the acceleration in the use of ground source heat, progress must be made by making the technology more competitive (IEA, 2006). This is related to cost reduction, sustainable use, and expansion of the technology for new applications and into new geographical regions. Profits from the ground is commonly obtained by using a borehole heat exchanger (BHE) that is installed in a previously drilled vertical borehole. A fluid circulates in the BHE, and energy is then delivered to a GSHP as illustrated in Figure 1.2. The heat transfer between the fluid and the surrounding ground will depend on the characteristics of the BHE and the ground. An increase of 1 °C of the out coming flow

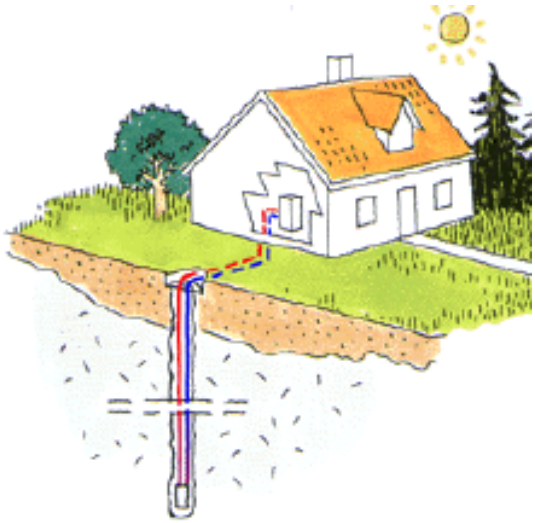

Figure 1.2: Illustration of ground source heat (Midttømme and Hauge, 2009), including a borehole heat exchanger and a ground source heat pump

from the boreholes gives a coefficient of performance (COP) increase of approximately 3 %, giving annual electricity savings in Norway of 0.1 TWh (Acuña and Palm, 2008a). Thus, by improving the performance of the BHE, large cost savings may be conducted.

At Mære Landbruksskole in Nord-Trøndelag, Norway, a large research-project has been developed in order to optimize an underground thermal energy storage (UTES). A greenhouse at the site requires large amounts of heat during both summer and winter, and therefore a dynamic system including ground source heat, heat from the sun through the greenhouse and short-term storage is being developed. In this master's thesis, the thermal and geological characteristics of the ground are found in order to dimension the pilot-system properly. Also, two BHE's are tested for pressure drop and vibrations to find which is more energy efficient. The flow regimes in the BHE's are investigated to ensure the best heat transfer at the lowest cost. In this manner, optimization of heat transfer between the ground and the circulating fluid is possible.

Chapter 2

Theoretical Background

The theory included in this master's thesis covers the general aspects of thermogeology as well as configurations of heat pump systems and their performance. Formulas relevant for the data analysis required in the fieldwork are also embedded in this chapter.

2.1 Geothermal energy

The term *Geothermal energy* is most often used to describe the high-temperature energy derived from heat flux from the earths interior, and may be found either in very deep boreholes or at specific locations on earth like Iceland. *Heat flux* is the amount of heat flowing through a unit area per time [W/m^2]. The study of *ground source heat*, *thermogeology*, is used to describe heat occurring at relatively low temperatures in the shallow subsurface (Banks, 2008). Ground source heat is usually dominated by solar energy absorbed and stored in the subsurface and may contain a component of genuine geothermal energy from the earth flux. This master's thesis covers the theory concerning ground source heat and thermogeology.

2.1.1 Thermal properties of the ground

The use of ground source heat is based on the ground working as a heat storage. The ground is heated by the sun during summer, and this heat is stored and can be extracted during winter. While extracting heat in the winter, cold is stored and can be used for cooling during summer. Therefore, the ground must have a high capacity to store heat, but also a modest release of heat to the surroundings.

Thermal conductivity

This property describes a materials ability to transfer heat by conduction. It is described by Fourier's law, as evident in the following equation:

$$Q_{heat} = -\lambda A \frac{d\theta}{dx} \tag{2.1}$$

where Q_{heat} is the heat flow [W], λ is the thermal conductivity [$W/(m \cdot K)$], A is the cross-sectional area of the block of material under consideration [m^2], θ is the temperature [K], x is the distance coordinate in the direction of the decreasing temperature [m] and $\frac{d\theta}{dx}$ is the thermal gradient [K/m].

Fourier's law leads to the foundation of computer-based numerical heat transfer models. Also, from Fourier's law, it is evident that if there is a geothermal gradient and rocks have a finite ability to conduct heat, the earth must be conducting heat from its interior to its exterior, even in the range of the shallow subsurface. Table 2.1 gives an overview of the thermal conductivity of some rocks.

Table 2.1: The thermal conductivity and volumetric heat capacity of selected rocks (Banks, 2008; Eskilson et al., 2000)

Rocks	$\lambda[\mathrm{W/(m \cdot K)}]$	$S_{VC}[\mathrm{MJ/(K \cdot m^3)}]$
Coal	0.3	1.8
Shale	1.5-3.5	2.3
Basalt	1.3-2.3	2.4-2.6
Sandstone	2.0-6.5	2.0-2.1
Gneiss	2.5-4.5	2.1-2.6
Granite	3.0-4.0	1.6-3.1
Quartzite	5.5-7.5	1.9-2.7
Amphibolite	2.1-3.6	2.6
Micaschist	1.5-3.1	2.2

Volumetric or specific heat capacity

Heat capacity is the property describing storage of heat. S_C, specific heat capacity, is the amount of heat locked up in a rock for every degree Kelvin. For water this value is particularly high, 4180 $\mathrm{J/(kg \cdot K)}$, while most rocks have values around 800 $\mathrm{J/(kg \cdot K)}$. One may also use the term volumetric heat capacity, S_{VC}, defined as Joules per degree Kelvin per unit volume. Most rocks have values in the range of 2.0-2.4 $\mathrm{MJ/(K \cdot m^3)}$ (see Table 2.1). For every cubic meter of rock, it is possible to release 10 MJ of energy by dropping the temperature by 4 K. The heat energy is stored as molecular vibrational or kinetic energy. S_{VC} decreases slightly with increasing temperature, partly due to changes in density.

2.1.2 Movement of heat

It is necessary to have an understanding of the transfer of heat between places or materials in order to optimize the use of ground source heat. Heat is transferred by three mechanisms:

- Conduction
- Convection
- Radiation

When it comes to ground source heat at low temperatures, conduction through minerals or pore fluids and convection *via* the groundwater are probably the most important mechanisms (Banks, 2008). There must be a temperature difference within a medium (conduction), or between mediums (convection and radiation) for heat transfer to take place.

Conduction

During heat conduction, heat diffuses through a material by the process of molecular interaction. As the temperature increase, molecules vibrate more strongly and cause their neighboring molecules to transfer this motion through the surrounding material. The amount of

heat that can be transferred is dependent on the diffusivity of the medium , α [m^2/s], as described in Equation 2.2:

$$\alpha = \frac{\lambda}{S_{VC}} = \frac{\lambda}{\rho S_C} \tag{2.2}$$

where λ is thermal conductivity [$W/(m \cdot K)$], S_{VC} is the volumetric heat capacity [$J/(K \cdot m^3)$], S_C is the specific heat capacity [$J/(kg \cdot K)$] and ρ is the density [kg/m^3].

As evident in Table 2.1, the thermal conductivity of rocks tends to fall in a range between 1 and 3 $W/(m \cdot K)$. However, among minerals, quartz has the highest thermal conductivity at around 7 $W/(m \cdot K)$. Therefore, the thermal conductivity of rocks will greatly depend on their quartz content (Banks, 2008). It is also, to a minor degree, dependent on temperature, increasing with increasing temperatures.

Convection

Convection is the transfer of heat due to the movement of a fluid (Banks, 2008). Within the bedrock this heat transfer is common between flowing groundwater and the rock, and the convection takes place in fracture sets (Brekke, 2003). Fractures are often filled with water that may receive from or release heat to the rock. The movement of groundwater with a different temperature than the surrounding bedrock leads to cooling or heating of the ground. Groundwater in the subsurface moves from areas of high head to low head, ultimately driven by gravitational forces. Convection is thus dependent on both the specific heat capacity of the rock and the flow of the groundwater.

Radiation

Heat transfer due to radiation takes place when energy is transported by electromagnetic waves. More energy is radiated when the body is hotter, as stated by Stefan and Boltzmann for an ideally radiating body, where the energy (E_b) [W/m^2] is proportional to the fourth power of the absolute temperature (θ [K]):

$$E_b = \sigma \theta^4 \tag{2.3}$$

where σ is the Stefan-Boltzmann constant of 5.67×10^{-8} $W/(m^2 \cdot K^4)$.

Absorption of radiated energy from bodies like the sun and the atmosphere are important heat transfer mechanisms at the surface of the earth. However, within the bedrock, heat transfer by radiation is small under normal circumstances compared with conduction and convection (Brekke, 2003). As the temperature of the ground is low, Equation 2.3 states that the energy radiated is also low.

2.1.3 The temperature of the ground

The temperature of the ground is a key parameter for how much energy is possible to extract. In order to optimize a thermal energy storage system, it is vital to know how the temperature in the ground is affected by different parameters. As illustrated in Figure 2.1, there are several parameters affecting the temperature of the ground:

- Solar energy
- Heat flux from the earth
- Heat from buildings
- Groundwater flow

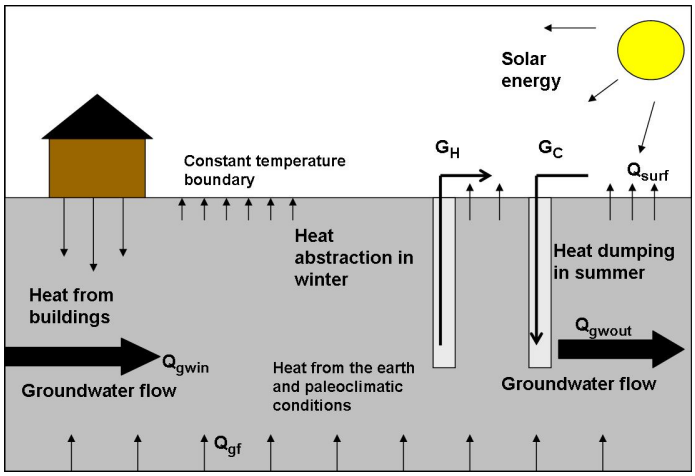

Figure 2.1: Illustration of a block of the subsurface showing elements in the heat budget. Q_{gwin} is groundwater flowing in to the aestifer, Q_{gwout} is groundwater flowing out, Q_{gf} us heat entering from the geothermal heat flux, Q_{surf} is heat to or from the ground surface, G_H is heat extracted and G_C is heat dumped in the aestifer. Mod. from Banks (2008)

- Paleoclimatic conditions
- Topography

Also, heat abstraction and dumping will affect the temperature of the ground. The balance of the *aestifer*, a heat reservoir, can be viewed in a heat budget as presented in Figure 2.1.

Solar energy

Solar radiation heats up the ground during summer, and contributes therefore to the the net heat that can be extracted during winter. As rocks have high values of heat capacity and modest values of thermal conductivity, they have rather low thermal diffusivities. Because of the slow propagations of heat waves through the rocks, the temperature of the subsurface is quite stable below a few meters depth. Seasonal variations of the ground temperatures due to changes in the ambient air temperature reach only some 15 m below the surface, as illustrated in Figure 2.2 (Ericsson, 1985). The annual average surface temperature is reflected by the ground temperature. Therefore, in regions with seasons, the earths subsurface temperature is warmer than the air temperature in winter, but cooler in the summer. In Norway, the average temperature of the shallow subsurface is 4-6 degree Celsius, caused by a rather low annual solar radiation (Banks, 2008). It is worth to note that the northern parts of Norway may have groundwater temperatures down to 2 °C (Sand, 1990). The heat extracted *via* ground source heating is thus dominantly derived from solar energy absorbed by the earth‘s surface.

Heat flux from the earth

The ground temperature is also affected by the geothermal heat flux from the earth‘s interior. The geothermal temperature gradient is superimposed on the annual average surface temperature. The geothermal gradient varies between different locations, but typical values are in the range of 1-3 °C per 100 m (Banks, 2008). The heat flux has a global average estimated at 87 mW/m^2. Figure 2.3 shows heat flux data from Norway as well as the heat production of Norwegian bedrock.

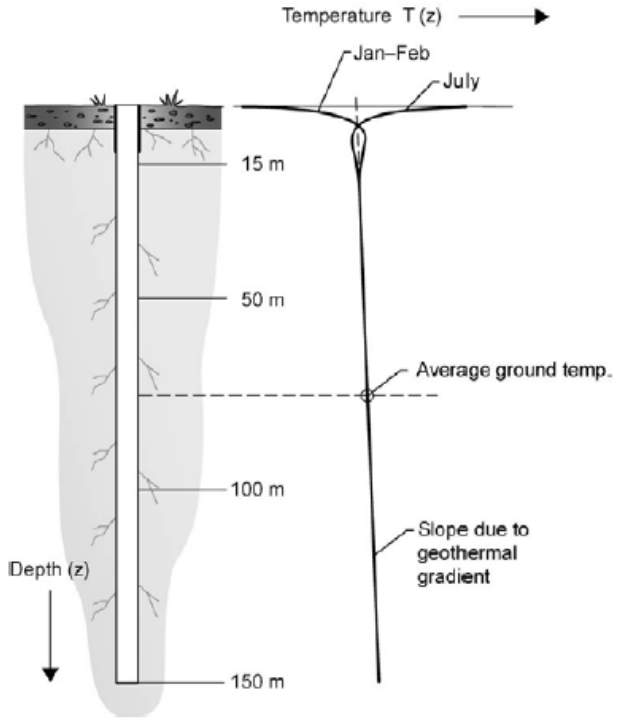

Figure 2.2: Temperature profile of the ground. Seasonal temperature variations does not reach below 15 m from the ground surface (Gehlin, 1998)

Heat from buildings

Buildings greatly affect the heat flux in the surrounding rock (Banks, 2008). Modeling in consistency with thermal recordings have shown influenced ground temperatures down to 150 m in the direct vicinity of a building (Roy et al., 1972; Liebel et al., 2009). In Figure 2.4 a simulated heat plume below Nordstrand skole in Oslo is shown. In urban areas, temperatures in the ground are found to be 2-3 °C higher than background temperatures (Banks, 2008). The effect of heat loss towards the ground depends on the insulation of the building, the thermal conductivity of the ground and the presence of groundwater flow. A thermal plume caused by urban areas affects the temperature of the ground and will thus influence the measured thermal conductivity and undisturbed ground temperature.

Groundwater flow

Field observations indicate that groundwater movement around the borehole influences the effective thermal conductivity significantly (Liebel et al., 2009; Gehlin, 1998; Gehlin and Hellström, 2003). Also, the presence of groundwater determines the section of the BHE that will be exposed to effective heat transfer (Acuña and Palm, 2008b). As the thermal conductivity of water is approximately 20 times that of air, the active borehole length is found at the height of the groundwater table. The convective heat transfer occurs either because of groundwater density differences along the borehole length or due to the presence of cracks around the borehole, improving the net heat transfer at local sections (Acuña and Palm, 2008b). An increased heat transfer influences the apparent thermal conductivity. Groundwater flow can be discovered by the comparison of standardized temperature profiles before and after a thermal response test (Liebel et al., 2009).

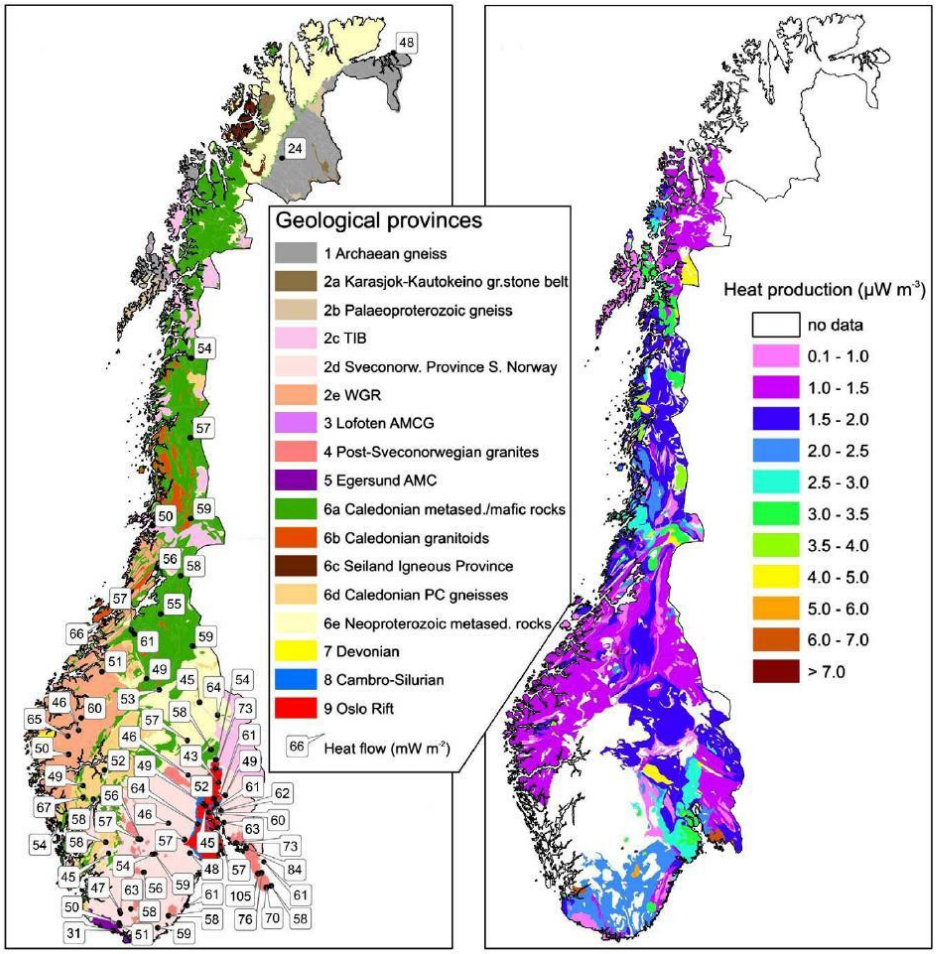

Figure 2.3: Left: Available paleoclimatically corrected heat flux data from Norway (Slagstad et al., 2009). Right: Heat production of Norwegian bedrock (Slagstad, 2008)

Paleoclimatic conditions

The effect of paleoclimatic changes on subsurface temperature might affect the measured heat flow (flow of heat depending on time [W]) down to at least 1000 m depth (Kukkonen et al., 1998). Temperature disturbances at the surface propagates into the subsurface at a rate determined by the diffusivity of the rock (Slagstad et al., 2009). The depth of the paleoclimatic change depends also on the amplitude and duration of the disturbance at the surface. Climatic changes are related to glacial and interglacial periods with known temperature changes at the surface. In Norway, paleoclimatic corrections are significant, and found by Slagstad et al. (2009) to constitute 10-20 % of the final heat flow values.

Topography

Topographic features may significantly influence subsurface temperatures and gradients (Blackwell et al., 1980; Slagstad et al., 2009). The temperature gradient should be lower below a hill than below a valley (Midttømme, 2000). Also slope orientation and the inclination of a hillside affects the heat flow. Topographic correction can be made by using the finite element method on topographic models based on elevation data (Slagstad et al., 2009). When interpreting temperature profiles from ground, topography effects should be

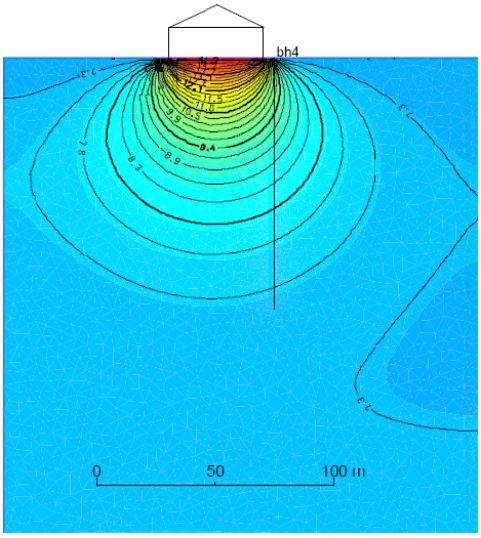

Figure 2.4: Simulated plume below Nordstrand skole (Liebel et al., 2009)

taken into consideration.

Heat energy budget

The heat energy budget of an aestifer consists of several natural components (Banks, 2008)

- Heat entering the aestifer from the geothermal heat flux, Q_{gf}
- Groundwater flow passing the aestifer, carrying a load of heat, Q_{gwin} and Q_{gwout}
- The aestifer may be gaining or loosing heat from the ground surface, Q_{surf}. Under natural conditions there will be a net loss equal to the geothermal heat flux.

Under natural conditions, in the long term:

$$Q_{gwout} + Q_{surf} = Q_{gwin} + Q_{gf} \tag{2.4}$$

If heat is extracted, G_H, at a greater rate than heat is dumped, G_C, then there is a net heating scheme:

$$G_H + Q_{gwout} + Q_{surf} > G_C + Q_{gwin} + Q_{gf} \tag{2.5}$$

In this situation, the heat stored in the aestifer is depleted and the temperature will fall both in the ground and in the groundwater (Banks, 2008). The temperature fall induces a flux of solar energy from the surface to the ground. A new equilibrium will ultimately be established, with the subsurface temperature at a lower but still acceptable level.

2.2 Ground source heat pumps

To utilize the energy from the shallow subsurface, GSHP's are used. By the means of the stable bedrock temperature, GSHP's can provide heating, cooling and domestic hot water to family homes and commercial buildings. The basic principle of a GSHP is illustrated in Figure 2.5. A geothermal heating and cooling system consists of three main components: A BHE, a heat pump and a heating system. The BHE and a generalized heat pump is further

discussed in this section. Thermal energy storage by the use of large systems of GSHP's is also described in this section, as they represent a solution for heating and cooling demands in larger buildings.

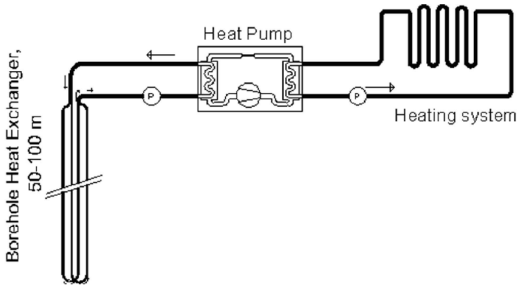

Figure 2.5: Sketch of a ground source heat pump (Sanner, 2001)

2.2.1 Heat pumps: Fundamentals

A heat pump is a machine than moves heat from one location (heat source) to another location (heat sink) by using mechanical work. The principles of the operating process are equivalent to the one used in a refrigeration unit, where heat is moved from a low temperature heat source to a higher temperature heat sink. Energy can then be used for heating or cooling purposes depending on the desired temperature, where the main difference is the purpose of the application, either heating or cooling.

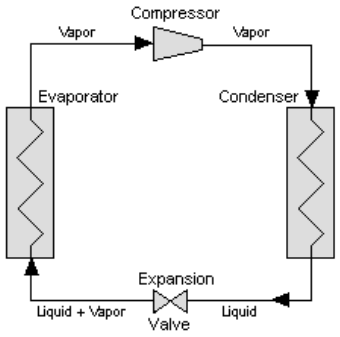

Figure 2.6: Typical vapor compression refrigeration (Wikipedia, 2006)

Figure 2.6 shows a vapor compression cycle (refrigerating process), which consists of a condenser, evaporator, compressor, expansion valve and refrigerant. Heat is absorbed at a lower temperature, compressed and then rejected at the higher temperature. First, the refrigerant runs through an evaporator, absorbs heat from the cold heat source and becomes a saturated vapor. As the refrigerant passes through the compressor it obtains a higher pressure and temperature level. The heated vapor is cooled and condensed by the condenser, and heat is delivered to the heat sink. Next, the expansion valve reduces the refrigerant pressure and temperature until a liquid-vapor state is reached. The cycle ends when the refrigerant circulates through the evaporator again.

There is a need for energy input, as the overall system is opposing the second law of thermodynamics which states that heat cannot pass from a colder to a hotter place. The energy is received by the system through the compressor. The energy required depends on the

difference between the temperatures of the source and the sink; the greater temperature difference the greater energy input needed by the pump. Therefore, the most beneficial heat source is one with a high and stable temperature level throughout the heating season (Palomares, 2008). Bedrock temperature has this property, as already stated in the previous sections.

2.2.2 Configurations of ground source heat systems

The ground source heat systems link the heat pump to the underground and allow for extraction of heat from the ground or injection of heat into the ground. There are two main configurations of ground source heat pump systems (Sanner, 2001; Lund et al., 2004):

- **Open systems**: Ground water or lake water is transferred directly to the heat pump
- **Closed system**: Heat exchangers are located in the ground, installed vertically or horizontally as illustrated in Figure 2.7. A heat carrier fluid is circulated in the heat exchangers, transporting heat from the ground to the heat pump or the opposite (Sanner, 2001).

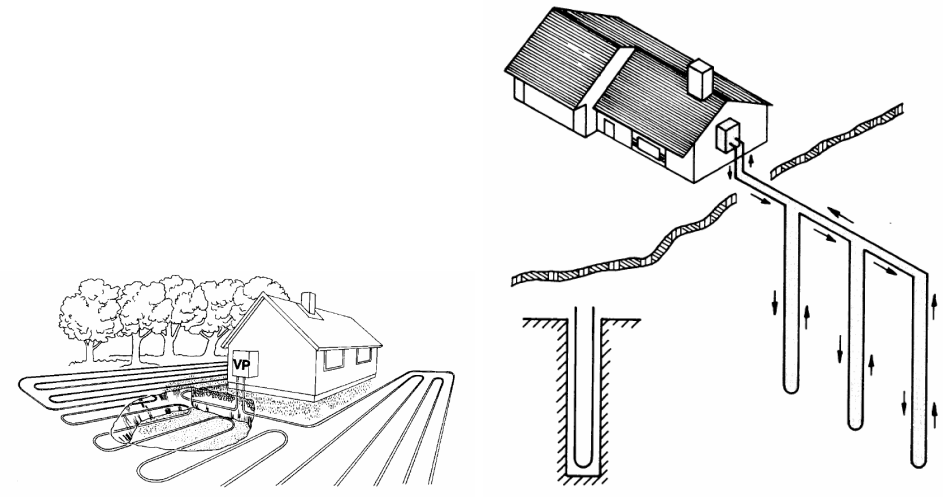

Figure 2.7: Horizontal (left) and vertical closed system (right) (Hellström, 2006)

Open systems are mostly used for larger installations with suitable aquifers. The advantage of an open system is a good heat transfer between the borehole and the circulating fluid due to direct contact between them. However, the geochemical properties of water may lead to a faster deterioration of the heat pump (Brekke, 2003). Closed systems are more common for domestic and commercial buildings (Sanner, 2001). The advantage with a closed system is a longer lifetime of the heat pump, and the possibility of using a heat carrier fluid with a temperature below zero. There is, however, a larger thermal resistance between the circulating fluid and the rock (Brekke, 2003). This thesis focuses on closed systems.

Horizontal closed systems

A horizontal closed system compromises a buried pipe, conveying an heat carrier fluid extracting heat from or dumping heat to the shallow subsurface. The horizontal closed system is the easiest and cheapest closed system to install (Sanner, 2001; Banks, 2008). Due to restrictions in available area, the individual pipes are laid in relatively dense patterns,

connected in either series or parallel, as shown in Figure 2.8. Spiral forms are popular in USA, mainly in the form of "slinky" collectors placed horizontally in a trench as seen in Figure 2.9. Single pipes may support 15-30 W/m in parallel trenches at 1 m spacings, while slinkies in trenches may support 100 W/m at 3-5 m spacings (Banks, 2008).

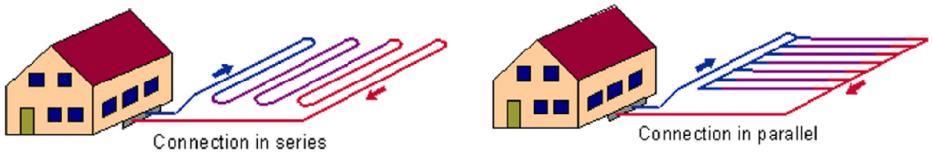

Figure 2.8: Horizontal ground heat exchanger (Sanner, 2001)

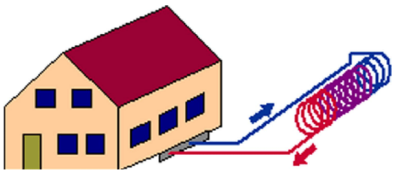

Figure 2.9: Spiral-type ground heat exchanger (Sanner, 2001)

The horizontal loops function mainly as subsurface solar collectors, as they are buried at depths around 1-2 m (Banks, 2008). Heat is extracted in the winter from the soil surrounding the collectors, and the system thus relies on the depleted heat reservoir to be replenished during summer. The extraction of thermal energy gives a temperature drop in the ground, and moisture freezes to ice which forms cylinders around the pipes. As long as there are no sensitive foundations above the loop this is positive as the formation of ice leads to an elevated thermal conductivity of the ground (Banks, 2008). The phase change also leads to a release of heat in the form of latent heat of freezing.

When heat is rejected into the ground, the air within the pore spaces is heated. The vapor pressure of the water is also increased, causing it to migrate by convection away from the loop. This might lead to drying out of the ground around the loop, causing a decrease in thermal conductivity and decline in the efficiency of the system. Generally, both thermal conductivity and the volumetric heat capacity of geological materials increase as they become wetter (Banks, 2008).

The main drawbacks with horizontally closed loops are areal constraints. Also, they are not the better choice for storing heat. According to Skarphagen (2010), these systems have a lower COP than vertical closed systems.

Vertical closed system

In vertical closed systems, a pipe is installed in a vertical borehole in the rock so that heat can be extracted from the ground at a reduced surface area. In a standard BHE, plastic pipes are installed and filled with a pumpable material, unless water is used as is common in Scandinavia.

Many different BHE's have been used and tested, but the two main designs are (Banks, 2008; Sanner, 2001; Hellström, 2006):

- **U-pipes**: Consists of a pair of straight pipes, connected with a 180 degree bend at the bottom.

- **Coaxial (concentric) pipes**: Two straight pipes having different diameters or in more complex configurations.

The most popular BHE is a closed U-pipe, through which heat carrier fluid travels up and down while collecting heat from the bedrock (Acuña and Palm, 2008a). The advantage of this type is the low cost of the pipe-material (Sanner, 2001). The double U-pipe has two up flow and down flow tubes, and is slightly more efficient than the single U although more difficult to emplace in a borehole (Banks, 2008). In the coaxial tube configuration heat exchange occur either in the downstream or the upstream direction. Coaxial tubes may be designed with or without a liner or outer tube, i.e. as a closed or open circuit. Illustrations of the different BHE's are shown in Figure 2.10 and Figure 2.11.

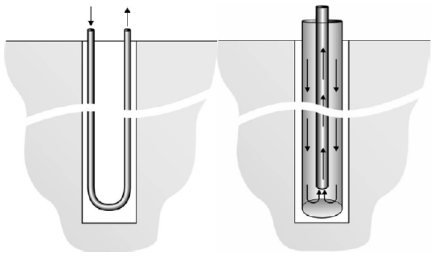

Figure 2.10: The two fundamental borehole heat exchanger designs - the U-pipe and the coaxial pipe (Gehlin, 2002)

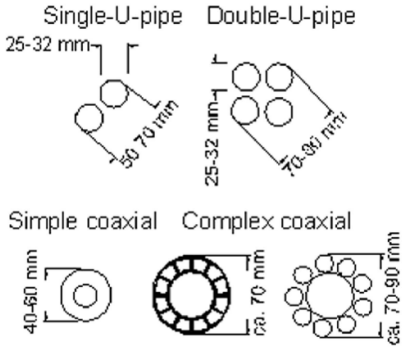

Figure 2.11: Cross-sections of different types of borehole heat exchangers (Sanner, 2001)

The BHE will be further investigated in Section 2.4.

2.2.3 Underground thermal energy storage

Energy storage helps match energy supply and demand. It also increases the potential of utilizing renewable resources such as ground source heat, solar energy and waste heat. In an underground thermal energy storage (UTES), the most frequently used system for energy storage, both heat and cold are stored in the ground (Midttømme et al., 2008). Cold storage is becoming increasingly popular, as the cost for space cooling is rather high (Sanner, 2001). Cold air in the winter is used to cool the underground storage, and this cold is used again in the summer. For heating, solar radiation or waste heat can be stored in the ground during summer and used in the winter. By using the ground as a heat store, supply and demand can be matched over at least a years cycle.

As for GSHP's, there are two main configurations:

- **Borehole storage (BTES)** - closed systems with boreholes and pipes
- **Aquifer storage (ATES)** - open systems with groundwater as heat carrier

This thesis treats BTES systems only.

Borehole Thermal Energy Storage

A borehole thermal energy storage is an underground structure for storing large quantities of heat or cold for use at a later season. The volumetric heat capacity of the rock alone is used for storage. BTES consists of arrays of boreholes resembling standard drilled wells, connected to form a larger system.

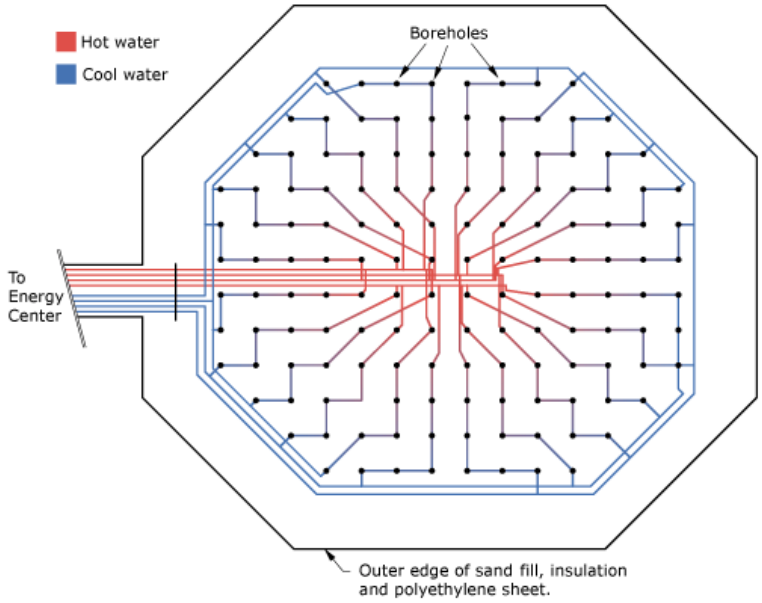

Figure 2.12: Areal view of a borehole thermal energy system (DLSC, 2005).U-pipes are connected in series of six radiating from the center to the outer edge

Figure 2.12 illustrates a typical large BTES planned for the Drake landing solar community in Canada (DLSC, 2005). It consists of 144 boreholes, each at a depth of 37 m. At the surface, the U-pipes installed in the boreholes are connected in series of six that radiate from the center to the outer edge, and then connect back to the center of energy building. The entire field is covered by insulation. When solar heated water is available for storage, it is pumped into the center of the BTES and through the series of U-pipes. Heat is then transferred to the surrounding ground, and the water cools as it heads back to the outer edges. Conversely, when the homes require heat, cooler water is pumped into the edges of the BTES, and as the water flows to the center it picks up heat. The heated water is transported to a short-term storage tank in the center of energy building, and is ultimately delivered to the homes through a district heating loop.

The ground offers a huge thermal store that can bank heat energy in times of surplus and drawn upon in need. Large BTES is a key technology for more efficient heating and cooling of large buildings.

Dynamic Thermal Energy Storage

UTES can be combined with other low- CO_2 energy technologies (wind, solar panel, air-air heat pumps etc.) to deliver integrated solutions (Midttømme et al., 2008). This technology is called *dynamic thermal energy storage* (DTES), and compromises the utilization of multiple energy sources for rapid dynamic usage by the means of storage of heat and cold. DTES can be a short-term storage tank(Gether, 2009). DTES will dynamically follow the the demand for heating and cooling with changing outdoor conditions or production patterns.

It is a rather new idea to combine the DTES with a BTES (Gether, 2010). The DTES typically has a fast response and high effect but a limited capacity for matching variations between seasons. Thus, there are large synergy effects by combining the system with a BTES as they can be used to store heat or cold between seasons (Gether et al., 2009). Initial theoretical evaluation points to a COP of 6-7, which is twice the ordinary gain of a BTES. One way to take advantage of the synergy between the two systems is to charge the DTES in the day, and transfer heat to the BTES both night and day. This will lower the resistance to the heat transfer between the borehole and the ground.

Figure 2.13 illustrates how energy may be gained by using dynamic thermal energy storage. Here, the heat pump is run at full capacity in mild weather when all of its capacity is not required to heat the building, loading the DTES. In a following cold period heat is obtained from the DTES while the heat pump is turned off. Economic savings can also be made when there is a price variation from day/night as the heat pump can be run during the night when prices are low.

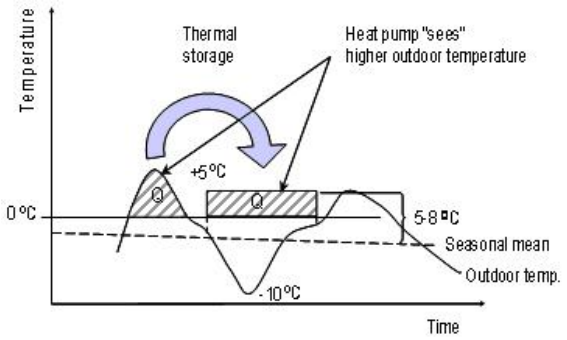

Figure 2.13: Energy gain by dynamic thermal energy storage (Gether, 2010). Heat it stored in a mild period and used in a cold period

Optimization of energy use and utilization by the means of combining DTES with BTES will enhance commercial and industrial heating and cooling processes. The integrated systems lead to a higher energy efficiency and a decrease in dependency of fossil fuel during peak loads.

2.3 Thermal response testing

This section will describe the various sources of thermogeological data, as well as the thermal response from the ground, the thermal response test (TRT) in detail and the analytical procedure used in the analyses of data from a TRT.

2.3.1 Sources of thermogeological data

When planning a borehole-based closed-loop heating or cooling system, values of the ground's thermal conductivity and its volumetric heat capacity are required as input parameters to the design process. These can be acquired by three ways:

- **Generic values**. The simplest method is to use the average value for Norwegian bedrock. A better approach is to classify the rock at the fieldsite by using a geological map and match this with the averaged thermal conductivity for the rock in question.
- **Laboratory testing**. A core or sample of geological material from the location in question can be returned to the laboratory and the thermal conductivity can be determined by the means of measuring heat flux of the material when subjected to a known temperature gradient (Banks, 2008). The mineral composition of the local bedrock can also be found.
- ***In situ* field tests**. By performing a TRT.

The thermal conductivity is a critical parameter for the sizing of the BTES, and may vary $\pm$ 20 percent from the average value of the rock (Gehlin, 1998). Determining the local thermal properties of the bedrock contributes therefore to optimization of the BTES. Laboratory tests have considerable limitations. They determine the properties of a small sample only, as compared to the heat scheme that may induce heat flow through thousands of cubic meters of rock. Fractures and discontinuities present in the aquifer are likely to reduce the bulk thermal conductivity of the rock. Also, ambient groundwater flow may enhance the heat transport in the aestifer by convection. These features can only be identified in field tests (Banks, 2008). For larger projects, a knowledge of the thermal conductivity of the subsurface will constrain the number of BHE's required to supply the energy needs of a given building, and thus the costs involved. Field tests significantly improve the accuracy of the estimated design values, and causes a cost reduction.

The most reliable source of thermogeological data is the TRT, conducted in a ready-to-operate BHE. This approach was first presented by Mogensen (1983) at a conference in Stockholm. The first mobile measurement devices were introduced in Sweden in 1995 (Eklöf and Gehlin, 1996), and in the U.S. three years later (Austin, 1998). The experimental methodology attempts to constantly heat or cool a heat carrier fluid that circulates in the BHE, measuring the fluid temperature at the inlet and outlet in order to attain the temperature development over time.

2.3.2 Thermal response

The borehole thermal response is the temperature development over time when a known heating or cooling load is imposed on the borehole, commonly by using a heat carrier fluid that circulates in the BHE. Information about the thermal properties of the rock close to the borehole is obtained by evaluating the temperature development. A low thermal conductivity is indicated by a steep gradient of the temperature development, as the temperature of the heat carrier fluid increases rapidly. Conversely, a high thermal conductivity leads to the energy being transferred to the surrounding rock at a higher rate thus obtaining a lower increase in the temperature of the heat carrier fluid. The response also gives information about the temperature difference between the heat carrier fluid and the borehole wall, the thermal resistance, as further explained in the next section.

In Europe, the most used analytical model for TRT evaluation is the *line-source model* (Carslaw and Jaeger, 1959). This model uses the concept of radial conduction of heat from a line heat source (borehole). Many have contributed to the development of the mathematics involved, but the Swedes Claesson and Eskilson have provided an investigation of numerical

and analytical solutions to the the extraction of heat from a closed-loop borehole that forms the basis for the following discussion (Claesson and Eskilson, 1987, 1988). The mathematics are also summarized by Gehlin (2002) and used in the following sections.

The basic equation is described as a linear function with constant initiation:

$$\Delta T(r_b, t) = \frac{q}{4\pi\lambda} \int_{r/2\sqrt{\alpha t}}^{\infty} \frac{e^{-\beta^2}}{\beta} d\beta \tag{2.6}$$

where $\Delta T(r_b, t)$ is the temperature increase of the heat carrier fluid [K], q is the heat injection rate per unit borehole length [W/m], λ is the thermal conductivity [W/(m · K], r is the radius from the borehole [m], α is the thermal diffusivity [m^2/s] and t is the time of after application of heat injection [s].

For a TRT, the solution of Equation 2.6 can be approximated by the following expression for the temperature of the borehole wall:

$$\Delta T(r_b, t) = \frac{q}{4\pi\lambda} \left(ln \frac{4\alpha t}{r_{b^2}} - \gamma \right) \tag{2.7}$$

where r_b is the borehole radius and γ is Euler's constant (0.5772..).The maximum error of this simplification is less than 10 % provided that $t > \frac{5r_b^2}{\alpha}$.

The above derivation assumes:

1. A *constant temperature* along the borehole, neglecting the geothermal gradient and considering the aestifer as initially having a uniform temperature equal to the average temperature over the borehole length. This is not the case in practice, as the axial temperature gradient is always small compared to the radial gradient (Gehlin, 1998).

2. *Infinite length* of the borehole. In real life, the borehole length is much larger than the borehole radius, and thus for short periods of time as is the case during the TRT, end effects can be ignored (Ingersoll et al., 1948).

The equations above are used for the transient phase of heat extraction, when the temperature of the ground is still increasing. After some time, a steady state phase begins, requiring other formulas.

Borehole thermal resistance

In addition to the specific heat capacity and thermal conductivity, the *borehole thermal resistance*, R_b [(K · m)/W], is an important factor for the design of borehole systems. The fluid-to-borehole wall thermal resistance gives the temperature difference between the fluid temperature of the collector, T_f [K], and the temperature of the borehole wall, T_b [K], for the specific heat transfer q [W/m] as seen in Equation 2.8:

$$T_f - T_b = R_b q \tag{2.8}$$

The borehole thermal resistance depends on the arrangement of the flow channels and the thermal properties of the materials involved (Gehlin, 1998). Figure 2.14 illustrates the principles of thermal resistance in a borehole. Thermal resistance imparts additional temperature loss between the aestifer and the heat carrier fluid, over that predicted by Equation 2.7. The equation in question thus becomes:

$$\Delta T_{fluid} = q \left[R_b + \frac{1}{4\pi\lambda} \left(ln \frac{4\alpha t}{r_b^2} - \gamma \right) \right] \tag{2.9}$$

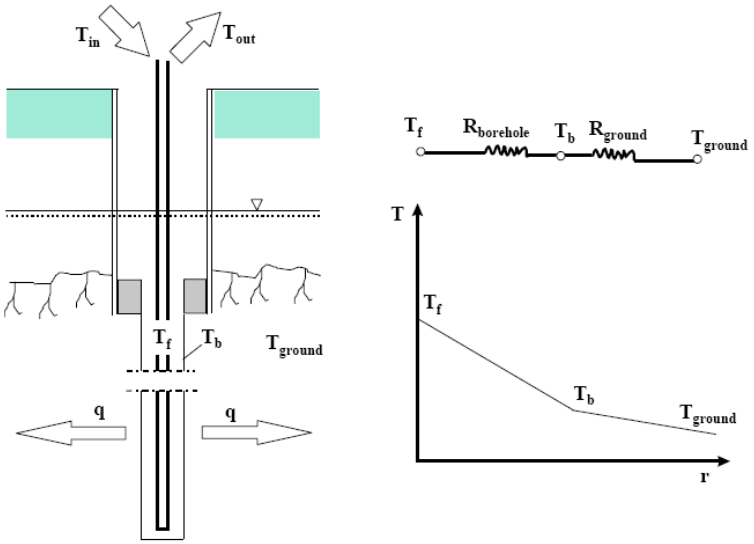

Figure 2.14: Illustration of the effect of thermal resistance in a borehole (Gehlin, 1998). The larger thermal resistance, the larger temperature loss in the material of the borehole

whereΔT_{fluid} is the difference from the initial temperature [K] and R_b is the thermal resistance [$(\mathrm{K} \cdot \mathrm{m})/\mathrm{W}$].

The borehole thermal resistance should be kept as low as possible, allowing for more heat to be transferred from the ground to the heat carrier fluid. R_b can be minimized by ensuring turbulent flow in the U-tube (further explained in Section 2.4.3), minimizing thermal short-circuiting by having a large and constant spacing between up flow and down flow tubes and finally backfilling the borehole around the U-tube with a material that has a high heat transfer coefficient.

2.3.3 Thermal response test

The initiator of the TRT, Mogensen (1983), suggested a simple arrangement including a circulation pump, a chiller with constant power rate and logging of the inlet and outlet temperature of the duct. His concept was used on full-scale BTES during their first days of operation. Later, mobile measurement equipment to be used on test-holes have been developed in order to attain parameters to be used in the design process. The mobile TRT equipment dealt with in this thesis, was developed in 1995-1996 at Luleå University of technology (Eklöf and Gehlin, 1996). Figure 2.15 illustrates the mobile test equipment, consisting of a pump, a heater and temperature sensors for measuring inlet and outlet temperature of the borehole. The equipment is set up on a small trailer to make it easily transported between boreholes. The equipment in a TRT will be further discussed in Section 3.2.

2.3.4 Data analysis

The calculation of the thermal conductivity and borehole resistance follows the suggestions by Gehlin (2002) and Signorelli et al. (2007). As already stated, the analysis of the response data is based on a description of heat as being injected from a line-source (Mogensen, 1983; Eskilson, 1987; Hellström, 1991). When heat is injected into the borehole a transient process starts that is approximated by:

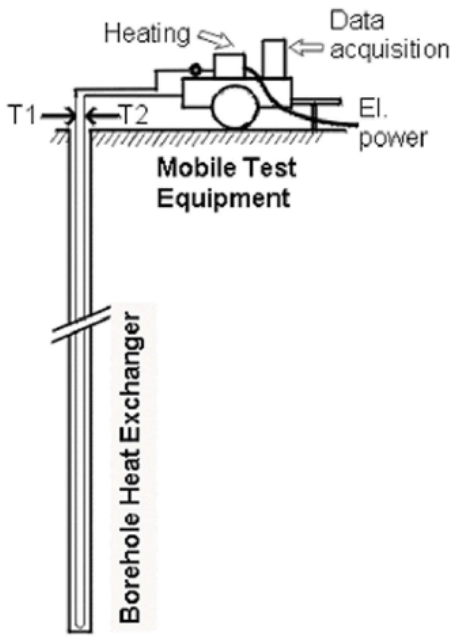

Figure 2.15: Schematic of thermal response test (Sanner, 2001), consisting of a pump, a heater, temperature sensors, a unit to log data and a borehole heat exchanger

$$T_f = \frac{Q}{4\pi\lambda H} ln(t) + \left[\frac{Q}{H} \left(\frac{1}{4\pi\lambda} \left(ln\left(\frac{4\alpha}{r_b^2} \right) - \gamma \right) + R_b \right) + T_{sur} \right] \tag{2.10}$$

where T_f is the heat carrier mean fluid temperature $= \frac{T_{in}+T_{out}}{2}$ [°C], Q is the injected heat power [W], H is the effective borehole depth [m], T_{sur} is the undisturbed initial temperature of the ground [°C] and the other parameters are as explained earlier in the text.

The equation can be simplified to a linear relationship between T_f and $ln(t)$:

$$T_f = kln(t) + m \tag{2.11}$$

where k is proportional to the thermal conductivity according to Equation 2.13 and m is a constant equal to:

$$m = \frac{Q}{H} \left(\frac{1}{4\pi\lambda} \left(ln\left(\frac{4\alpha}{r_b^2} \right) - \gamma \right) + R_b \right) + T_{sur} \tag{2.12}$$

By plotting the mean fluid temperature versus the dimensionless time parameter $\tau = ln(t)$ the thermal conductivity, λ is found from the inclination of the graph as:

$$\lambda = \frac{Q}{4\pi H} \frac{ln(t_2) - ln(t_1)}{T_f(t_2) - T_f(t_1)} \tag{2.13}$$

By this formula, not only the temperatures t_1 and t_2 is used to calculate the regression line to estimate the thermal conductivity by Equation 2.13, but also all the temperatures measured in between. In order to calculate the thermal conductivity over time, the first point of the evaluated data interval is set at a certain time, while the end time, t_2, varies.

Now, the effective thermal conductivity found in Equation 2.13 is used in Equation 2.10 to calculate the borehole thermal resistance between the heat carrier fluid and the borehole wall, R_b. Next, the experimental mean fluid temperature, T_f is plotted and matched with different thermal resistances according to equation 2.10. When the thermal conductivity is

graphically estimated according to the inclination of the curve, the borehole thermal resistance is found by matching the temperature development over time with different calculated borehole thermal resistances.

This graphical method has an accuracy of $\lambda \pm 0.05$ W/(m · K) and $R_b \pm$ 0.005 (K · m)/W (Gehlin, 1998).

2.3.5 Sources of errors

There are many sources for uncertainties in the estimation of the thermal conductivity of the ground, including both systematic and random errors. Signorelli et al. (2007), has found that the added effects of different errors by basing the analysis on the line-source model can easily reach 10 percent. The critical parameters for the analysis are the power rate, groundwater level and undisturbed ground temperature, and the main sources for errors are (Gehlin, 1998).

1. Heat leakages
2. Variable electric power supply
3. Determination of the undisturbed ground temperature
4. Gradient-driven horizontal groundwater flow
5. Density-driven vertical groundwater flow

Heat leakages

External effects such as large temperature changes in the ambient air and subsequent heat leakages may strongly disturb the measurements. Even though the heat loss to the air is much lower than the heat added to the ground, the analysis of the temperature profiles may be affected. A proper thermal insulation of the equipment is necessary in order to reduce errors related to heat leakages. Also, by logging the ambient air temperature, corrections for energy losses to the surroundings can be made.

Variable electric power supply

When using current directly from the net, variations in the voltage is likely to occur. This again leads to a non-constant transfer of heat as the power on the heat elements and the pump may fluctuate. When calculating the thermal conductivity, a mean value of the power over the time period of the testing is being used. Variations in the power supply must therefore be accounted for in the analysis. Provided it is known how the power supply varies with time, inverse modeling can be used to calculate the thermal conductivity (Banks, 2008). The power input should be measured with an accuracy of <2 % (ASHRAE, 2002).

Undisturbed ground temperature

The undisturbed ground temperature is an essential parameter for the design of a BHE, as it significantly affects the borehole thermal resistance. According to Eskilson (1987), it is not necessary to consider the temperature variations along the borehole. For a homogeneous medium, the mean temperature along the borehole is sufficient for a good approximation of the undisturbed ground temperature.

In order to attain a correct estimate of the undisturbed ground temperature, the borehole must be in thermal equilibrium with the surrounding ground. Therefore, there must be a

delay after drilling procedures, such that thermal equilibrium can be reached. If not, the measured undisturbed temperature will be too high. A minimum of 3-5 days is suggested by ASHRAE (2002). Also, if several TRT's are to be conducted in the same borehole, there must be a delay of two weeks between the tests.

To ensure the quality of the temperature measurements, it is recommended that the fluid temperature should be measured with an accuracy of < 0.3 °C (ASHRAE, 2002).

Gradient-driven horizontal groundwater flow

As previously mentioned in Section 2.1.3, heat transfer within a borehole may be significantly enhanced due to groundwater flow. Groundwater flow is caused by the hydraulic gradient, depending on the flow of water and the hydraulic conductivity of the material (Banks, 2008). The effect is present only in geological material with high hydraulic conductivities (sand, gravel), or rocks containing fractures or solution channels (Chiasson et al., 2000). Groundwater flow can be discovered by comparing standardized temperature profiles before and after a TRT (Liebel et al., 2009).

Density-driven vertical groundwater flow

Thermally induced groundwater flow due to the expansion of heated water is called the thermosiphon effect. It causes vertical groundwater flow that increases the measured thermal conductivity.

During a TRT, the temperature of the borehole is being raised. This temperature increase leads to a water volume expansion and consequently less dense water. The upper part of the borehole is likely to be more or less fractured, and the hydraulic pressure causes the heated water to drain through fractures. Following, the surrounding hydraulic pressure will be higher at the bottom of the borehole, causing a thermally induced groundwater flow into the borehole in order to reestablish the hydraulic equilibrium. This flow carries thermally undisturbed groundwater (colder). The flow will continue as long as there exists a density difference between the borehole water and the undisturbed groundwater. An illustration of the principles can be seen in Figure 2.16.

Modeling by Gehlin et al. (2003) and field tests in Norwegian shale suggest that high hydraulic conductivities may allow for large thermisophon flows, increasing the effective thermal conductivity. The thermisophon effect is also shown to be proportional to the injected heating power rate.

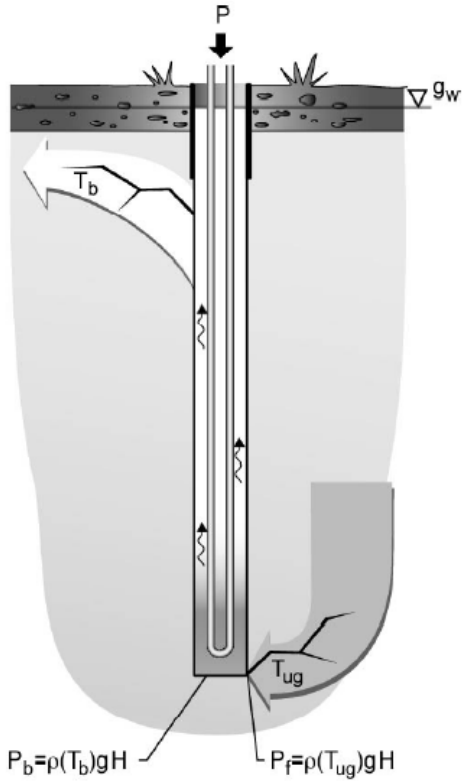

Figure 2.16: The principle of the thermisophon effect (Gehlin, 2002), induced by pressure differences between heated water and groundwater at undisturbed temperature. The heated and less dense water at temperature T_b is leaving the borehole through fractures at the top, while groundwater at temperature T_{ug} is entering the borehole at the bottom to reestablish the hydraulic equilibrium

2.4 Performance of borehole heat exchangers

In the design process of a BTES, it is of great concern to maximize the heat extraction performance of the borehole heat exchangers in order to reduce costs and increase the energy gain. In addition to the influence of groundwater flow and the ground thermal properties which has already been discussed, there are several factors affecting the heat extraction performance:

1. Temperature profile of the heat carrier fluid
2. Borehole geometry and characteristics
3. Flow conditions
4. Choice of BHE

This section will also include the equations required to analyze the heat extraction performance.

2.4.1 Temperature profile

The thermal energy obtained from the ground depends on the temperature at which the heat carrier fluid returns from the borehole, in comparison with the entrance temperature. A higher temperature provides more heat to the heat pump. The borehole thermal resistance, as already stated in Section 2.3.2, is the proportional relationship between the heat flow rate in the borehole and the temperature difference between the heat carrier fluid and the borehole wall. Thus, in order to have the most efficient heat transfer, the borehole thermal resistance should be minimized.

When a GSHP is in operation, the borehole thermal resistance may vary with depth, and it is therefore desirable to measure the temperature profiles of the BHE at many points. Heat can be transferred between the collector pipes from the upcoming pipe to the downgoing pipe causing a short circuiting effect (Acuña and Palm, 2008b). This may cause a temperature drop in the circulating fluid and decrease the system efficiency. The borehole thermal resistance between the two collectors going up and down must therefore be as high as possible, in contrast to the value for the borehole wall where a lower thermal resistance is desirable.

2.4.2 Borehole characteristics

Borehole characteristics such as the borehole diameter, depth and deviation all affects the heat transmission between the heat carrier fluid and the borehole.

The borehole diameter affects the borehole thermal resistance, as the temperature difference between the borehole wall and that of the collector fluid depends on the diameter. The temperature difference is larger when the distance between the outer wall of the BHE is increased, thus a larger diameter leads to a larger temperature decrease, and an increase in thermal resistance. The thermal conductivity is independent of the diameter of the borehole (Brekke, 2003).

The depth of the borehole has a large influence on the heat extraction. An increased depth of the borehole will in most cases lead to higher heat extraction values as the temperature of the ground increases with depth. However, borehole deviations must be accounted for as they lead to lower borehole lengths than expected, causing a lower groundwater temperature. The deviation may also cause thermal influence by other boreholes and lead to the BHE pipes to rest on one of the borehole sides having better contact with the borehole wall. The borehole thermal resistance is in theory not dependent on depth as the resistance is measured per meter well. However, there will always be some heat transfer between the BHE‘s, and this increases with depth. Some of this energy is transferred to the fluid in the collectors, thus leading to an uncertainty in the measured borehole thermal resistance.

2.4.3 Flow conditions

The type of flow of the heat carrier fluid, laminar or turbulent, greatly affect the amount of heat exchange in the boreholes. Convection in the heat carrier fluid during laminar flow may give rise to higher thermal resistance between the BHE pipes and the heat carrier fluid than in turbulent flow (Acuña and Palm, 2008a). In order to reduce the thermal resistance in the borehole it is therefore desirable to keep the flow within the turbulent region.

In laminar flow, all the fluid particles move in straight lines parallel to the pipe wall with an ordered motion (White, 2003). Turbulent flow, on the other hand, is irregular and characterized by random motions of the fluid particles. Sketches of both flows are shown in Figure 2.17. Higher motion of the fluid causes a greater heat transmission. Field studies by Kassabian (2007) suggest that higher volumetric flows yield more energy extracted from boreholes.

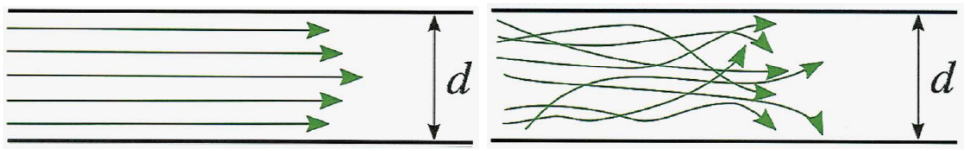

Figure 2.17: Illustration of laminar (left) and turbulent (right) flow in a pipe (ABK, 2009). In laminar flow, fluid particles move parallel to the pipe wall while in turbulent flow, the fluid particles move in random manner

The nature of the flow is determined by calculating the dimensionless Reynolds number, as seen in Equation 2.14:

$$Re = \frac{u_m \rho D}{\mu} \tag{2.14}$$

where u_m is the velocity of the flow [m/s], D is the inner diameter of the pipe [m], ρ is the density of the fluid [kg/m^3] and μ is the dynamic viscosity of the fluid [kg/(m $\cdot$ s)].

For circular pipes, the critical value for the onset of turbulence is believed to be in the range Re=2000-3000 (Banks, 2008). However the point of transmission will vary to a great extend depending on parameters such as the roughness of the pipe, bends etc., thus making it hard to address the exact value. Re increases as (and turbulent flow is more likely) density increases and viscosity decreases. With water, dynamic viscosity decreases with increasing temperatures. Also density decreases as the temperature increase, but at a slower rate. By adding antifreeze, the characteristics of the fluid change.

Even though turbulent flow optimizes heat exchange, it leads to greater losses of heat in the pipes between the ground array and the building (head loss). Also, a greater amount of energy is used as the pump requires more energy at higher volumetric flows. The pumping power must therefore be regulated to achieve the best heat transfer conditions at the lowest energy cost.

2.4.4 Choice of borehole heat exchanger

Heat exchangers are devices that transfer heat between two fluids (Banks, 2008). The thermal potential of the borehole is not influenced by externalities, and the choice of borehole heat exchanger will thus not have an direct effect on the efficient thermal conductivity of the well. The borehole thermal resistance, on the other hand, is greatly dependent on the type of BHE, and may vary significantly.

As discussed in Section 2.2.2, the most used BHE is the *U-pipe*. Recently, a new version of the standardized BHE pipe has been introduced to the market. This is called a "turbo collector", and has micro fins in helix form on their inner surface as evident in Figure 2.18.

Figure 2.18: Turbo collector (Accio, 2010). Notice microfins in a helix shape on the inside

In situ measurements conducted by Acuña and Palm (2008a), showed that the turbo collector had lower thermal resistance values compared with the standard collector, implying the best thermal performance. The turbo collector also showed a lower pressure drop, causing the required pumping power for this collector to be less than for the standard collector. Laboratory tests by Hansson (2009), showed similar results, where the pressure drop was up to 20 % lower for the turbo collector compared with the standard collector for Reynolds numbers less than 9000.

It is suggested that the micro-fins in helix form causes the fluid to travel a longer distance thus increasing the effective Reynolds number, as well as causing turbulence at an earlier stage. However, there is not a considerable amount of research on this topic. Still, the design of the BHE may cause significant differences in the borehole heat performance.

2.4.5 Analysis of heat extraction performance

The performance of the BHE is determined by the relationship between the energy added and the energy gained. The added energy depends on the energy required to run the pump, while the gained energy is the heat extracted from the well. This thesis will focus on the first, as this is a parameter that can easily be investigated in cooperation with a TRT.

The pumping power, i.e. the energy needed to pump the heat carrier fluid, is proportional to the pressure drop in the BHE channels:

$$E_{pump} = \frac{\Delta P \cdot \dot{V}}{\eta_{pump}} \tag{2.15}$$

where E_{pump} is the pumping power [W], ΔP is the pressure drop [Pa], $\dot{V}$ is the heat carrier fluid volumetric flow [m^3/s] and η_{pump} is the pump efficiency.

The pressure drop is mainly due to friction and is greater at higher velocities (Acuña and Palm, 2008a). From the equation for pressure drop one can deduce the dimensionless parameter f, the friction factor:

$$f = \Delta P_f \cdot \frac{2}{\rho u_m^2} \cdot \frac{D}{L} \tag{2.16}$$

where ΔP_f is the pressure drop due to friction [Pa], ρ is the density [kg/m^3], D is the inner pipe diameter [m], L is the total tube length [m] and u_m is the mean fluid velocity [m/s].

The friction factor depends on whether the flow is laminar or turbulent. If the pressure drop is known, f can be found by Equation 2.16 and plotted against the Reynolds number. The shape of the curve may then be used to investigate whether the flow is laminar or turbulent. As evident in the Moody diagram shown in Figure 2.19, the characteristics of laminar and turbulent flow are very different. For laminar flows, the theoretical friction factor is:

$$f = \frac{64}{Re} \tag{2.17}$$

not including the friction added by bends and turns. Turbulent flow is strongly affected by the roughness of the pipes as opposed to laminar flow where this effect is negligible (White, 2003). The relative roughness ϵ/D, where ϵ is the roughness [mm] of the pipe wall and D is the diameter of pipe [mm], is thus important when calculating the theoretical friction number for turbulent flows. If the Reynolds number is known, the friction factor for turbulent flows can be estimated by Haalands equation (White, 2003):

$$f = \left(\frac{1}{-1.8log(\frac{6.9}{Re} + (\frac{\epsilon/D}{3.7})^{1.1})}\right)^2 \tag{2.18}$$

where ϵ is the roughness [mm] and D is the diameter of the pipe [mm]. As shown in the Moody chart, the shaded area indicates the range where transition from laminar to

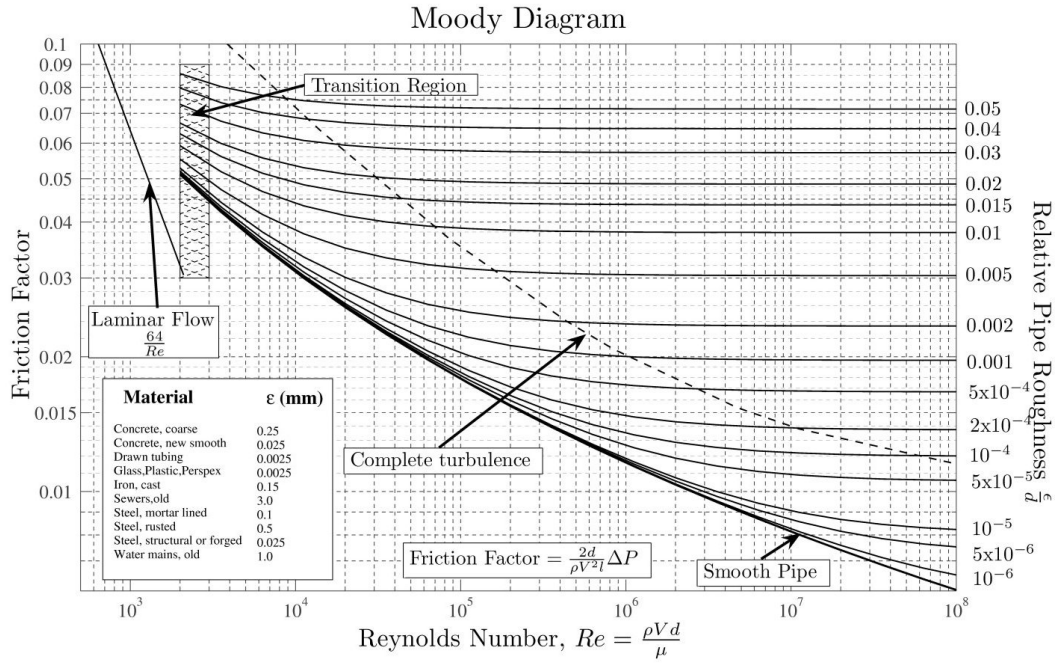

Figure 2.19: Moody diagram (Beck and Collins, 2008)

turbulent flow occurs. There are no reliable friction factors in this range. Notice also how the roughness curves are nearly horizontal in the fully turbulent regime to the right of the dashed line.

As a low friction factor means low pressure drop and less required pumping power, this is an important parameter for testing the performance of the BHE. Also, in combination with the Reynolds number, one may investigate the transition of the flow from laminar to turbulent.

Chapter 3

Fieldwork

3.1 Site description

The fieldwork was conducted in the county of Nord-Trøndelag in Norway, at Mære Landbruksskole. The location is shown in Figure 3.1.

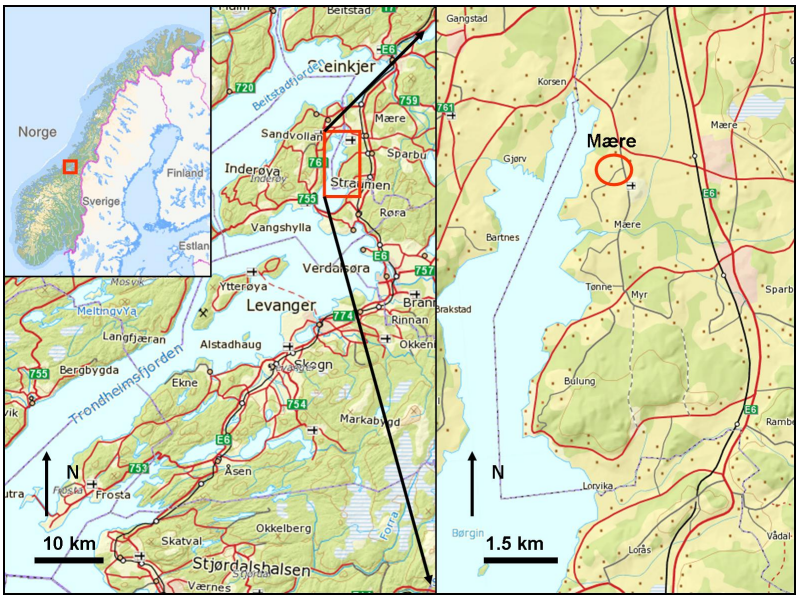

Figure 3.1: Map showing the location of Mære Landbruksskole. The red circle indicates the location of the fieldsite

Mære Landbruksskole was chosen as a case study for the project "active dynamic thermal storage for industrial processes" due to to their greenhouse facilities. In Norway, there is a concern regarding energy use with the horticulture industry where greenhouses are energy-intensive in a cool climate (Gether, 2009). A typical greenhouse of 1000 m^2 may generate 500 kW of heat in strong sunshine, and it may absorb 200-300 kW on a cold night. Greenhouses are thus great solar collectors while simultaneously acting as production units e.g. for vegetables. However, using the solar energy collected in summer efficiently and at the same time heating the greenhouse during all seasons requires a complex system of energy exchange. If one masters the thermal dynamics of a greenhouse, one may also be able to handle many uses of cooling and heating in industrial processes or comfort in residential

buildings.

The borehole was drilled by the Norwegian company Båsum Boring Trøndelag A/S. It is located in UTM-zone 32, with EW 617212 and NS 7092366. The diameter of the borehole is 165 mm, and the casing is 6 m long with a diameter of 193 mm. The borehole length is 150 m, but the BHE's only reached down to 139 m. Two different BHE's were tested in this master's thesis, a standard and a turbo collector. Both collectors have an outer diameter of 40 mm and a thickness of 2.4 mm. While the standard collector has a smooth inner surface, the turbo collector has micro fins in a helix form.

3.1.1 Geology

Mære Landbruksskole is situated in the geological region in Norway called "Trondheimsfeltet", one of the main regions of the Caledonian mountain range (Løset, 2006). The geological map in Figure 3.2 represents the geology and Quaternary geology at the site and the immediate surroundings. The rocks are mainly Silurian or Ordovician, but some are also from the late Precambrian supereon. The typical allochthonous features of the rocks mean that they have been transported by thrusting. This is due to the formation of the Caledonian mountain chain about 400-500 million years ago.

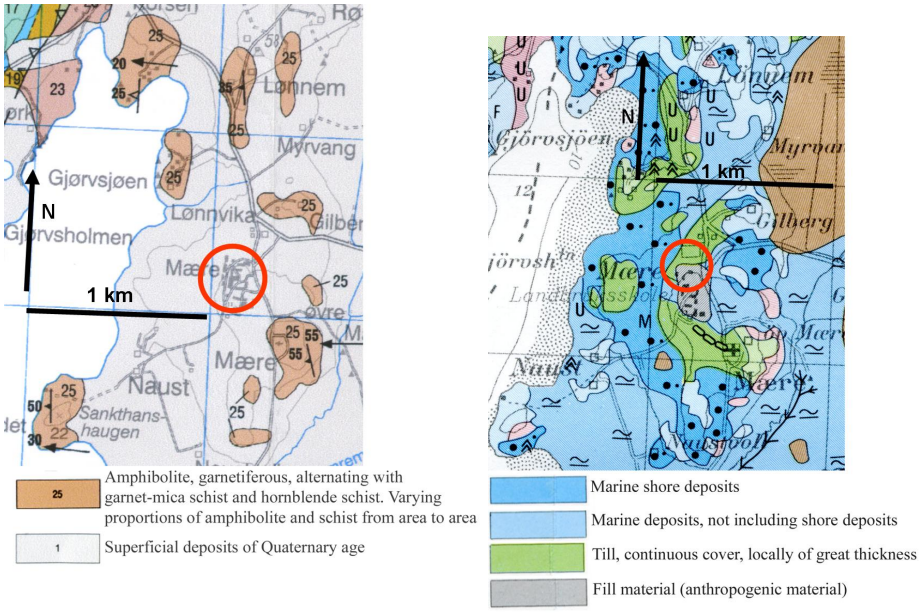

Figure 3.2: Geological map (left) and Quaternary geology (right) showing the local geology of Mære (Roberts, 2010; Sveian, 1985). The red circles represents the fieldsite

In the transition between Cambrian and Ordovician (approx. 500 Ma), the historic ocean Iapetus was closing by the converging continents of Baltika (todays Europe) and Laurentia (todays North-America and Greenland). This created a huge continental collision, in which flakes of different geological origin were thrusted upon each other, creating the Caledonian mountain chain (Ramberg et al., 2007). The mountain chain thus consists of a mix of rocks from the Precambrian continental rock from Baltika, late Precambrian to Ordovician continental sediments from Baltika, oceanic rocks from Iapetus and also possibly some remains from Laurentia. The Caledonian thrust sheets found in Trondheimsfeltet, are dominated by metagrey wackes, phyllites, mica schist, and also marbles and ophiolitic greenschists (Slagstad, 2008). Typically, they are metamorphosed under greenschist to upper amphibolite-facies conditions. The metasedimentary and metavolcanic rocks constitute

nappe and nappe complexes. Stretching lineations (mineral lineations) are well represented in Caledonian thrust sheets (Fossen and Gabrielsen, 2005).

At Mære, the rocks are mainly amphibolites and schists in various proportions (Roberts, 2010). They are a part of the Ofiolites, describing the deep oceanic rocks from Iapetus, including Gabbro, Greenstone, Amphibolites and ultramafic rocks. The rocks have large persistent faults and fractures. As seen in Figure 3.2, the main foliation close to Mære has a dip varying from 35-55 ° in the south-southwest direction. Mineral lineations are present and have a dip of 20-55 ° towards west. Large amounts of displacement have occurred in this area, and the rocks are strongly folded (Løset, 2006). Weak layers of faults with chlorite or clay may give low stability.

The Quaternary geology at the fieldsite is fill material at the immediate site of the school, surrounded by till locally of great thickness, marine shore deposits and pure marine deposits (Sveian, 1985). This corresponds with the data from the drilling as seen in Appendix B, where the upper 4.5 m consists of unconsolidated sediments. The borehole is 135 m long, and consists of various degrees of hard and weak rock. These sections are cut by faults, one at 72-75 m and one at 91-94 m. It is also worth to note that the drilling of the original well was not completed due to a fault.

3.1.2 Hydrogeology

According to the drilling company the well was extremely dry, in fact the driest they have encountered. There are no groundwater sources in this area, and the interactive map by the Geological Survey of Norway (NGU) states that there is no to low potential for groundwater at the site (NGU, 2004).

3.1.3 Thermogeology

Amphibolite and micaschist have recommended values for thermal conductivity of 2.9 $\mathrm{W/(m \cdot K)}$ and 2.0 $\mathrm{W/(m \cdot K)}$, respectively (Eskilson et al., 2000). As evident in Table 2.1, the volumetric heat capacity of amphibolite and mica schist are 2.6 $\mathrm{MJ/(K \cdot m^3)}$ and 2.2 $\mathrm{MJ/(K \cdot m^3)}$.

Samples from the Caledonian Orogen show a median heat production of 1.4 $\pm 1.39\,\mu\mathrm{W/m^3}$, and an area-weighted heat production of 1.47 $\mu\mathrm{W/m^3}$ (Slagstad, 2008).

3.2 Equipment and methodology

In this master's thesis, the focus of the investigation was the geology of the field site, obtaining thermal parameters from the ground and test two different types of BHE's by gaining an understanding of their performance under different flow conditions. The type of equipment and methodology used to complete these investigations is described in this section. For additional information on the equipment and computer software used, look to Appendix C.

The well was drilled in December of 2009 and the measurements were carried out during March and April 2010. An investigation of the fieldsite was carried out in January.

3.2.1 Geological investigation

The geological mapping was performed on the 27th of April, after having studied the area beforehand by the use of geological and hydrogeological maps. The mapping included registering the strike and dip direction of fractures, collecting representative samples for further

laboratory investigations (thermal conductivity, x-ray diffraction and differential thermal analysis) and gather information about the geological features of the area. Coordinates of the sample sites were found by the use of a handhold GPS. Unfortunately, not many outcrops were available for gathering data. Figure 3.3 shows were the sample locations are situated. The coordinates of the sample locations can be found in Appendix E.

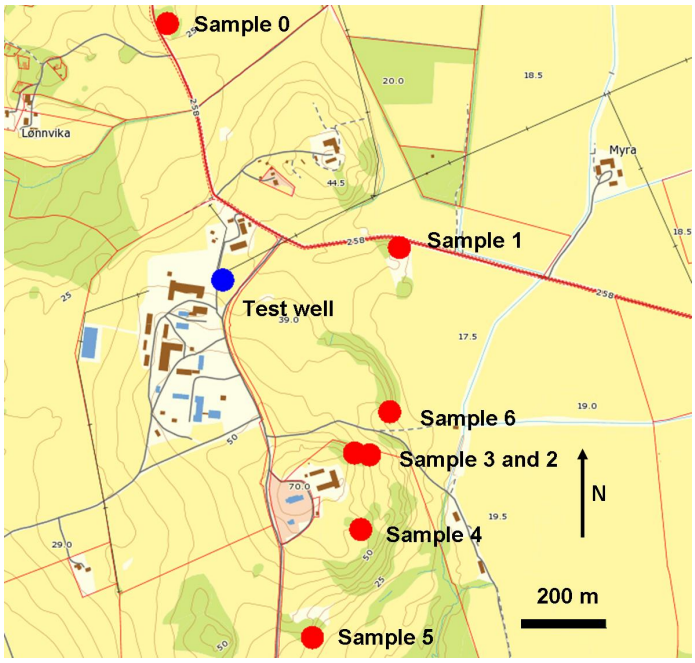

Figure 3.3: Map showing the location of samples (red dots) and well (blue dots). Map made in `http://www.gislink.no/gislink/` 2nd of June 2010

3.2.2 Thermal properties of the fieldsite

The goal for the TRT was to gather information about the thermal properties of the ground, and also compare the results for two different BHE's. The standard test equipment used for the TRT in this master's thesis was an rig owned by NGU, described in detail by Gehlin (1998). The equipment is set up on a small trailer, and consists of a pump circulating the heat carrier fluid through the borehole collector system and through a heater with adjustable and stable heating power. The fluid temperature is measured at the inlet and outlet of the borehole with thermistors, and are recorded at intervals set by the data logger. The equipment is powered by 16 A electricity. A sketch and a photo of the TRT equipment is shown in Figure 3.4.

The connection between the trailer and the borehole had was insulated in order to minimize energy losses and the influence of changes in temperatures of the ambient air. Both TRT's were carried out for at least 72 hours, as suggested by Gehlin (2002), and the pump was run at 22.4 Hz, ensuring turbulent flow. The thermal conductivity and borehole thermal resistance was calculated by the standard procedure used by NGU and presented in Section 2.3.4. The thermal conductivity was also calculated as it changed over time by using the same method as Signorelli et al. (2007).

Temperature profiles were measured with the use of temperature data loggers, connected to a sinker with a 200 m long chord. In order to determine the undisturbed ground temperature, a temperature profile was found before both TRT's. Four hours after the TRT, another temperature profile was made in order to investigate the groundwater flow (Liebel et al.,

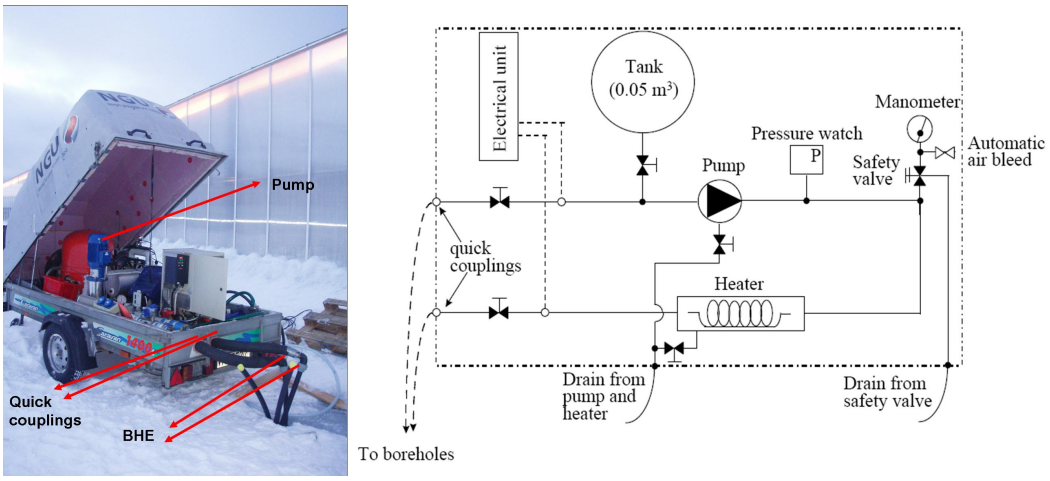

Figure 3.4: TRT equipment in field (left) and as a sketch (right) (Gehlin, 1998). Photo: Marie Stølen

2009). The time interval for the recordings of the temperature profile was set at one minute to ensure that the data logger adapted to the fluid temperature even at steep temperature gradients. To increase the validity of the first recording, the data logger was placed 3 m below the casing of the borehole for 10 minutes because of the temperature difference between the ambient air and the borehole wall. The next three measurements had time intervals of two minutes. The depth interval was set at 4 m with regard to the temperature measurements after the TRT, keeping the measurement time low to reduce the effect of the temperature recovery of the ground.

Also, four temperature data loggers were lowered down in the collector not being used in the TRT. These were used to investigate the temperature development, and thus the thermal conductivity, at different depths during the TRT, and after. The data loggers were set at depths of 40 m, 73 m, 93 m and 101 m; chosen to correspond with sections of hard rock and thrust zones.

3.2.3 Flow conditions

Flow conditions were tested by using a differential pressure transmitter and accelerometer in addition to the standard TRT equipment. The main goal was to investigate the difference between the two BHE's to with regard to pressure drop and vibrations. Previous investigations of these collectors have never been performed in the same borehole.

In addition to the standard test equipment, a differential pressure transmitter was used to measure the total pressure drop in the collectors. The differential pressure transmitter was connected to the pressure taps located at the collector inlet and outlet lines. The set-up of the differential pressure transmitter can be viewed in Figure 3.6. The uncertainty of the instrument is given to be $\pm$ 0.25 %. Also, an ammeter was used to measure the current used by the pump. The uncertainty of the instrument was $\pm$ 3 %, and working temperature 0-50 °C. Finally, an accelerometer was used to measure the vibrations from the flow in the collectors. Figure 3.5 shows the accelerometer during testing, and how the vibration indicators were connected to the collectors. It was important to ensure that the in-going and out-going pipe did not come in contact with each other and thus transfer vibrations. Also, the sensors had to be glued onto the pipe as far as possible from the pump. A preliminary analysis of the vibration data was conducted by Frode Haukland at SINTEF.

The flow conditions of the system were measured twice. The first measurement period was

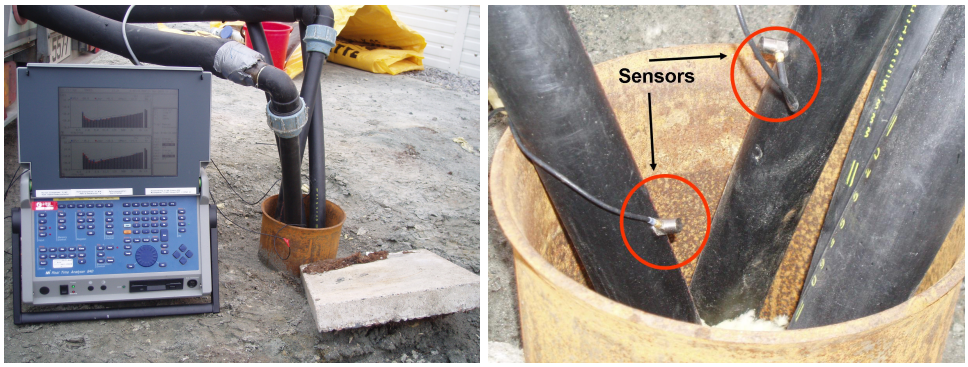

Figure 3.5: The accelerometer during testing. The sensors glued onto the borehole heat exchanger are indicated with red circles. Photo: Marie Stølen

conducted in March 2010, before the first TRT. The pump was set at the lowest revolution per minute, and after letting the borehole recover for five minutes the volumetric flow, current, pressure drop and vibrations were recorded. The revolution per minute was then increased in steps of 1 Hz until reaching 29.2 Hz when steps of 2 Hz were used. The volumetric flow was recorded by measuring the time for 0.01 m^3 of water to pass through the pipe. Both collectors were tested by using the same procedure.

The second measurement period was conducted in April 2010. To attain a lower volumetric flow a restriction valve was used. The restriction valve is located on the out-going pipe downstream of the differential pressure transmitter, as shown in Figure 3.6. By tightening the restriction valve, a lower volumetric flow was reached. The volumetric flow was then measured to investigate whether the desired flow was obtained. If so, the borehole was given ten minutes to recover and subsequently the volumetric flow, current, pressure drop and vibrations were recorded. The pump was set at the lowest revolution per minute possible while the restriction valve was loosened and recordings at higher volumetric flows were completed. Measurements on the vibrations of the pump and the BHE's before the pump was started were also conducted in order to record noise from the external environmental.

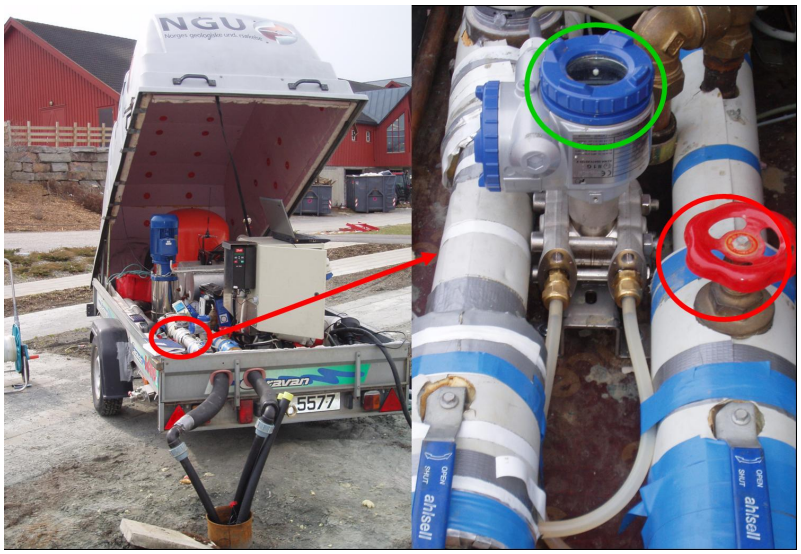

Figure 3.6: Thermal response test rig (left) showing the location of the differential pressure transmitter (right - green circle) and restriction valve (right - red circle). Photo: Marie Stølen

Chapter 4

Results

4.1 Field investigations

4.1.1 Hydrogeology

The water table was found to be 2.21 m below surface before the first TRT. After the test, the water table was increased to 1.33 m below surface. Before TRT 2, the water table was found to be 1.57 m. During the period of time between the measurements the outdoor temperature was increased from a minimum of -15 °C to a maximum of 4 °C. This lead to snow- and ice-melting in and around the casing of the borehole, and a flow of melting-water into the borehole.

4.1.2 Geological conditions

During the geological mapping, it was evident from both the rock samples and the bedrock that quartz ores up to 7 cm thick were present. Figure 4.1 shows both thick and thin ores. Mineral lineations were present in the same direction as the quartz ores.

Figure 4.1: Quartz-ores in rock close to Mære. Large ore on the left and smaller ores to the right. Photo: Marie Stølen

A stereoplot of fractures measured at outcrops in the area is given in Figure 4.2. Even though a small population of fractures were measured, three fracture-sets are evident. Average strike/dip directions are 132/36.6 °SW for K1, 30.7/66.3°SE for K2 and 70.9/28.8°NW for K3. The observed fractures were parallel to the foliation. Small folds were also observed.

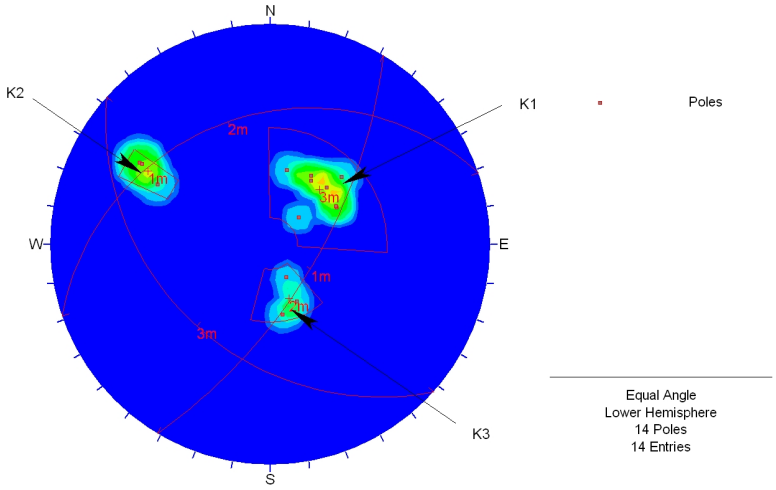

Figure 4.2: Equal area stereoplot and contourplot (lower hemisphere - Fisher distribution method) of rock in Mære. There are three main fracture sets, K1, K2 and K3

4.2 Laboratory analysis

4.2.1 Mineralogy

Rock samples from Mære were analyzed with the x-ray diffraction (XRD) method to identify mineral types. It is a semi-quantitative method, i.e. quantity of minerals are only approximate. The results from XRD are presented in Table 4.1. See complete results in Appendix D.

Table 4.1: Results from XRD

	Sample numbers						
Minerals	0	1	2	3	4	5	6
Albite [%]	12	16	20	10	13	19	18
Chlorite [%]	12	2	11	2	3	3	1
Microcline [%]	6	4	11	3	2	2	2
Quartz [%]	35	49	32	4	44	40	43
Mica [%]	16	5	3	3	10	22	2
Hornblende [%]	12	18	19	75	20	5	28
Calcite [%]	4	3	3	1	5	7	1
Dolomite [%]	3	3	1	2	3	2	5
Classification	Mica schist	Mica schist	Mica schist	Amphi-bolite	Mica schist	Mica schist	Mica schist

By studying the rocks, the presence of amphibole, mica and quartz were evident. The presence of calcite was verified for sample 4 and 5 by hydrochloric acid. Calcite is concentrated to diffuse bands in intact rock and as mineral filling, also proven by previous field investigations in this area (Haraldseth, 2009). The rocks had various degrees of foliation, but in general, the rock samples showed schistous structures. From the XRD-results and observations, all rocks but one were classified as mica schists. Sample no. 3 was classified as an amphibolite due to a very high hornblende content (Prestvik, 2001).

4.2.2 Quartz-content

Because of the large influence quartz has on the thermal conductivity, differential thermal analysis (DTA), was used to detect the quartz-content specifically. A brief explanation of the method is found in Appendix F, together with the results. The results are also shown in Figure 4.4, where the quartz-content is plotted against the thermal conductivity.

The results from DTA varies from less than 5 % to close to 50 %. It is also worth to note that sample 3 stands out with a very low content of quartz compared to the other samples.

4.2.3 Thermal conductivity

The thermal conductivity of samples from the fieldsite was measured at the lab at NGU on the 9/3-2010 and 4/5-2010. The sample cores were drilled either parallel or normal to the foliation of the sample rock. An extensive laboratory report can be found in Appendix E, where all the measurements and details concerning the cores are presented. A statistical analysis of the averaged measurements from each sample location is shown in Figure 4.3.

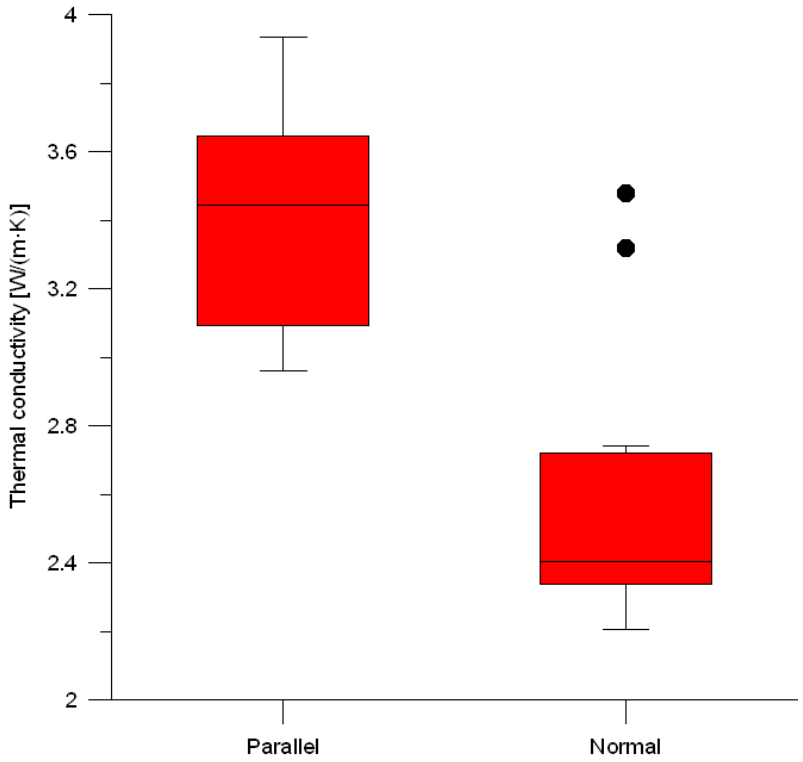

Figure 4.3: Box and Whisker plot showing statistical variations of the thermal conductivity (25% percentile, median, 75% percentile, whiskers indicate 10% and 90 % percentiles if more than 9 samples are available, outliers are dotted) for samples measured in the laboratory both parallel and normal to the direction of the foliation

The mean thermal conductivity for the parallel samples is 3.4 $\pm$ 0.3 W/(m $\cdot$ K), where as the normal samples have a mean thermal conductivity of 2.5 $\pm$ 0.3 W/(m $\cdot$ K). From the statistical analysis, it is clear that the samples measured in the parallel direction have a larger thermal conductivity than the samples measured normal to the foliation. This is only deviated from for sample 4, noted in Figure 4.3 as outliers. A sample containing close to 80 % quartz had an averaged thermal conductivity of 4.7 W/(m $\cdot$ K). The average of all rock samples, including both parallel and normal oriented samples, is 3.0 $\pm$ 0.5 W/(m $\cdot$ K).

The relationship between the quartz-content and averaged thermal conductivity for each sample is found in Figure 4.4. Several different fit equations were tested to see which fitted the most, and a linear equation showed to have the highest R-squared. Following, by enforcing a linear relationship, there is an R-squared of approximately 0.6. There was no or an insignificant relation found when plotting the quartz-content against the averaged parallel and normal oriented samples.

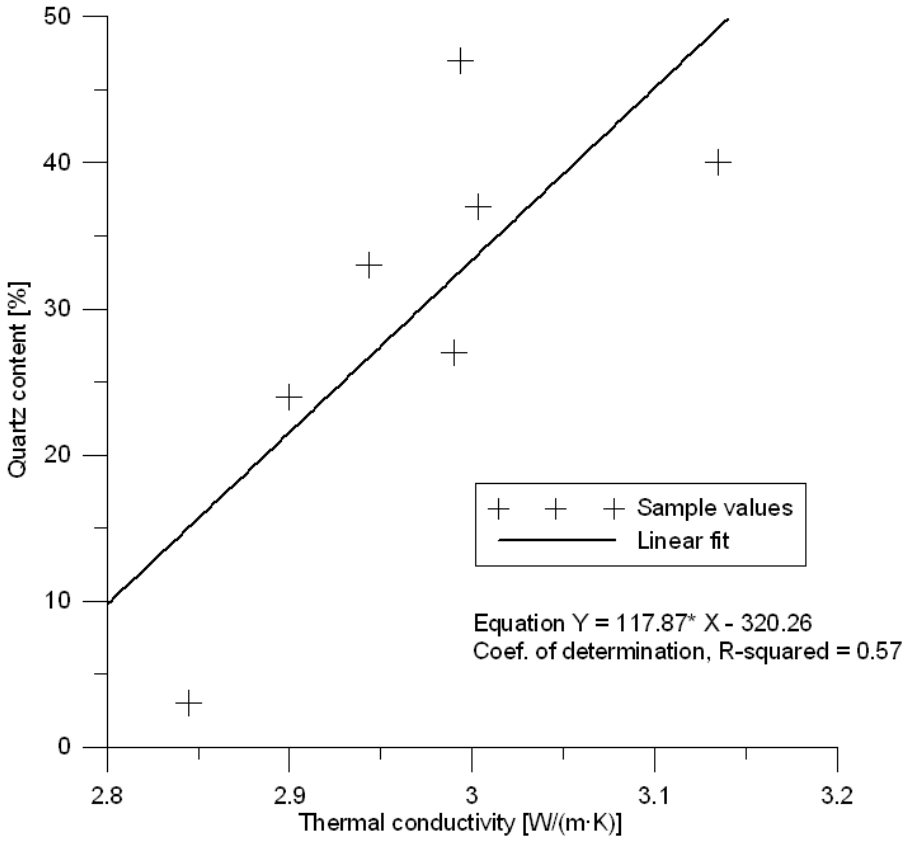

Figure 4.4: Relationship between quartz content and thermal conductivity

4.3 Thermal properties of the field site

4.3.1 Thermal response test

The TRT's were carried out consecutively with a waiting period of 14 days in between. The borehole was heated up to 11 °C during the first test, and was then allowed to recover to about the same temperature as before the first TRT. The undisturbed ground temperature was reinstalled during the waiting period.

Both tests were carried out in March, with temperatures as low as -15 °C. The TRT for the turbo collector was completed first during a period at which the temperature increased from -15 °C to 5 °C, as evident in Figure 4.5. As the ground was covered in ice and snow this lead to extensive snow-melting in and around the area of the test-well. The well was not closed during the test so that water may easily have entered. Before the start of the test there was ice present in the casing of the well, and after the test the casing was clean. The cold weather lead to some frozen equipment, and the air-valve did not seem to function properly during the pressurizing of the system. The temperature during the second test also

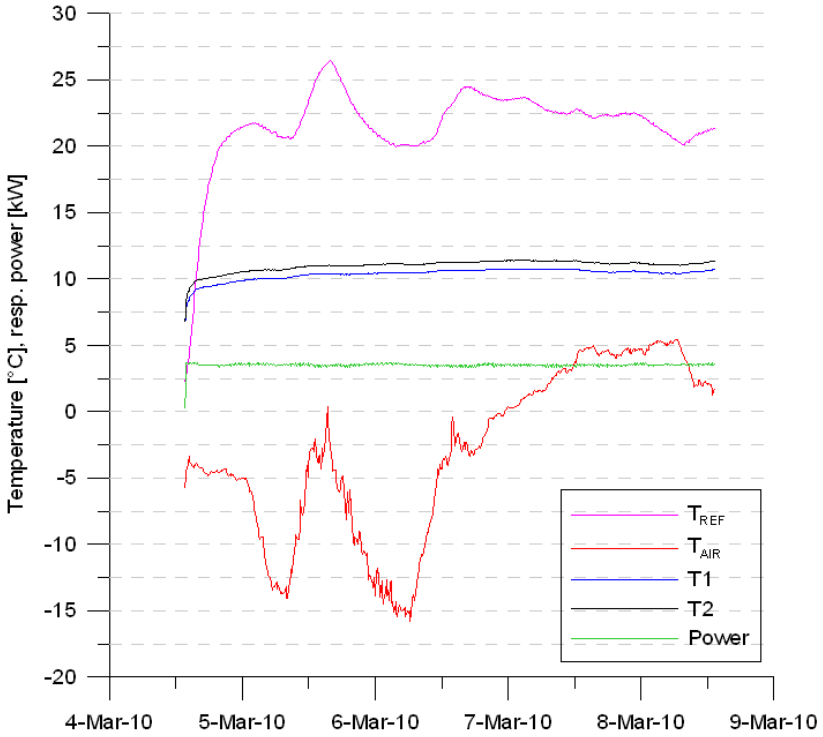

Figure 4.5: TRT 1 for turbo collector. T1:up-flow temperature, T2:down-flow temperature, T_{REF}:reference temperature inside the TRT trailer, T_{AIR}:temperature of ambient air, Power is the consumption of heat elements and the circulation pump.

increased from -6 °C to 5 °C Celsius (Figure 4.6). However, there was no ice present and only small amounts of snow.

Table 4.2 gives an overview over the calculated effective thermal conductivities, (λ_S), and the borehole thermal resistances using standard procedures for the two TRT's conducted at the borehole in Mære. The diagrams used to find the borehole thermal resistance at Mære are presented in Appendix A. The thermal conductivity measured in the first TRT is larger than for the second TRT.

Table 4.2: Thermal conductivity and borehole thermal resistance at Mære

Type of collector	λ_S [W/(m · K)]	Borehole thermal resistance [(K · m)/W]
Turbo	4.8	0.07
Standard	4.0	0.07

Figure 4.7 and Figure 4.8 shows how the calculated thermal conductivity develops over time. Equation 2.13 was used in the calculations. For the first TRT, the thermal conductivity seems to stabilize between 40-60 hours at about 4.2 W/(m · K) before it increases greatly.

The temperature development at different depths during TRT 1 is shown in Figure 4.9 and TRT 2 in Figure 4.10. These were measured from the collector not being used during the test.

Thermal conductivity was calculated by standard procedures at each depth, using the temperature development at that depth. The results are shown in Table 4.3.

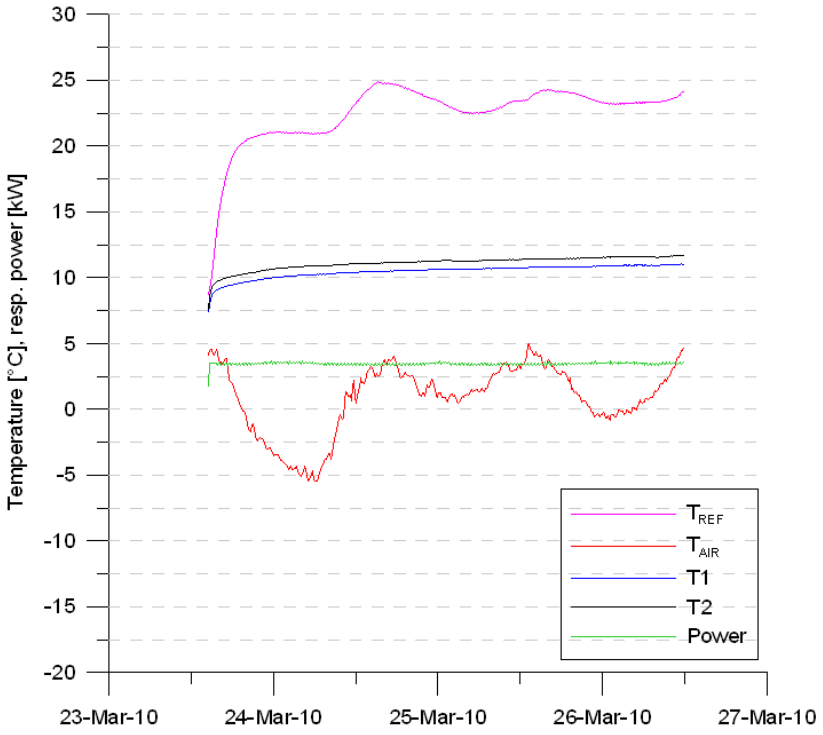

Figure 4.6: TRT 2 for standard collector. T1:up-flow temperature, T2:down-flow temperature, T_{REF}:reference temperature inside the TRT trailer, T_{AIR}:temperature of ambient air, Power is the consumption of heat elements and the circulation pump.

Table 4.3: Thermal conductivity at varying depths

TRT test	λ_{40} [W/(m · K)]	λ_{73} [W/(m · K)]	λ_{93} [W/(m · K)]	λ_{101} [W/(m · K)]
1	3.8	4.8	41.7	3.9
2	3.7	3.9	5.0	4.2

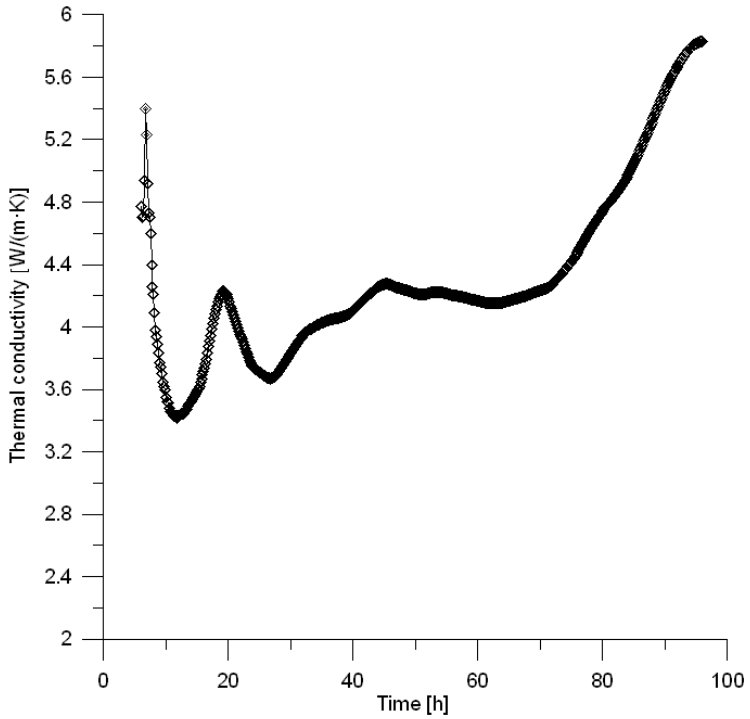

Figure 4.7: Calculated thermal conductivities over time during TRT 1. The first point of the evaluated data interval is set at t_0=5h; the end time varies. There is a sharp increase of the thermal conductivity at around 70 hours

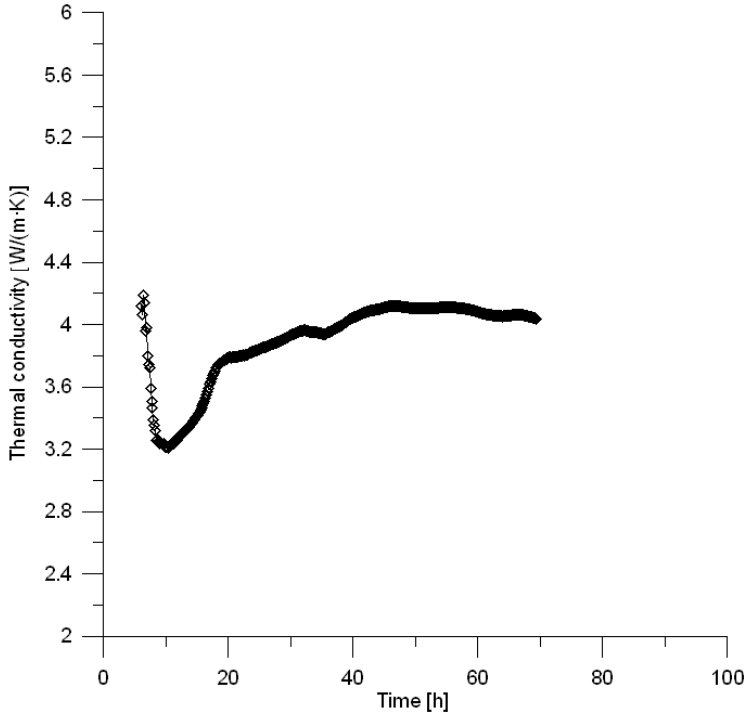

Figure 4.8: Calculated thermal conductivities over time during TRT 2. The first point of the evaluated data interval is set at t_0=5h; the end time varies

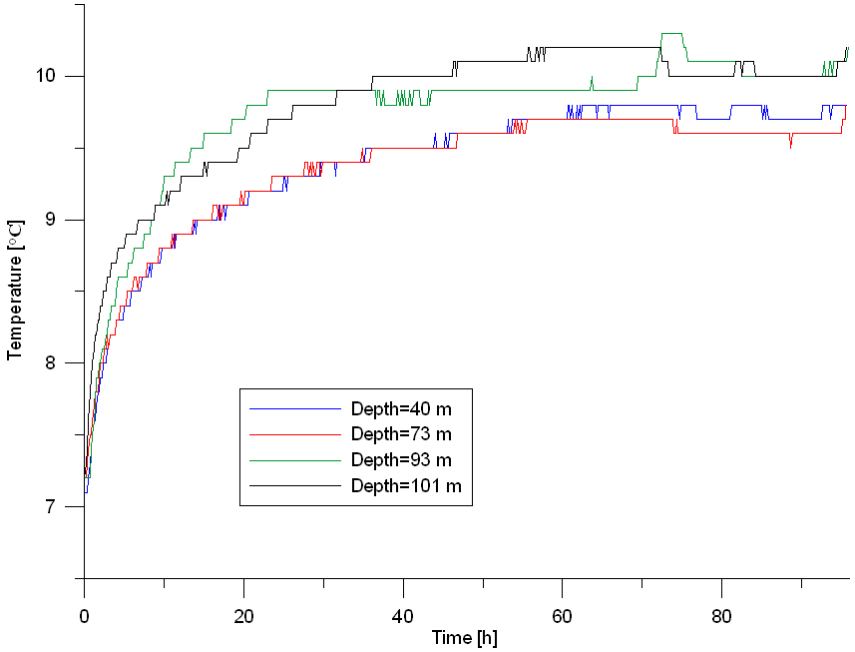

Figure 4.9: Temperature development at different depths during TRT 1, turbo collector. The temperature development at depths of 40 m, 73 m, 93 m and 101 m is shown

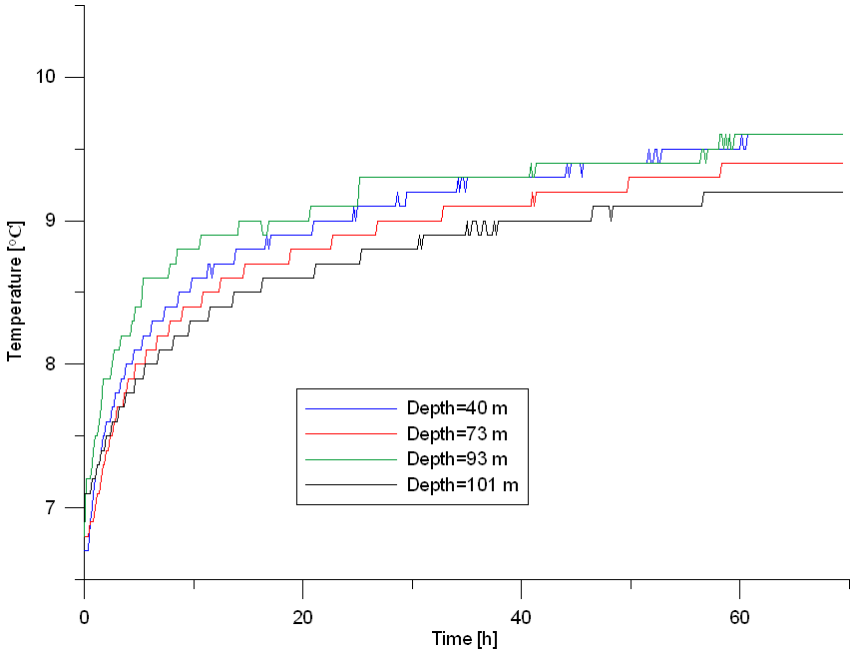

Figure 4.10: Temperature development at different depths during TRT 2, standard collector. The temperature development at depths of 40 m, 73 m, 93 m and 101 m is shown

4.3.2 Temperature profiles

The temperature profiles are used to calculate the average undisturbed ground temperature, as well as giving an indication about the geothermal gradient and heat flow in the area.

Figure 4.11 shows the undisturbed temperature profiles taken before the TRT's for both turbo collector and standard collector, respectively.

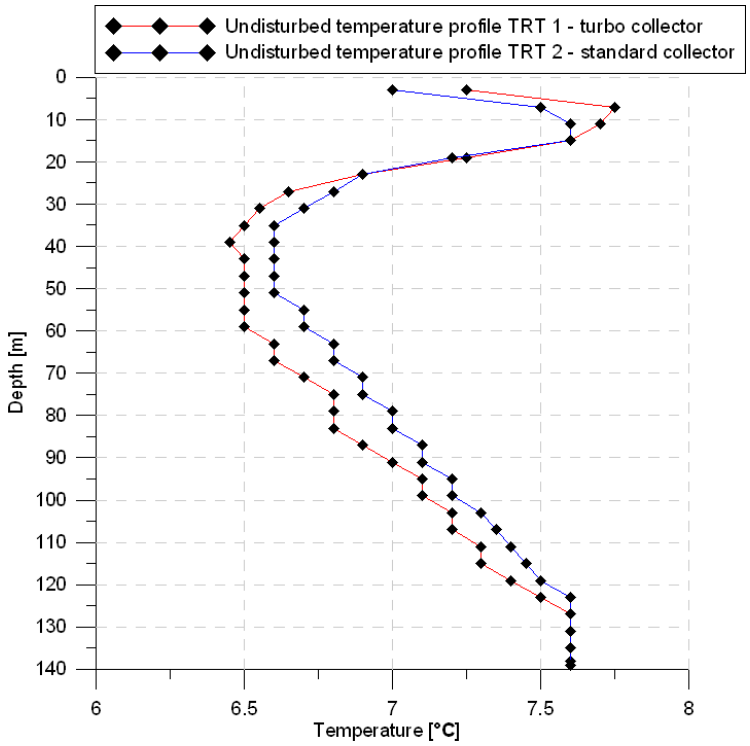

Figure 4.11: Undisturbed temperature profile TRT 1 (red line) and TRT 2(blue line)

As a temperature profile also was completed after the TRT's, these profiles were compared by subtracting them from each other:

$$\Delta T(z) = T_{after}(z) - T_{ini}(z) \tag{4.1}$$

where $T_{after}(z)$ is the temperature measured a certain time after the TRT at depth z and $T_{ini}(z)$ is the temperature measured before TRT at depth z.

For the first TRT test (turbo collector), the temperature profile was measured 4 hours after the TRT-test, while for the second test the measurements were done after 5 hours. It was tried to measure after 4 hours, but the logger did not go further than 95 m. The measurements were therefore completed at the other side of the collector, 5 hours after the TRT-test. The delta temperature profiles for each TRT is seen in Figure 4.12.

The geothermal gradients and heat flow data were calculated by Fourier's law (Equation 2.1). The method used for calculating the geothermal gradient is as suggested by Liebel et al. (2009). 20 m intervals is used from the temperature profile to calculate the gradient. If a temperature profile starts at 10 m depth, the first value is calculated by subtracting the temperature at 30 m with the temperature at 10 m, assigning this value to a depth of 20 m. The same procedure is followed for each step in depth. Figure 4.13 shows the thermal gradient measured before each of the TRT's. Now, the heat flow can be calculated by using the thermal conductivity value achieved *via* the TRT performed in the same borehole, and the measured thermal gradient for a certain depth interval (Figure 4.14 and Figure 4.15).

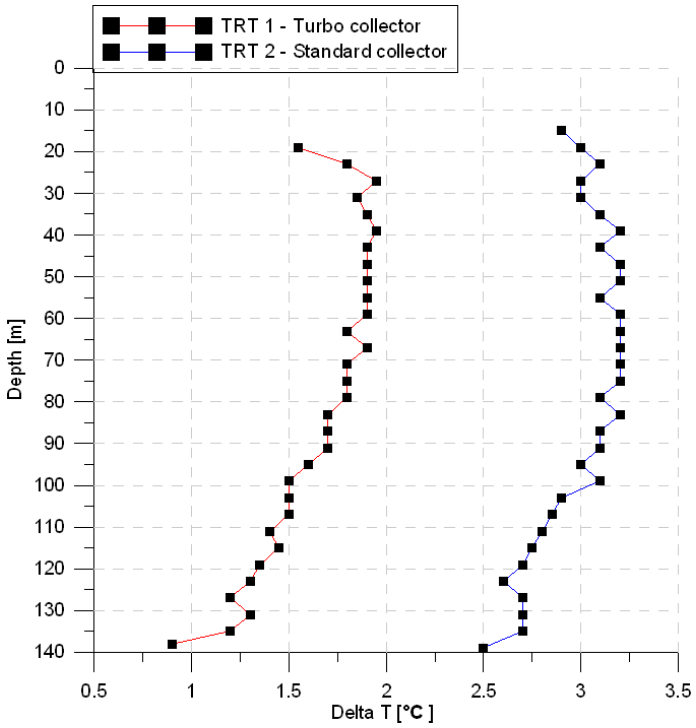

Figure 4.12: Delta temperature profiles TRT 1 (red line) and TRT 2 (blue line)

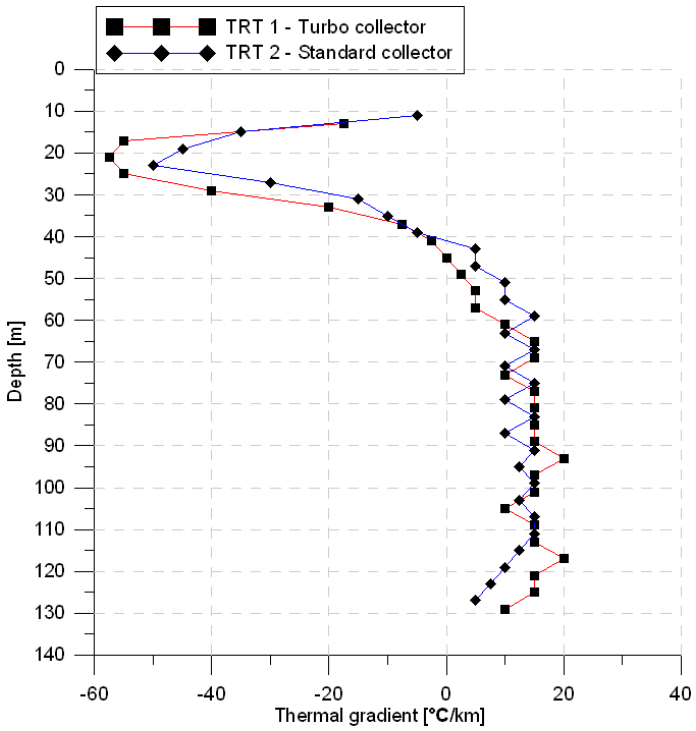

Figure 4.13: Thermal gradients for TRT 1 (red line) and TRT 2 (blue line). 20 m intervals has been used to calculate the thermal gradient

The mean values for the geothermal gradient and heat flow were calculated for depths below 63 m, as those values appeared in Figure 4.15 and Figure 4.14to be less influenced by

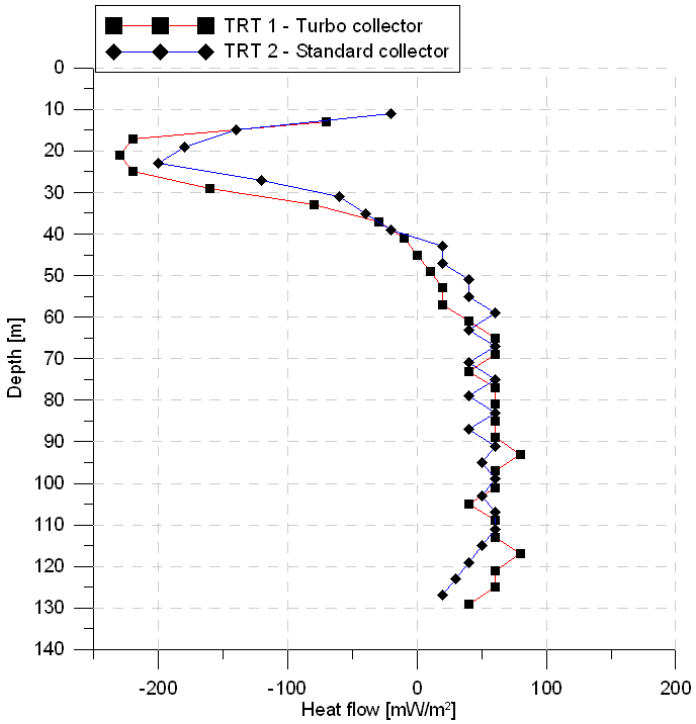

Figure 4.14: Heat flow calculated for the first TRT (red lines) and the second TRT (blue lines) from temperature profiles before TRT

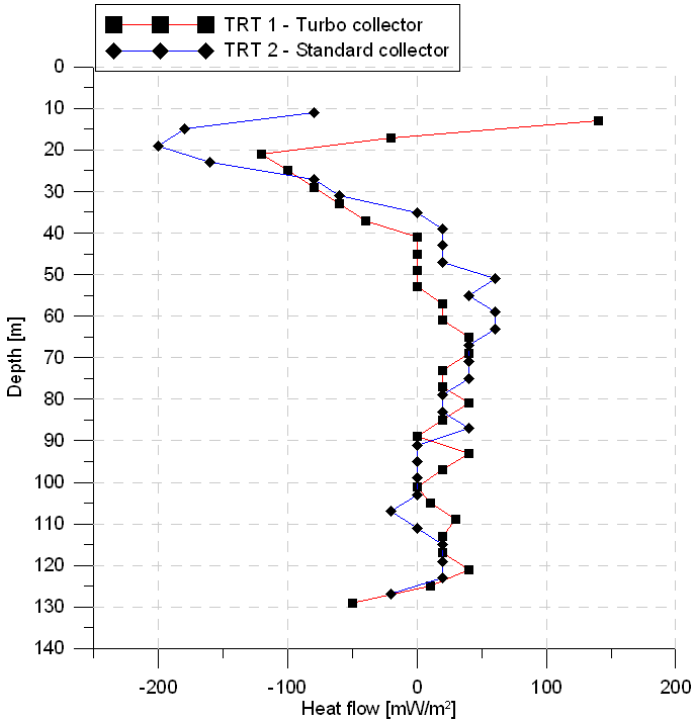

Figure 4.15: Heat flow calculated for the first TRT (red lines) and the second TRT (blue lines) from temperature profiles after TRT

external factors. The mean geothermal gradient before TRT 1 was 14.7 ± 3.0 °C/km and 12.0± 3.2 °C/km before TRT 2. For heat flow, the mean value before TRT 1 was 58.7 ± 11.9 mW/m^2 and 48.4 ± 12.7 mW/m^2 before TRT 2.

4.4 Flow conditions

4.4.1 Pressure drop

The pressure drop *versus* the volumetric flow were measured twice, the first time on the 2nd and 3rd of March, and the second time on 26th and 27th of April. In the first measurement, the flow did not reach expected laminar flow as the pump was too strong.

For correlating the results of experimental research, it is essential to employ dimensionless parameters. Thus, it was chosen to portray the results using the Reynolds number, Re, and the friction factor f. The friction factor was calculated with a roughness of ϵ=0.0015 mm, the value for a drawn plastic tubing with an uncertainty of ± 60 % (White, 2003). A logarithmic scale was used to emphasize the measurements with lower Reynolds number as these are of most interest when comparing the two BHE's. The calculated experimental friction factor against Reynolds numbers for both tests is shown in Figure 4.16, together with theoretical values for laminar and turbulent flow.

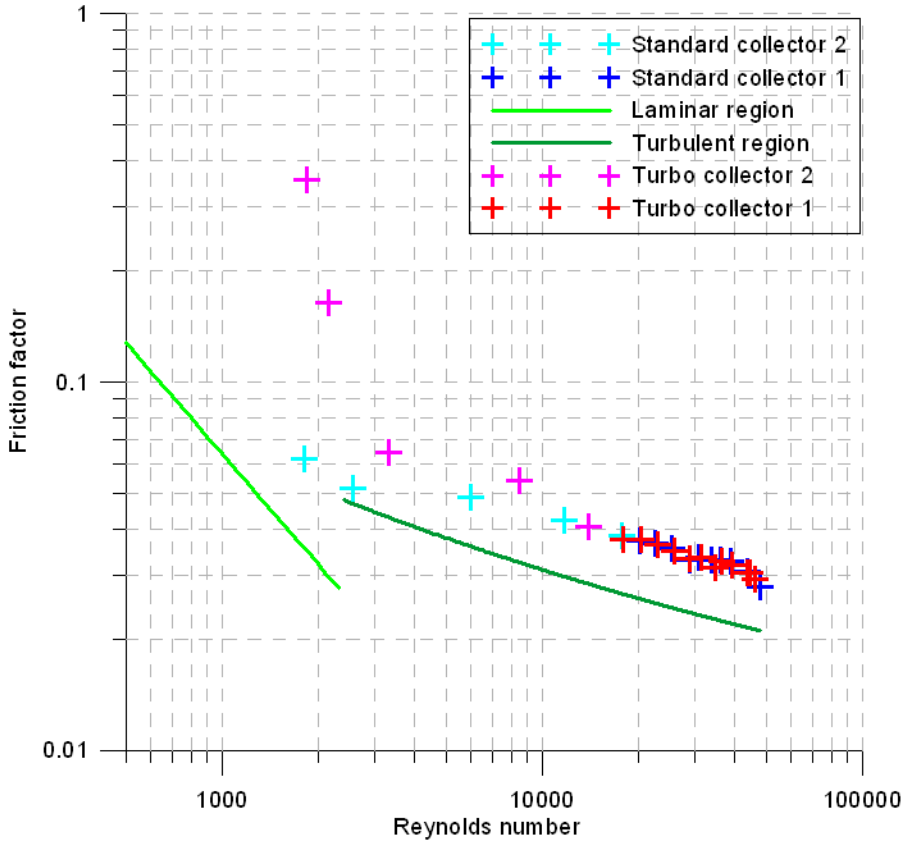

Figure 4.16: Friction factor plotted against Reynolds number for TRT 1 and TRT 2 and both collectors. The predicted theoretical values for laminar and turbulent flow are represented by the light green and dark green line. Note logarithmic scale on the axes

To see how much the experimental friction factor deviated from the predicted value, these were plotted against each other as evident in Figure 4.17. Figure 4.18 emphasises the

experimental values closest to the theoretical values, not including some measurements from the second test of the turbo collector.

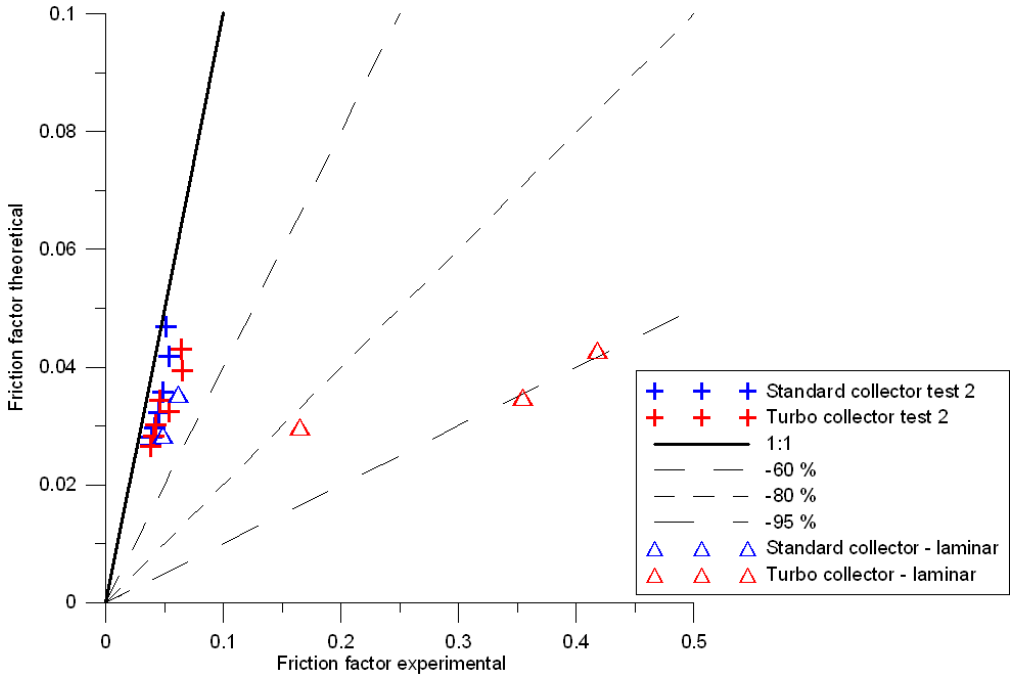

Figure 4.17: Experimental friction factor *versus* predicted value

The temperature in the BHE's were logged during the measurements, and showed a mean temperature of 7 ° C for all the tests. Thus a dynamic viscosity of 0.001429 kg/(m · s and a density of 999.96 kg/m^3 was used to calculate Reynolds numbers. However, 10-15 l of antifreeze was still in the system together with pure water, which is maximum 3% of the circulating fluid. Since the amount was so small it was not accounted for in the calculations.

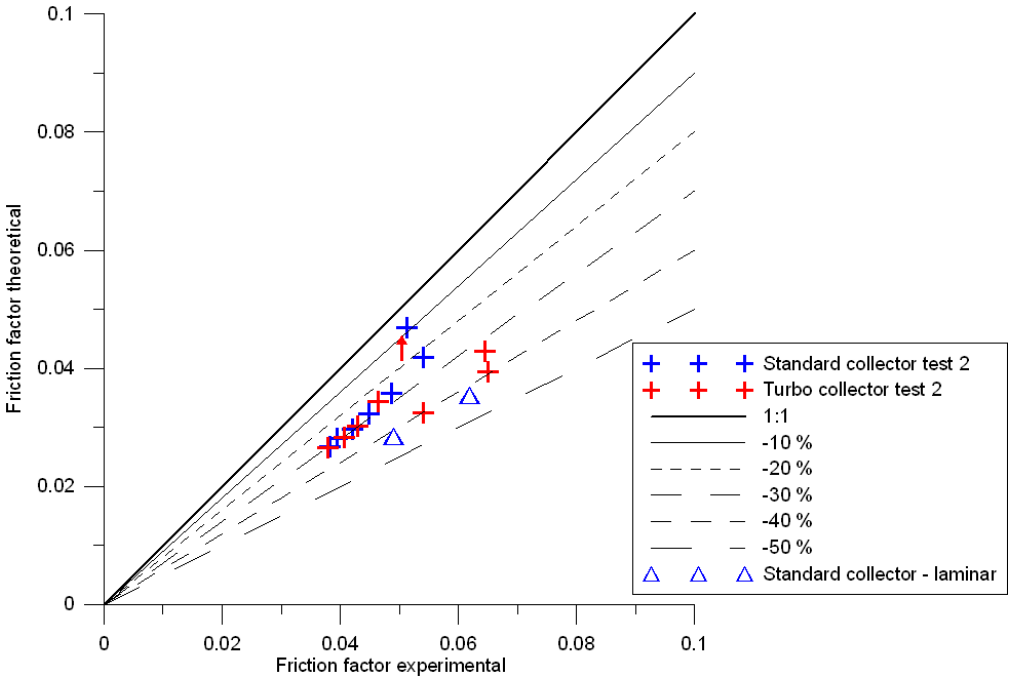

Figure 4.18: Experimental friction factor *versus* predicted value. This figure does not include the measurments at assumed laminar flow for the turbo collector, emphasising the similar values. Notice the red arrow pointing at a measurement in the transition zone

4.4.2 Vibration measurements

The vibration measurements presented in this section were carried out the 26th and 27th of April. All the measurements are listed in tables and graphs in Appendix G, and the main findings are presented here.

In Figure 4.19, vibration measurements with Reynolds numbers of about 1880 and 18000 are shown, representing assumed laminar and turbulent flow. Only measurements from the out-going pipe are shown, as these are comparative to each other. Note that the turbo collector shows a larger mechanical vibration (represented by acceleration) than the standard collector. When comparing the curves representing turbulent and laminar flow, there is no clear pattern pointing to a higher or lower level of vibration.

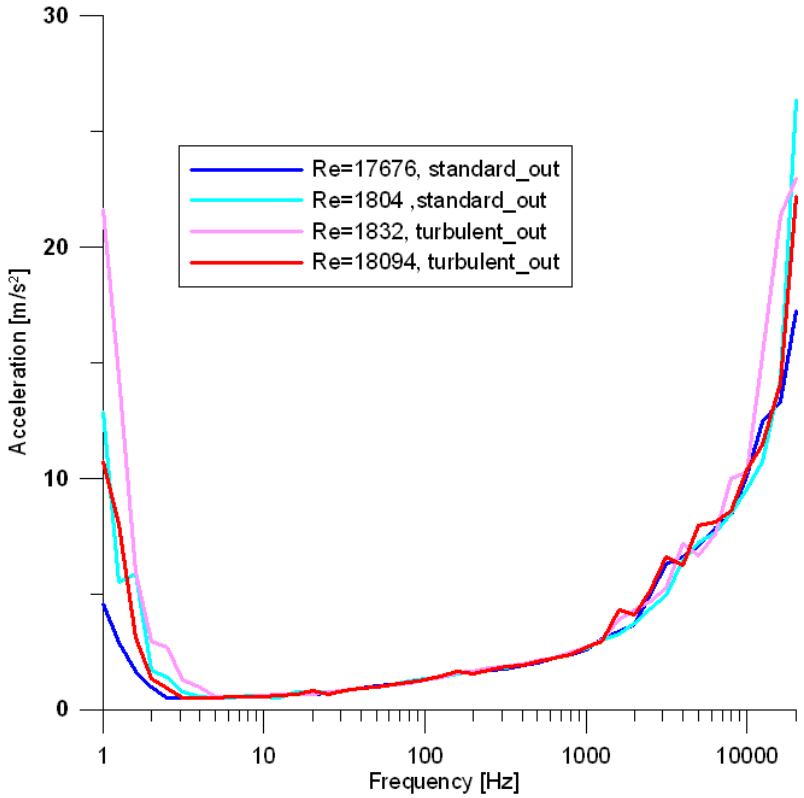

Figure 4.19: Comparison of vibration measurements with different Reynolds number

Figure 4.20 shows measurements of assumed turbulent flow (Re above 2300), and Figure 4.21 shows measurements of assumed laminar flow (Re below 2300). Both collectors as well as the in- and out-going pipe are represented by curves in the diagrams. There are larger vibrations in the out-going pipe than in the in-going.

Measurements of the vibration of the pump are shown in Figure 4.22 together with measurements from the turbo collector including both the in- and out-going pipe. The curve representing the pump seems to be close to that of the out-going pipe than the in-going pipe until large frequencies where the pump seems to have large mechanical vibrations.

Also, from the graphs in Appendix G, a larger variation in the measurements from the turbo collector compared to the standard collector, is shown.

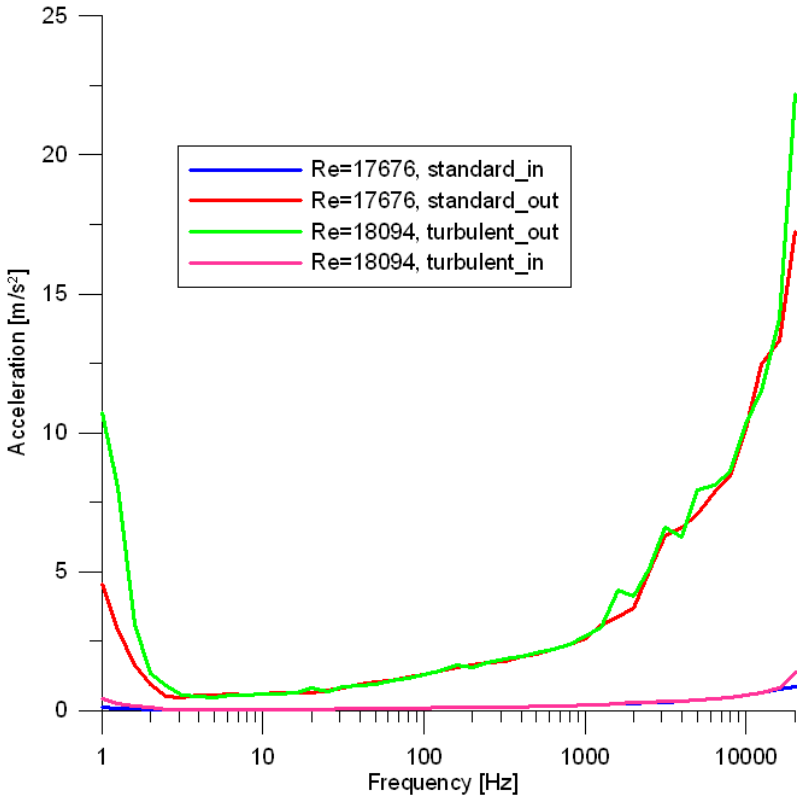

Figure 4.20: Comparison of all vibration measurements at assumed turbulent flow

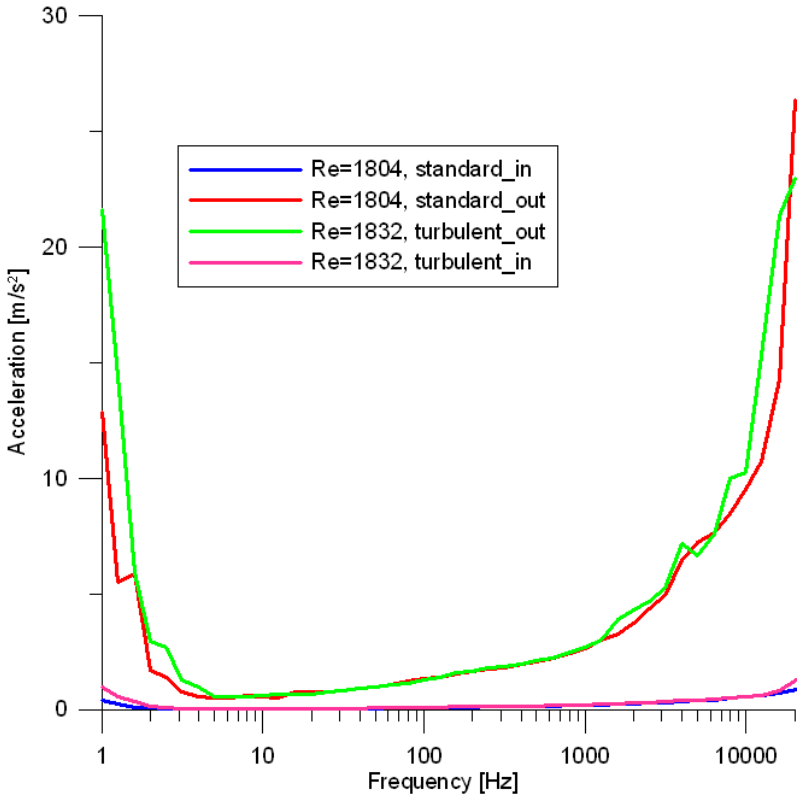

Figure 4.21: Comparison of all vibration measurements at assumed laminar flow

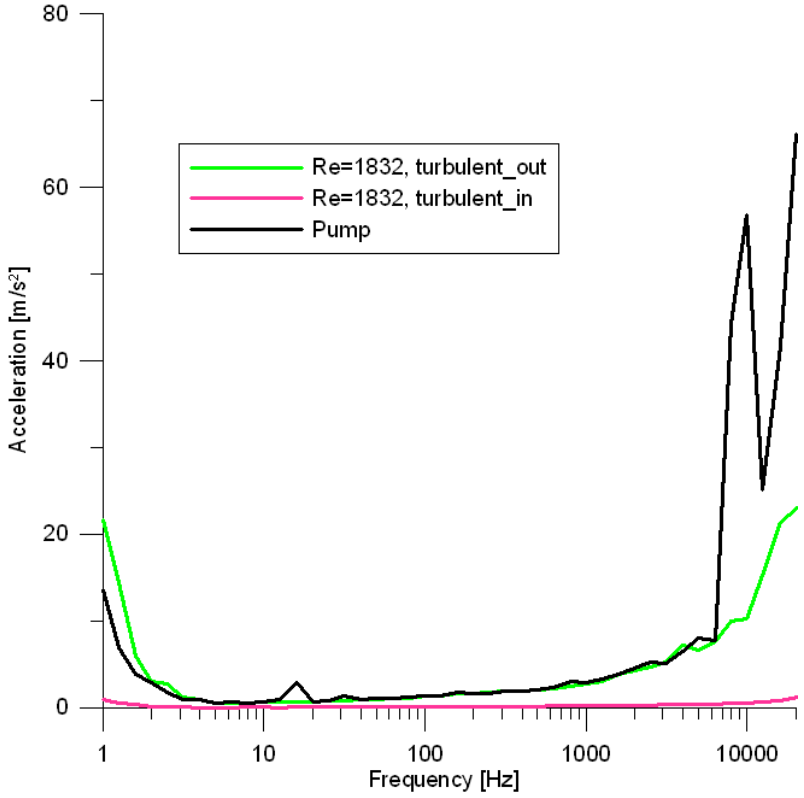

Figure 4.22: Vibration measurements of the pump compared to measurements of the pipe

Chapter 5

Simulation

Simulation of the temperature development of the planned BTES at Mære was used to investigate the sustainability of the BTES. In addition, simulations of the required borehole length was conducted to compare how much the thermal conductivity derived from different sources affects the total cost of the BTES. By comparing the total cost of the BTES based on the thermal conductivity obtained from generic values, laboratory testing and *in situ* field tests, it is possible to find which method is most profitable in terms of optimizing the BTES. It is costly to oversize the BTES, however, it also costly to undersize it as this leads to extra costs when the BTES is under operation.

5.1 The program and assumptions

Simulation of the borehole performance was completed in Earth Energy Designer, a program used for BHE design (Eskilson et al., 2000). Details concerning the software can be found in Appendix C. As planned in the project at Mære, the BTES was modeled with 12 wells, all having a depth of 150 m. As the projected DTES is rather complex, results from simulations performed by NIVA are used as input parameters in this simulation for the base load in the BTES. These are not real values, but valid estimations of cooling and heating loads based on climatic data and energy data for the greenhouse. Regarding peak load, a short-term storage tank is used to distribute the heat acquired during summer equally through the day, thus including the peak load in the base load. During the winter, the heat pump is run at full capacity, and peak load is supplied from a gas-stove. A complete list of the design data can be found in Appendix H. The base-load data are portrayed in Table 5.1.

The generic value being used for thermal conductivty was 2.0 $\mathrm{W/(m \cdot K)}$, as this is the average value for mica schist, the rock most prominent in the geological mapping of the area. The value for thermal conductivity found by laboratory testing was 3.0 $\mathrm{W/(m \cdot K)}$, and for the *in situ* field test a value of 4.0 $\mathrm{W/(m \cdot K)}$ was used. This was the result of the second TRT, being less influenced by varying temperatures.

In the simulation performed by NIVA, climatic data for 2009 was used, leading to unexpected values in the simulations. Also factors regarding the greenhouse affect the results of the simulations:

- **Climatic data from 2009**. The results from the simulations show that October and November require the same heating capacity. In 2009, October was colder than normal and November milder, leading to unexpected results from the simulations.
- **DTES not in the model**. The short-term storage tank is not yet accounted for in the simulations. The DTES will most likely give a more efficient storage of heat e.g.

Table 5.1: Simulation data from NIVA for base-load heating and cooling

Month	$BTES\_out$ [kWh]	$BTES\_in$ [kWh]
January	21748.5	16.5
February	28748.6	1.0
March	26019.6	2.3
April	12764.1	7986.0
May	4876.8	23901.1
June	3262.6	27877.7
July	0	23942.2
August	166.6	26971.7
September	2977.9	21973.9
October	21250.0	5.4
November	21502.5	40.8
December	29651.1	0.5
The whole year (2009)	172968.4	132719.1

by loading the boreholes by night.

- **Greenhouse empty in January and July**. It is assumed that no plants are growing in the greenhouse in January and July, and less heat is needed these months.
- **Heat storage in winter.** Due to the fact that there is no heat storage in January, the average temperature in the greenhouse is less and excess heat from the outside air (if $T > 2°C$) is used to load the boreholes.

The simulations are being improved at the moment, and will be used to master the DTES at Mære.

5.2 Results

The results from simulating different thermal conductivities can be found in Table 5.2 and Table 5.3, having a heat capacity of 2.2 $\text{MJ}/(\text{K} \cdot \text{m}^3)$ (mica schist) and 2.6 $\text{MJ}/(\text{K} \cdot \text{m}^3)$(amphibolite), respectively.

Table 5.2: Results of the simulation with a heat capacity of 2.2 $\text{MJ}/(\text{K} \cdot \text{m}^3)$

	2 $\text{W}/(\text{m} \cdot \text{K})$	3 $\text{W}/(\text{m} \cdot \text{K})$	4 $\text{W}/(\text{m} \cdot \text{K})$
Borehole length [m]	240.3	142.9	110.1
Price per borehole [kr]	48788	31402	25548
Price 12 boreholes [kr]	672310	429685	341935

Table 5.3: Results of the simulation with a heat capacity of 2.6 $\text{MJ}/(\text{K} \cdot \text{m}^3)$

	2 $\text{W}/(\text{m} \cdot \text{K})$	3 $\text{W}/(\text{m} \cdot \text{K})$	4 $\text{W}/(\text{m} \cdot \text{K})$
Borehole length [m]	229.6	135.6	107.5
Price per borehole [kr]	46878	30099	25084
Price 12 boreholes [kr]	644956	408695	331580

The development of the temperature over a period of 25 years was also simulated with a conservative value of 3.0 $\text{W}/(\text{m} \cdot \text{K})$ for the thermal conductivity and a heat storage capacity of 2.2 $\text{MJ}/(\text{K} \cdot \text{m}^3)$ (mica schist). The minimum and maximum temperatures over 25 years is plotted in Figure 5.1. The resulting temperature of the fluid in the BHE after 25 years of BTES is presented in Figure 5.2.

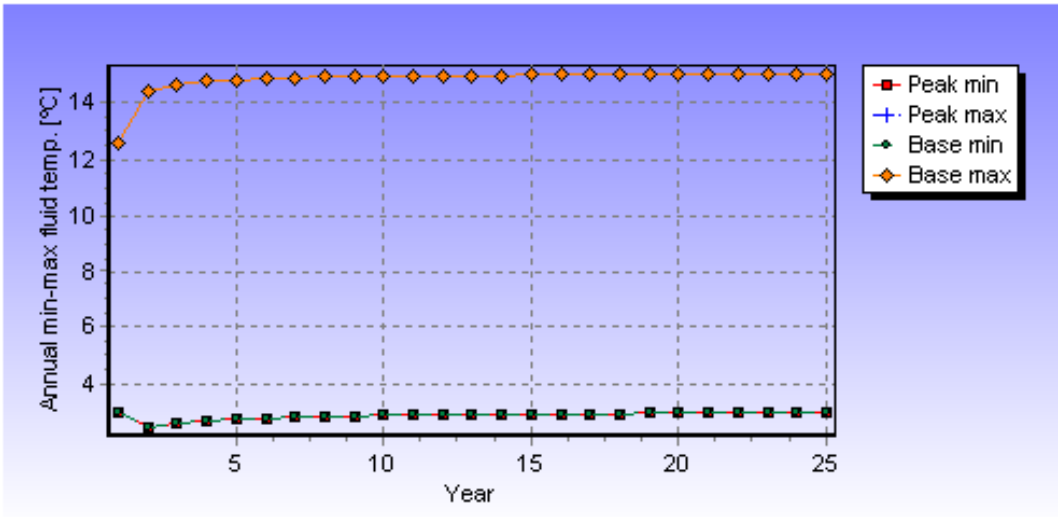

Figure 5.1: Minimum and maximum temperatures over 25 years

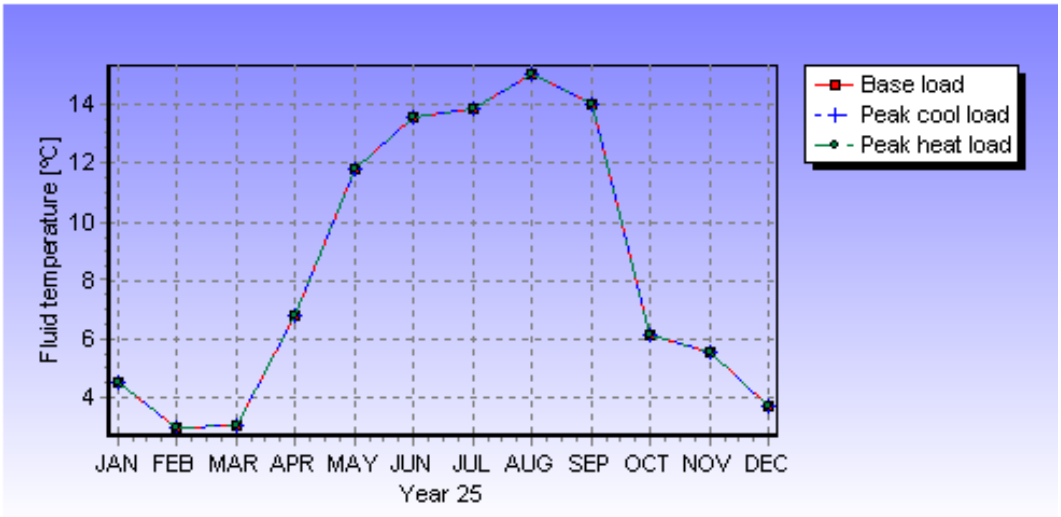

Figure 5.2: Fluid temperature after 25 years of BTES

Chapter 6

Discussion

The discussion relates the results from fieldwork and laboratory work to theoretical considerations. Uncertainties and errors are also discussed.

6.1 Geology

6.1.1 Geological conditions

Mica schist and amphibolite were found during geological mapping, as suggested by the regional geology of this area. However, the low numbers of outcrops makes it difficult to predict the exact geology at the location of the well.

Folding was observed, as the presence of small folds suggests the presence of larger folds (Fossen and Gabrielsen, 2005). This correlates well with the expected behavior of "Trondheimsfeltet", being transported by thrusting and thus creating large folds and fracture zones (Løset, 2006). Fractures may also be caused by pressure release from eroded material or ice from the last glaciation. Observations at the outcrops of fractures being parallel to the foliation suggest that these fractures have the latter origin. The stereoplot shows three different fracture sets with strike/dip directions of 132/36.6 °SW, 30.7/66.3°SE and 70.9/28.8°NW, where the first (and largest) group corresponds well with the foliation suggested by the geological map of the area (Roberts, 2010). Although the number of measured fractures in this case is too low to be sure to have covered all fracture sets (few outcrops available), it does suggest that fractures represents geological structures one should be aware of when drilling wells. As the main foliation measured at the fieldsite corresponds with the value derived from the geological map, it is likely that fractures are present at the site of the BTES has a dip of 35-55 ° in the southwest direction. The first well to be drilled was not completed due to fractures, so fractures are present close to the greenhouse and represents a complicating factor in the making of a BTES.

6.1.2 Mineralogy and thermal conductivity by laboratory analysis

The mineralogy was investigated both by XRD and DTA. XRD indicated the presence of the minerals albite, chlorite, microcline, quartz, mica, hornblende, calcite and dolomite. Because of the schistous structure of the rocks and the presence of mica and quartz they were classified as mica schists. One of the samples contained less quartz and more amphibole and was thus classified as an amphibolite. Even though XRD is only semi-quantitative, it does find the mineral present in the sample and makes a relative comparison possible between the samples as the same analyzing model is used for all.

The quartz content measured with DTA has a lower detection limit of 1 % and values within ± 5 % (Hagen, 2010). Compared with the XRD meaurements they are much more accurate. Since the difference between XRD-measurements and DTA for quartz is in the range 4-32% less for DTA than XRD and varying in the same manner, the DTA verifies, to a certain extent, the reliability of the XRD measurements.

The thermal conductivity measured in lab shows an average of 3.0 ± 0.5 $W/(m \cdot K)$, calculated for 65 samples. This is above average for mica schist (2.0 $W/(m \cdot K)$), but almost the same as for amphibolite. The calibration samples showed a standard deviation of 8.3 %, close to the 10 % accuracy NGU uses for thermal conductivity measurements, where as the standard deviation for all field samples, given in percentage, is close to 20 %. The large difference in the standard deviation for the field samples and the calibration samples indicates that there are other parameters than the uncertainty of the measurements that affect the variation in the field samples. The standard deviation for samples measured in normal and parallel direction to the foliaton is close to 10 %, indicating that the orientation has a large influence on the variation of the samples.

The difference between the samples measured in normal and parallel directions is 0.9 $W/(m \cdot K)$, a close 30 % difference from 2.5 $W/(m \cdot K)$ for the normal samples and 3.4 $W/(m \cdot K)$ for the parallel samples. Consequently, there is a large anisotropy in the rock concerning it's thermal conductivity. The reason for this might be quartz ores leading heat as quartz has a high thermal conductivity relative to other minerals. By investigating the relationship between the quartz content and averaged thermal conductivity for each sample, a linear relation was found with a R-squared of 0.6 telling us that 60 % of the variation in thermal conductivity might be explained by the quartz-content. The variation in the averaged thermal conductivity, however, is rather small as it varies from approximately 2.9-3.2 $W/(m \cdot K)$ while the quartz-content varies from 3-47 %. When comparing the quartz content against the averaged thermal conductivites for the two different orientations, no significant relation is found. Thus, it seems like the orientation of the rock has a greater importance than the actual quartz-content for this specific rock.

As the average value for thermal conductivity in the core samples is much higher than the literature value for mica schist, it might be the presence of quartz in ores and not in individual lenses that accounts for the difference. Heat is transported at a higher rate along ores with higher thermal conductivity than the surrounding rock. Also, the precipitation of quartz in 'pressure-shadows' is common in metamorphized rocks (Fossen and Gabrielsen, 2005). A phenomenon called quartz-rodding, common in mica schists, lead to a streaked appearance of quartz aggregates. The rods and pressure-shadows lead to enhanced heat transfer in the direction of the mineral lineation. Thus, quartz lead to a greater thermal conductivity both present in ores parallel to the foliation and in the direction of the mineral lineation.

6.1.3 Groundwater movement

The groundwater movement was investigated by measuring a temperature profile of the well before the TRT's and a temperature profile after the TRT's. Unfortunately, the measurements were not conducted at the same time after the TRT's. One of the assumptions to be fulfilled for comparison of ΔT profiles is that temperature measurements has to be measured exactly four hours after a TRT (Liebel et al., 2009). If not, the temperature recovery of the rock will be different for each test. Even though the ΔT temperature profiles does not fulfill one assumption for comparisons of temperature profiles, the general characteristics of the profiles can still be compared.

The difference between the temperature before and after the test (ΔT) is largest if the thermal conductivity is poor, e.g. the temperature cannot recover as fast as if the thermal conductivity is high. Thus, groundwater movement can be seen when there is a deviation

in the temperature difference (less). The thermal conductivity increases if groundwater is present and the added heat is therefore transported at a faster rate. At Mære, neither of the temperature profiles measured after the TRT's show such deviations. The presence of large groundwater movements is therefore unlikely, especially considering the observations made during drilling of the well seeing that it was extraordinary dry.

6.2 Thermal properties of the fieldsite

6.2.1 Thermal response test

Both TRT's were performed successfully even though there were large temperature variations in the temperature of the ambient air. Both results regarding the borehole thermal resistance and the thermal conductivity calculated in various ways are discussed here.

Thermal conductivity

The first TRT, completed for the turbo collector, showed an unusual high thermal conductivity of 4.8 $\mathrm{W/(m \cdot K)}$. The temperature of the ambient air increased by 20 °C from -15 °C to +5 °C. Observations were made suggesting that melting-water from ice of the casing of the borehole wall or the surrounding snow entered the well and caused the water-table to rise. The melting-water was colder than the water in the well, and most likely sunk due to a higher density than the heated water in the well. The colder water caused the temperature of the heat carrier fluid in the BHE to decrease. This would cause the expected temperature increase in the well (thermal response) to be less and the calculated thermal conductivity to increase. There is a correlation between the time where ambient air temperature reached 0 °C causing melting and the time where the calculated thermal conductivity over time had a sharp increase. Therefore, the melting water seems to have had a large influence on the calculated thermal conductivity, by overestimating it. The more accurate estimate for the thermal conductivity in TRT 1 is to use the thermal conductivity calculated over time. The thermal conductivity attained right before the sharp increase suggests a value of 4.2 $\mathrm{W/(m \cdot K)}$.

TRT 2, using the standard collector, did not have the complicating factor with melting water entering the well. Here, a thermal conductivity of 4.0 $\mathrm{W/(m \cdot K)}$ was found, using standard calculations. This was verified by the thermal conductivity calculated over time, achieving approximately the same value when the thermal conductivity was stabilized. The value of about 4.0 $\mathrm{W/(m \cdot K)}$ is therefore the most reliable value for the thermal conductivity when comparing the two TRT's.

The thermal conductivity was also calculated for various depths, chosen because they represent different geological sections of the borehole. In general, the values calculated at 40 and 101 m depth, representing hard rock sections, were more realistic than λ_S for TRT 1, and similar to the results from TRT 2. The temperature development over time at 40 m does not show a strong influence from the melting water, supporting the theory about cold water sinking down in the well. However, at 101 m depth there is no large influence of melting water to be seen in the temperature development, suggesting that the cold water has increasingly heated up during it's journey down the well, not reaching a depth of 101 m. Another interesting feature is that the thermal conductivities at 43 m are slightly lower than λ_S, suggesting that this section of the borehole represents a rock with a lower thermal conductivity than in the averaged borehole.

The depths representing thrust zones, 73 and 93 m, show more deviating values for thermal conductivity. At 73 m depth, the value for TRT 2 seems reliable as it is close to λ_S. The result from TRT 1 is also close to λ_S, and thus likely to have been influenced by melting

water as λ_S for TRT 1 was. The results at 93 m depth show extremely high values for the thermal conductivity calculated for TRT 1, at approximately 42.0 $W/(m \cdot K)$ which is not realistic. Looking at the temperature development, the temperature is stable from about 23 hours to 70 hours, which is actually before the ambient air reached 0 degrees at 60 hours after the start of the TRT. Also the value measured for TRT 2 is rather large compared with the other measurements during this test, at 5.0 $W/(m \cdot K)$. This suggest that other parameters than only the melting water accounts for the unusual high thermal conductivity measured at 93 m. It could be due to the presence of a quartz-ore, but this is hard to validate as the only geological feature known to be present is a thrust zone. As a concluding remark, the thermal conductivity calculated at different depths has been a useful way of validating and comparing the results from the standard TRT.

Comparing the effective thermal conductivity with the rock core sample data, there is a 25 % difference in favour of the value derived from the TRT. As already noted in the theoretical chapter, this is a common phenomenon, and might be explained by vertical movement of water due to convection or thermosiphon effects (Gehlin and Hellström, 2003). At this site, groundwater flow has not shown to be present and affect the effective thermal conductivity. The rock core samples may not represent the rock actually present at the well, ecpecially as this landscape has a complex and varying geology. As observed in the field, large quartz ores are present in the area and could lead to an enhanced thermal conductivity in sections of the well. The mineral lineation indicated at Mære in the geological map (Roberts, 2010), has a dip of 20-55 ° to the west. The orientation of the well in relation to the mineral lineation of the rock might therefore contribute to the effective thermal conductivity. However, the large difference in thermal conductivity between the TRT's and laboratory tests cannot be explained by geological variation alone. Therefore, when dimensioning the BTES, a conservative value should be used, preferably the lowest value measured during the TRT's.

Borehole thermal resistance

The calculated borehole thermal resistance for the two BHE's were the same (0.07 $(K \cdot m)/W$), despite the expected result where the turbo collector should have shown a slightly lower thermal resistance. One reason could be that the turbo collector and the standard collector actually have the same properties for thermal resistance. Another explanation is that the curve-fitting analysis is not sensitive enough to find small differences. Gehlin (1998) has found that that thermal resistance values derived from TRT's varies with less than ± 10 %, which is ± 0.007 $(K \cdot m)/W$ for the results from Mære. A better curve-fitting analysis tool would be a significant improvement to the method of estimating the borehole thermal resistance.

The thermal resistance is dependent both upon the power-load and the undisturbed ground temperature. The power load was consistent during both TRT's, and did not pose a significant source of error. The undisturbed ground temperature was measured before each TRT using the same method, indicating a 0.07 °C higher temperature before TRT 2. This could be due to the ground not being properly recovered even though there were 14 days between the measurements, or purely uncertainties in the loggers. Still, the temperature difference was not shown to alter the results of the calculations. Consequently, the difference in borehole thermal resistance by the two collectors is not shown to be significant in this field experiment.

6.2.2 Temperature profiles

Undisturbed temperature profile

The temperature profiles measured before the TRT's show similar features for both tests. The most pronounced feature is the rather rapid increase in temperature from 5-10 meter,

followed by a rapid decrease down to 30 m. This can be explained by heat from the greenhouse, influencing the temperature profile down to 10 m. However, the greenhouse is only two years old. Other sources of heat might be the parking lot or barn close to the test-well.

The profile measured right before TRT 2 shows a slightly higher temperature than before TRT 1, indicating that the recovery has not been fully completed. The temperature at 4 m depth was 0.25 °C higher before the TRT 1 than TRT 2, which is unexpected as the ambient air temperature was higher before the second test. It could be explained by seasonal lag in the ground, as the date of the minimum temperature of the ground is delayed until after the minimum temperature of the ambient air. This phenomenon is caused by the slow propagation of heat and cold through the ground. The undisturbed ground temperature, averaged for the whole borehole, was7.0 °C before TRT 1 and 7.1 °C before TRT 2.

Geothermal gradient

The thermal gradients calculated before the two TRT's also show similar features. The gradient is negative until about 45 m due to heat from the greenhouse. After about 60 m it stabilizes at $14.7 \pm 3.0\,°C/km$ for TRT 1 and $12.0 \pm 3.2\,°C/km$ for TRT 2, a variation that lies within the standard deviation of the results. The geothermal gradient is known to vary considerably between sites (Liebel et al., 2009), and the value attained in this fieldwork is realistic for this this rock.

Heat flow

As for the geothermal gradient, the heat flow is influenced by local factors such as the nearby buildings, surface temperature and so forth down to a threshold value of approximately 60 m. Below this value, the heat flow is positive towards the surface. However, it might be affected by paleoclimatic conditions. As the last glaciation covered the whole of this area it is not likely that local differences at the fieldsite are present.

Heat flow calculated for the temperature profiles measured after the TRT's show slightly different characteristics, but it has to be kept in mind that the profile after TRT 2 was given one more hour to recover. This is evident at the depth of 20 m where the standard collector has recovered to it's initial heat flow while the turbo collector is still recovering.

6.2.3 Simulation

The minimum and maximum temperatures over 25 years illustrates that the planned system at Mære is stable over time. The temperatures reaches a steady state after 5 years, and the minimum temperature is never below 0 °C which is the freezing point of the ground and should be avoided. The maximum temperature is never above 15 °C, which is the limit of when to use direct cooling in a building (Midttømme, 2010). The fluid temperatures during the 25th year of the BTES are within the recommended values, and show that the system is sustainable. Even though there are large uncertainties regarding the assumed base-loads, input-parameters and EED itself, the simulation using conservative input-values justifies the long-term sustainability of the system.

By comparing the simulations based on different thermal conductivities, it was found that the use of only generic values in the design process of this BTES is particularly costly. The required borehole length is larger than for values revealed by laboratory tests and TRT's. Considering the most conservative value of specific heat storage, the simulated required borehole length using values for λ attained from generic values and laboratory tests gives a difference in the total cost of 242 625 kr in favor of laboratory tests. The total required borehole length for all 12 boreholes is 1.1 km longer by using generic values compared with values from samples measured in the laboratory. The cost reduction by using a TRT

compared with laboratory values is less, but still significant with 87 750 kr. The difference in the total required borehole length is 0.4 km in favor of the TRT. A TRT costs approximately 96 000 kr (Grandetrø, 2010) and measuring one core-sample at NGU costs 450 kr. For large installations with several wells like the BTES at Mære, it is therefore recommended to use laboratory tests with core-samples from the site or preferably TRT's. If groundwater is present at the site, the difference between the thermal conductivity measured by laboratory and *in situ* tests is likely to be even larger. Even considering single wells with similar thermogeology as Mære, it is justified economically to test core-samples from the site in order to gain more precise knowledge of the thermogeology. If the generic values were to underestimate the thermal conductivity, it could be even more costly to use these values as an undersized BTES leads to increased investment costs.

The results with different heat capacities show that changing this parameter has a rather small influence on the resulting cost. The required borehole depth for one well is maximum 11 m larger for the conservative value of the heat capacity and the lowest value for thermal conductivity. This results in an extra cost of approximately 27 000 kr for 12 boreholes. However, this is a rather small difference compared with changing the values of thermal conductivities. It is therefore recommended to use conservative values for specific heat capacities.

6.3 Flow conditions

6.3.1 Pressure drop

During the flow measurements, the differences between the two BHE's were investigated. In the first test, only volumetric flows with Reynolds numbers above 17000 were used, thus obtaining a turbulent flow. No difference between the collectors were noted. This validates previous tests where no difference is seen above a Reynolds number of 9000. When comparing the calculated experimental values for friction factor with the theoretical values, the friction factor determined experimentally is slightly higher, but following the same trend. This is expected as the theoretical friction factor does not account for the 180° bend at the bottom of the U-pipe. It also validates the measurements as they are in the expected range and behaves like predicted by theory.

The second set of tests operated with Reynolds number down to 1800, thus expecting laminar flow at low volumetric flows and also lower friction numbers for the turbo collector as observed in previous experiments (Acuña and Palm, 2008a). The results actually show the opposite, where the standard collector has lower pressure drop and lower friction factor than the turbo collector. When comparing experimental values for the friction factor with theoretical values, it is clear that that the measurements for the turbo collector for $1830 < Re < 2150$ (expected laminar flow) deviates. Here, the measured experimental values are between 80-95 % higher than the predicted values, as opposed to the measurements with Re>2150 that seem to cluster around values that are 30 % higher than predicted.

One reason could be that turbulent flow has already occurred at these Reynolds numbers and thus showing deviating results when compared to theoretical calculations. However, even when applying the turbulent formulas for all measurements they still have anomalously high friction factors compared with theoretical values. Another explanation being proposed is that the turbo collector is damaged at some place along the pipe, causing a larger pressure drop. It was noted before the second test that it was not possible to lower the temperature logger in the standard collector below 92 m. However, a deviating pressure drop would then be expected to be measured at all volumetric flows, not only the lower ones. Also, the antifreeze polluting the water in the BHE's may have increased the viscosity of the fluid thus leading to lower Reynolds numbers. The calculation of the experimental friction factor does not impart viscosity and the values are still anomalously high. If one assumes the

measurements to be correct, one explanation could be that the helix shape of the pipe leads to high pressure drops when the water in a laminar flow is forced through the 180 degree bend. At the onset of turbulence, the water may no longer be forced to follow the helix shape, leading to a lower pressure drop. Nonetheless, the results are surprising, and it is a reason to study the turbo collector further.

When studying the results in Figure 4.17, where the "non-deviating" results from the second test is presented, it is evident that the values representing turbulent flow follow a similar pattern. The relationship between the experimental friction factor and the predicted is the same, suggesting that the experimental values are reliable. The values representing suspected laminar flow and transition flow are distributed more randomly. After a Reynolds number of 4000, both values from the standard collector and turbo collector show about the same relationship between theoretical and experimental values, even though the turbo collector still shows a higher pressure drop up to about Re=10 000.

6.3.2 Vibration analysis

The vibration data was difficult to analyze as there were large amounts of data, and restrictions concerning the resolution of the frequency from the equipment. However, some cautious interpretations might be done with the guidance of Frode Haukland at SINTEF, an engineer in this field (Haukland, 2010).

Mechanical vibration is detected 90 degrees on the flow. Therefore, as laminar flow is parallel to the pipe, less mechanical vibration is expected. The working hypothesis was that turbulence characterized by random movements would lead to more mechanical vibration and thus indicate the transition from laminar to turbulent flow.

It was hard to detect the transfer from laminar to turbulent flow from these recordings. This might be due to noise from the pipe and the environment, as the vibrations from the pump will influence the recordings to a much higher degree than the onset of turbulence. It was visually observed that vibrations from the pump were affecting the pipes. Also, if the flow transfer is related to a certain area of frequencies, the resolution in frequency of the real-time analyzer might have been to low to detect the changes in mechanical vibration. There was a frequency resolution of 40 Hz near the rotational speed of the pump, and a resolution of 250 Hz at 1000 Hz, suggesting that the frequency resolution might have been too low. Another possibility is that the flow was turbulent from the start, and hence no change in vibrations should occur.

There are, however, three features evident from the recordings. First of all, there is a large difference between the recordings from the in-going and out-going pipe. This might be due to the pipe being more or less influenced by the pump. The pump was seen to have vibrations on high frequencies (9-10000 rpm). The curves showing the vibration for the out-going pipe was quite similar to the curve for the pump, suggesting that the out-going pipe was more affected by vibrations from the pump than the in-going pipe. Another explanation is that the calibration of the nodes were not conducted properly (Haukland, 2010). If this is the case, the results are still usable as the the same accelerometers are being compared. The second feature is the turbo collector showing a higher degree of mechanical vibration than the standard collector. One explanation is that the presence of fins is causing more radial flow than without. Thirdly, the results from the turbo collector portrays a larger variation between the recordings than the standard collector. No explanation has been found for the latter point.

It should be possible to measure the onset of turbulence in the in-going and out-going pipe, however, this requires more sensitive equipment and a thorough frequency analysis using other equipment.

Chapter 7

Conclusions

The main practical goals of this master's thesis was to gain geological and thermogeological knowledge within the rock mass and to test properties of a new type of BHE, the turbo collector, in comparison with a standard collector. These goals are accounted for by summarizing the geological parameters affecting the heat extraction and making a relative comparison between the two BHE's with regard to flow conditions.

7.1 Geological parameters affecting the heat extraction

Only the parameters identified as most important in this particular case are listed here.

7.1.1 Geological conditions

- **Groundwater**. At Mære, no significant amount of groundwater flow has been proven by measurements or observed during drilling. One may therefore assume that groundwater flow will not affect the heat storage in the ground, and does not have to be accounted for in the dimensioning process.
- **Fractures**. Fractures in and around the area of the planned thermal storage at Mære have been observed, and are likely to appear at the fieldsite having a dip of 35-55 ° in the southwest direction. The fractures have not proven to lead a large amount of groundwater at the test well, although they could pose problems in other wells. It is necessary to account for some extra costs related to drilling.
- **Anisotropy**. There are large anisotropies concerning thermal conductivity in the rock-samples at Mære. Measurements conducted parallel to the foliation show values 25 % higher than those conducted normal to the foliation.
- **Quartz-content**. The quartz-content in the rock-samples at Mære show large variations, and there is a correlation between the averaged thermal conductivity and the quartz-content. However, it is most likely the orientation of quartz ores that affect the thermal conductivity the most.

7.1.2 Thermogeology

- **Thermal conductivity**. The thermal conductivity by generic values is estimated from literature as 2.0 $\mathrm{W/(m \cdot K)}$ (mica schist), from laboratory measurements as 3.0 $\mathrm{W/(m \cdot K)}$ and from the TRT's as 4.0 $\mathrm{W/(m \cdot K)}$. The TRT is the more accurate

method, and a conservative value of approximately 3.7 $\mathrm{W/(m \cdot K)}$ is recommended as an input parameter for the design of the BTES, being the lowest value measured *in situ* .

- **Borehole thermal resistance**. The borehole thermal resistance is calculated from the field-tests, and the recommended value is 0.07 $\mathrm{K \cdot m/W}$.
- **Volumetric heat capacity**. The recommended volumetric heat capacity for mica schist is 2.2 $\mathrm{MJ/(m^3 \cdot K)}$.

The fieldwork illustrates how winter conditions may alter the results from the TRT significantly. Therefore, it is not recommended to perform TRT's when the likelihood of experiencing large temperature variations and melting water is present. However, by using temperature loggers at different depths in the borehole, this problem might be overcome. Economically, simulations have shown by calculating the required borehole length for different thermal conductivities that it is not recommended to use generic values only. The thermal conductivity and borehole thermal resistance of this fieldsite allows for a sustainable use of the planned BTES.

7.2 Comparison of two borehole heat exchangers with regard to flow conditions

The TRT did not show any difference in the borehole thermal resistance between the two collectors. This is either because the collectors share the same borehole thermal resistance when subjected to the same conditions, or because the equipment and curve-fitting methods are not sensitive enough to find the differences. Above a Reynolds number of 10 000, the calculated friction factor showed no difference between the collectors. At lower Reynolds numbers, the standard collector had a lower friction factor than the turbo collector, thus being the better option (regarding pressure drop) since the required pumping power for the fluid would be slightly lower for this collector. However, more tests are required to verify this result showing the opposite features than previous tests. To find the most energy efficient BHE, also heat transfer properties must be tested. With regard to the vibration data, the turbo collector showed a higher degree of mechanical vibrations, possibly due to more radial flow. It was not possible to detect the transition from laminar to turbulent flow from the vibration data nor the flow tests. Further experiments must be done to find how the flow can be altered to optimize energy gain.

Chapter 8

Suggestions of Further Work

With regard to the geological conditions of the field-site, it would be of interest to have data from an optical televiewer including information about the dip, strike, frequency and fracture aperture. This would be useful in terms of evaluating the temperature development at different depths, as well as returning information of possible groundwater presence through fractures and the direction towards the foliation of the rock. In accordance, optical fiber cables that examine the temperature distribution along the entire cable length could be used to calculate the thermal conductivity along the whole borehole and compare it with the results from the optical televiewer.

The surprising results regarding low pressure drop for the standard collector should be further investigated in field tests with similar conditions and Reynolds numbers less than 10 000. To further analyze the flow conditions, it would be of interest to use a transparent pipe with the characteristics of the turbo collector, to visualize the fluid by adding ink. As suggested by Acuña (2010), one could in this way perhaps observe flow patterns and the transitions between laminar and turbulent flow. Another option is to use particle image velocimetry (PIV), which is an optical method for fluid visualization. In PIV, the fluid is seeded with tracers particles and the motion of these particles is used to calculate velocity information of the flow. Following, a detailed vibration analysis should be conducted by professionals in this field. Analysis should be done to find which frequencies the pipe will vibrate at for laminar and turbulent flow. Next, measurements should be performed with a logging frequency 4 times larger than the highest relevant frequency to be able to assess the vibrations in a frequency spectrum with fast Fourier transform (Seim, 2010).

Bibliography

ABK. Ny 'Turbulence'-type energikollektor for grunnvarmepumper. Reklamemateriell, 2009.

Accio. Effektivare geoenergisystem med ny kollektor. `http://www.geocalc.accio.se/index.php?option=com_content&view=article&id=75&Itemid=70` Cited:02.05.2010, 2010.

J. Acuña. Personal comment per mail correspondence, March 2010.

J. Acuña and B. Palm. Experimental comparison of four borehole heat exchangers. In *8th Gustav Lorentzen Conference on Natural Working Fluids, Copenhagen*, 2008a.

J. Acuña and B. Palm. Characterization of boreholes - results from U-pipe borehole heat exchanger installation. In *9th International IEA Heat Pump Conference*, 2008b.

ASHRAE. Methods for determining soil and rock formation thermal properties from field tests. Technical report, American Society of Heating, Refrigerating and Air-Conditioning Engineers, 2002.

W. A. Austin. Development of an in situ system for measuring ground thermal properties. Master's thesis, Oklahoma State University, 1998.

D. Banks. *An Introduction to Thermogeology : ground source heating and cooling.* Oxford : Blackwell Publ., 1st edition, 2008.

S. Beck and R. Collins. Moody Diagram. `http://upload.wikimedia.org/wikipedia/commons/8/80/Moody_diagram.jpg` Cited:10.05.2010, 2008.

D. D. Blackwell, J. L. Steele, and C. A. Brott. The terrain effect on terrestrial heal flow. *Journal of Geophysical Research*, 85(1):4757–4772, 1980.

E. Brekke. Energiuttak fra fjell : Et studium av data fra termisk responstesting. Master's thesis, Norwegian University of Science and Technology, 2003.

H.S. Carslaw and J.C. Jaeger. *Conduction of heat in solids.* Oxford University Press Inc., 2nd edition, 1959.

A. D. Chiasson, S. J. Rees, and J. D. Spitler. Preliminary assessment of the effects of groundwater flow on closed-loop ground-source heat pump systems. In *2000 ASHRAE Winter Meeting*, 2000.

J. Claesson and P. Eskilson. *Conductive heat extraction by a deep borehole: analytical studies.* University of Lund, Departement of Mathematical Physics, 1987. Doctoral dissertation.

J. Claesson and P. Eskilson. Conductive heat extraction by a deep borehole: thermal analysis and dimensioning rules. *Energy*, 13(6), 1988.

DLSC. Borehole thermal energy storage. http://www.dlsc.ca/borehole.html Cited:01.06.2010, 2005.

C. Eklöf and S. Gehlin. TED - a mobile equipment for thermal response test. Master's thesis, Luleå University of Technology, 1996.

L. O. Ericsson. Värmeutbyte mellan berggrund och borrhål vid bergvärmesystem. Technical report, Department of Geology, Chalmers University of Technology and University of Göteborg, 1985.

P. Eskilson. *Thermal analysis of heat extraction boreholes*. PhD thesis, University of Lund, 1987.

P. Eskilson, G. Hellström, J. Claesson, T. Blomberg, and B. Sanner. Earth Energy Designer version 2.0, software parameter database. Blocon software, Sweden, 2000.

H. Fossen and R. H. Gabrielsen. *Strukturgeologi*. Fagbokforlaget, Bergen, 1st edition, 2005.

S. Gehlin. Thermal response test - In situ measurements of thermal properties in hard rock. Luleå University of Technology, 1998. Licentiate thesis.

S. Gehlin. *Thermal response test. Method development and evaluation*. PhD thesis, Luleå University of Technology, 2002.

S. Gehlin and G. Hellström. Influence on thermal response test by groundwater flow in vertical fractures in hard rock. *Renewable Energy*, 28(1), 2003.

S. Gehlin, G. Hellström, and B. Nordell. The influence of the thermosiphon effect on the thermal response test. *Renewable Energy*, 28(1), 2003.

Gether. Prosjektbeskrivelse Mære Landbruksskole – senter for klimatiltak og fornybar energi i landbruksnæringa. http://www.ntfk.no/bibliotek/saker/2008/FR/Vedlegg/FR08108_1.htm Cited:12.04.2010, 2009.

Gether. Active dynamic thermal storage for industrial processes - Project description. By mail: harald.gether@ntnu.no, 2010.

K. Gether, H. Gether, H. Skarphagen, and J. Gether. Principles of saving energy with dynamic thermal energy storage. In *The European Council for an Energy Efficient Economy (ECEEE) 2009 Summer Study - Panel 7: Innovative buildings technologies*, 2009.

H. A. Grandetrø. Personal comment per phone, May 2010.

S. A. Hagen. Personal comment per mail correspondence, May 2010.

F. Hansson. Experimentel jämförelse av turbokollektor och slät energikollektor. Technical report, Accio AB, 2009.

K. Haraldseth. Characteristics of rock slides at Løsberga. Norwegian University of Science and Technology, 2009. TGB4500 Ingeniørgeologi og bergmekanikk, fordypningsprosjekt.

F. Haukland. Personal comment per mail, 2010. 10th of May.

G. Hellström. *Ground Heat Storage*. PhD thesis, University of Lund, 1991.

G. Hellström. Market and Technology in Sweden. http://www.kraac.or.kr/upload/board_techData/market\%20and\%20technology\%20in\%20sweden.pdf Cited:05.03.2010, 2006. Licentiate thesis.

IEA. *Renewable energy: RD and D priorities*. International Energy Agency, 2006.

L.R. Ingersoll, O.J. Zobel, and A.C. Ingersoll. *Heat conduction with engineering and geological application*. McGraw Hill, New York, 1st edition, 1948.

M. Kassabian. Ground source heat pumps : Analyzing the brine flow in boreholes, Mariehäll. Master's thesis, KTH School of Energy and Environmental Technology, 2007.

I. T. Kukkonen, W. D. Gosnold, and J. Šafanda. Anomalously low heat flow density in eastern Karelia, Baltic shield: a possible paleoclimatic signature. *Tectonophysics*, 291(1), 1998.

H. T. Liebel, K. Huber, B. Frengstad, R. K. Ramstad, and B. Brattli. Thermogeology in the Oslo region and Kristiansand - Results from thermal response tests with and without artificially induced groundwater flow. Technical report, Geological Survey of Norway and the Norwegian University of Science and Technology, 2009.

F. Løset. *Norges tunnelgeologi*. Norges Geotekniske Institutt, 1st edition, 2006.

J. W. Lund. Characteristics, development and utilization of geothermal resources. *Geo-Heat Center Quarterly Bulletin, Oregon*, 28(2), 2007.

J. W. Lund, B. Sanner, L. Rybach, R. Curtis, and G. Hellström. Geothermal (ground-source) heat pumps - a world overview. *Geo-Heat Center Quarterly Bulletin, Oregon*, 25 (3), 2004.

J. W. Lund, D. H. Freeston, and T. L. Boyd. Direct application of geothermal energy: 2005 worldwide review. *Geothermics*, 34(6):691–727, 2005.

B. Metz, O. R. Davidson, P. R. Bosch, R. Dave, and L. A. Meyer. Summary for policymakers. In: Climate change 2007: Mitigation. Contribution of working group 3 to the fourth assessment report of the intergovernmental panel on climate change. Technical report, IPCC, 2007.

M. F. Middleton. A transient method of measuring thermal properties of rocks. *Geophysics*, 58(3), 1993.

K. Midttømme. Temperaturgradienter, varmestrøm og radioaktiv energi i Osloområdet. Technical report, Geological Survey of Norway, 2000.

K. Midttømme. Norway's geothermal energy situation. In *Proceedings World Geothermal Congress 2005, Antalya, Turkey*, 2005.

K. Midttømme. Personal communication, May 2010.

K. Midttømme and A. Hauge. Geovarme - nytt fagområde, nye geofaglige utfordringer. Presentation for members in the Norwegian Geotechnical Society 26.10.2009, 2009. Midttømme can be contacted by mail: kirsti.midttomme@ngi.no.

K. Midttømme, D. Banks, R. K. Ramstad, O. M. Sæther, H. Skarphagen, and T. Slagstad. Ground-source heat pumps and underground thermal energy storage; Energy for the future. *Geology for society*, 11(1):93–98, 2008. The Geological Survey of Norway - Special publication.

P. Mogensen. Fluid to duct wall heat transfer in duct system heat storage. In *Proceedings of the International Conference on Surface Heat Storage in Theory and Practice, Stockholm, Sweden*, 1983.

NGU. Oversikt over løsmassene i Norge. `http://www.ngu.no/kart/losmasse/` Cited:06.04.2010, 2004.

M. T. Palomares. Thermal comparison of two borehole heat exchangers. Master's thesis, KTH School of Industrial Engineering and Management, 2008.

T. Prestvik. *Petrologi og geokjemi*. Vett & Viten, 1st edition, 2001.

I. B. Ramberg, I. Bryhni, and A. Nøttvedt, editors. *LANDET BLIR TIL - Norges geologi*. Norsk Geologisk Forening, 2nd edition, 2007.

R. K. Ramstad, H. Beer, K. Midttømme, J. Koziel, and B. Wissing. Thermal diffusivity measurement at NGU - Status and method development 2005-2008. Technical report, Geological Survey of Norway, 2008.

D. Roberts. Berggrunnskart STIKLESTAD 1722 IV, 1:50 000 forløpig utgave. Geological Survey of Norway, 2010.

R. F. Roy, D. D. Blackwell, and E. R. Decker. *Continental heat flow*, chapter 19, pages 506–544. McGraw Hill, New York, 1972.

K. Sand. Grunnvannstemperaturer i Finnmark. Technical report, Geological Survey of Norway, 1990.

B. Sanner. Shallow geothermal energy. *Geo-Heat Center Quarterly Bulletin, Oregon*, 22(2), 2001.

B. G. Seim. Personal comment per mail correspondence, May 2010.

S. Signorelli, S. Bassetti, D. Pahud, and T. Kohl. Numerical evaluation of thermal response test. *Geothermics*, 36(1):141–166, 2007.

R. E. H. Sims, R. N. Shock, A. Adegbululgbe, J. Fenhann, W. Moomaw I. Konstantinaviciute, H. B. Nimir, B. Schlamadinger, J. Torres-Martínez, C. Turner, Y. Uchiyama, S. J. V. Vuori, N. Wamukonya, and X. Zhang. Energy supply. In: Climate change 2007: Mitigation. Contribution of working group 3 to the fourth assesement report of the intergovernmental panel on climate change. Technical report, IPCC, 2007.

H. Skarphagen. Personal communication, May 2010.

T. Slagstad. Radiogenic heat production of Archean to Permian geological provinces in Norway. *Norwegian Journal of Geology*, 88(1), 2008.

T. Slagstad, N. Balling, H. Elvebakk, K. Midttømme, O. Olesen, L. Olsen, and C. Pascal. Heat-flow measurements in late Palaeoproterozoic to Permian geological provinces in south and central Norway and a new heat-flow map of Fennoscandia and the Norwegian-Greenland sea. *Tectonophysics - The International Journal of Integrated Solid Earth Sciences*, 473(1):341–361, 2009.

N. Stern. The Stern review report on the economics of climate change. Technical report, Cambridge University Press, UK, 2006.

H. Sveian. STIKLESTAD 1722 IV, Kvartærgeologisk kart - 1:50 000. Geological Survey of Norway, 1985.

UN. Copenhagen Accord. `http://unfccc.int/files/meetings/cop_15/application/pdf/cop15_cph_auv.pdf` Cited:03.03.2010, 2009. Advanced unedited version.

F. M. White. *Fluid Mechanics*. McGraw Hill, 5th edition, 2003.

Wikipedia. Typical single stage vapor compression refrigeration. `http://en.wikipedia.org/wiki/File:Refrigeration.png` Cited:05.04.2010, 2006.

Appendix A

Borehole Thermal Resistance

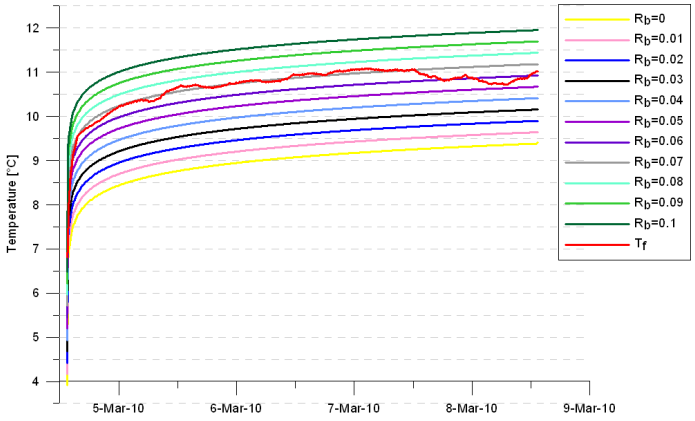

Figure A.1: Average fluid temperature in the collector (T_f) and borehole thermal resistance type curves [$(\mathrm{K} \cdot \mathrm{m})/\mathrm{W}$] during TRT 1, turbo collector

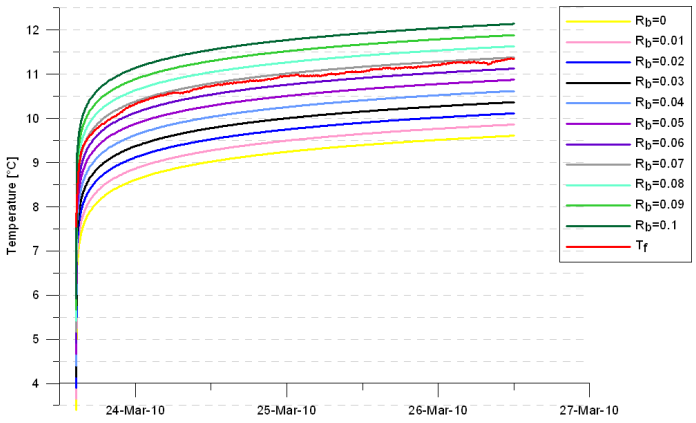

Figure A.2: Average fluid temperature in the collector (T_f) and borehole thermal resistance type curves [$(\mathrm{K} \cdot \mathrm{m})/\mathrm{W}$] during TRT 2, standard collector

Appendix B

Brønnskjema

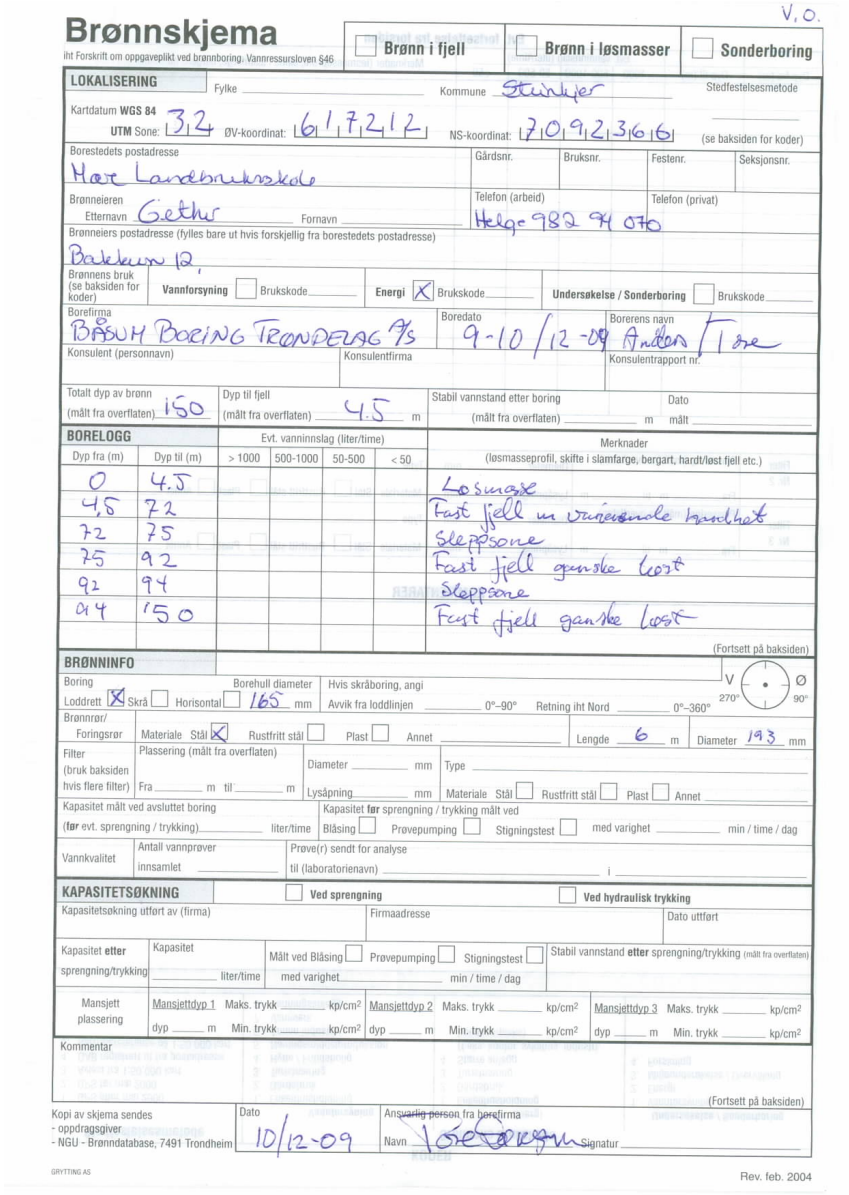

V.O.

Brønnskjema

iht Forskrift om oppgaveplikt ved brønnboring. Vannressursloven §46

☐ Brønn i fjell ☐ Brønn i løsmasser ☐ Sonderboring

LOKALISERING

Fylke _____ Kommune Steinkjer Stedfestelsesmetode _____

Kartdatum WGS 84 UTM Sone: 32 ØV-koordinat: 617212 NS-koordinat: 7092366 (se baksiden for koder)

Borestedets postadresse: Hoe Landbruksskole | Gårdsnr. | Bruksnr. | Festenr. | Seksjonsnr.

Brønneieren Etternavn Gether Fornavn _____ | Telefon (arbeid) Helge 982 94 070 | Telefon (privat)

Brønneiers postadresse (fylles bare ut hvis forskjellig fra borestedets postadresse): Bakkeun 12,

Brønnens bruk (se baksiden for koder): Vannforsyning ☐ Brukskode _____ Energi ☒ Brukskode _____ Undersøkelse / Sonderboring ☐ Brukskode _____

Borefirma: BÅSUM BORING TRØNDELAG A/S | Boredato 9-10/12-09 | Borerens navn Anders Tore

Konsulent (personnavn) | Konsulentfirma | Konsulentrapport nr.

Totalt dyp av brønn (målt fra overflaten) 150 | Dyp til fjell (målt fra overflaten) 4.5 m | Stabil vannstand etter boring (målt fra overflaten) _____ m | Dato målt _____

BORELOGG

Dyp fra (m)	Dyp til (m)	Evt. vanninnslag (liter/time) > 1000	500-1000	50-500	< 50	Merknader (løsmasseprofil, skifte i slamfarge, bergart, hardt/løst fjell etc.)
0	4,5					Løsmasse
4,5	72					Fast fjell m vannførende brudd
72	75					Sleppsone
75	92					Fast fjell gamske bost
92	94					Sleppsone
94	150					Fast fjell gamske bost

(Fortsett på baksiden)

BRØNNINFO

Boring: Loddrett ☒ Skrå ☐ Horisontal ☐ | Borehull diameter 165 mm | Hvis skråboring, angi: Avvik fra loddlinjen _____ 0°–90° Retning iht Nord _____ 0°–360° (V 270° Ø 90°)

Brønnrør/ Foringsrør: Materiale Stål ☒ Rustfritt stål ☐ Plast ☐ Annet _____ | Lengde 6 m | Diameter 193 mm

Filter (bruk baksiden hvis flere filter): Plassering (målt fra overflaten) Fra _____ m til _____ m | Diameter _____ mm Lysåpning _____ mm | Type _____ Materiale Stål ☐ Rustfritt stål ☐ Plast ☐ Annet _____

Kapasitet målt ved avsluttet boring (før evt. sprengning / trykking) _____ liter/time | Kapasitet før sprengning / trykking målt ved: Blåsing ☐ Prøvepumping ☐ Stigningstest ☐ med varighet _____ min / time / dag

Vannkvalitet: Antall vannprøver innsamlet _____ | Prøve(r) sendt for analyse til (laboratorienavn) _____ i _____

KAPASITETSØKNING ☐ Ved sprengning ☐ Ved hydraulisk trykking

Kapasitetsøkning utført av (firma) | Firmaadresse | Dato utført

Kapasitet etter sprengning/trykking: Kapasitet _____ liter/time | Målt ved Blåsing ☐ Prøvepumping ☐ Stigningstest ☐ med varighet _____ min / time / dag | Stabil vannstand etter sprengning/trykking (målt fra overflaten)

Mansjett plassering: Mansjettdyp 1 dyp _____ m Maks. trykk _____ kp/cm² Min. trykk _____ kp/cm² | Mansjettdyp 2 dyp _____ m Maks. trykk _____ kp/cm² Min. trykk _____ kp/cm² | Mansjettdyp 3 dyp _____ m Maks. trykk _____ kp/cm² Min. trykk _____ kp/cm²

Kommentar

(Fortsett på baksiden)

Kopi av skjema sendes
- oppdragsgiver
- NGU - Brønndatabase, 7491 Trondheim

Dato 10/12-09 | Ansvarlig person fra borefirma Navn [illegible] Signatur _____

GRYTTING AS

Rev. feb. 2004

Appendix C

List of Equipment and Software

Table C.1 gives details of the equipment used in this fieldwork, and Table C.2 gives details of computer software used in this master's thesis.

Table C.1: Equipment used in field

Name	Description	Company	Country of production
8-bit Minilog TDR	Temperature logger	Vemco	Canada
FCX-A2-V5	Differential pressure transmitter	Fuji Electric	France
Tangamperemeter AC/DC	Ammeter	Biltema AS	Sweden
Norsonic 840: Dual Channel Real Time Analyzer	Vibration analyzer	Norsonic AS	Norway
GPSmap 60CSx	Handheld GPS	Garmin	U.S.

Table C.2: Computer software

Name	Description	Version	By
Earth Energy Designer	Ground source heat dimensioning	2.0	Eskilson et al. (2000)
Grapher	Graphing system	7.0	Golden Software, Inc.
Mapsource	Trip and waypoint manager	6.11.6	Garmin Ltd.
Dips	Analysis of orientation based geological data	5.107	Rocscience

Appendix D

XRD

X-ray diffraction (XRD) was conducted at the laboratories of the department of Geology and Mineral Resources Engineering at NTNU. They were completed by senior engineer Kjell R. Kvam.

XRD finds the geometry and shape of molecules by using x-rays. The technique is used to characterize the crystallographic structure, grain size or the preferred orientations of the powdered solid sample. Unknown samples may in this way be identified by comparing diffraction data against an international database. In this master's thesis, XRD was used to find the mineral compositions of the samples in field, and thus the rock type.

This semi-quantitative method provides rough estimates of the quantity of each mineral. TOPAS quantification was used to improve the accuracy of the estimation.

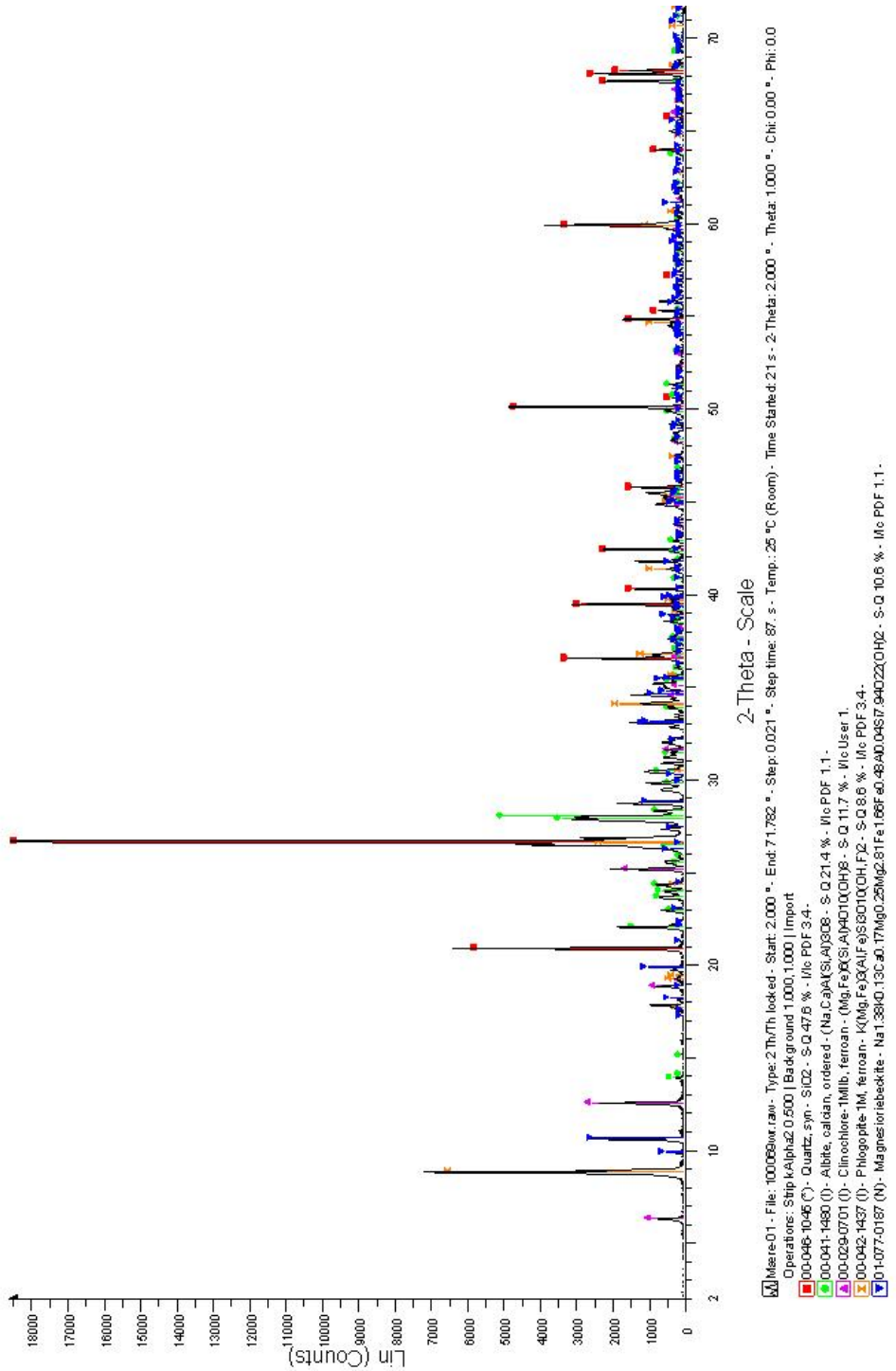

Figure D.1: Results XRD sample 0

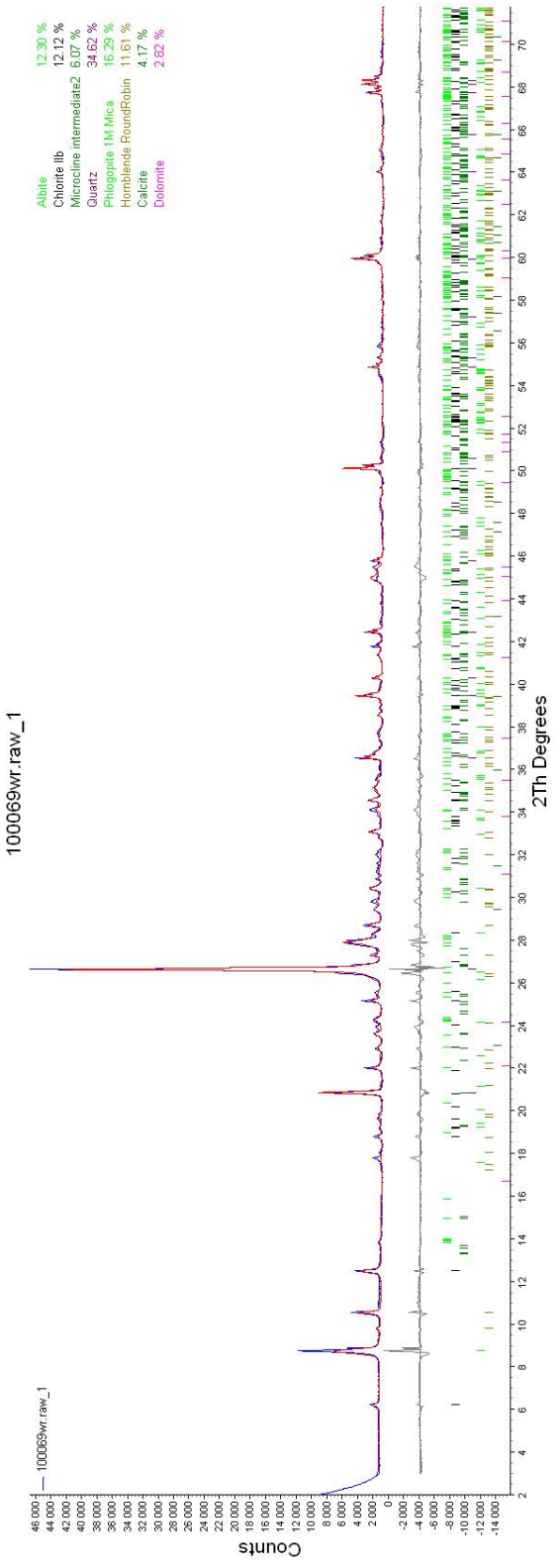

Figure D.2: Results TOPAS quantification sample 0

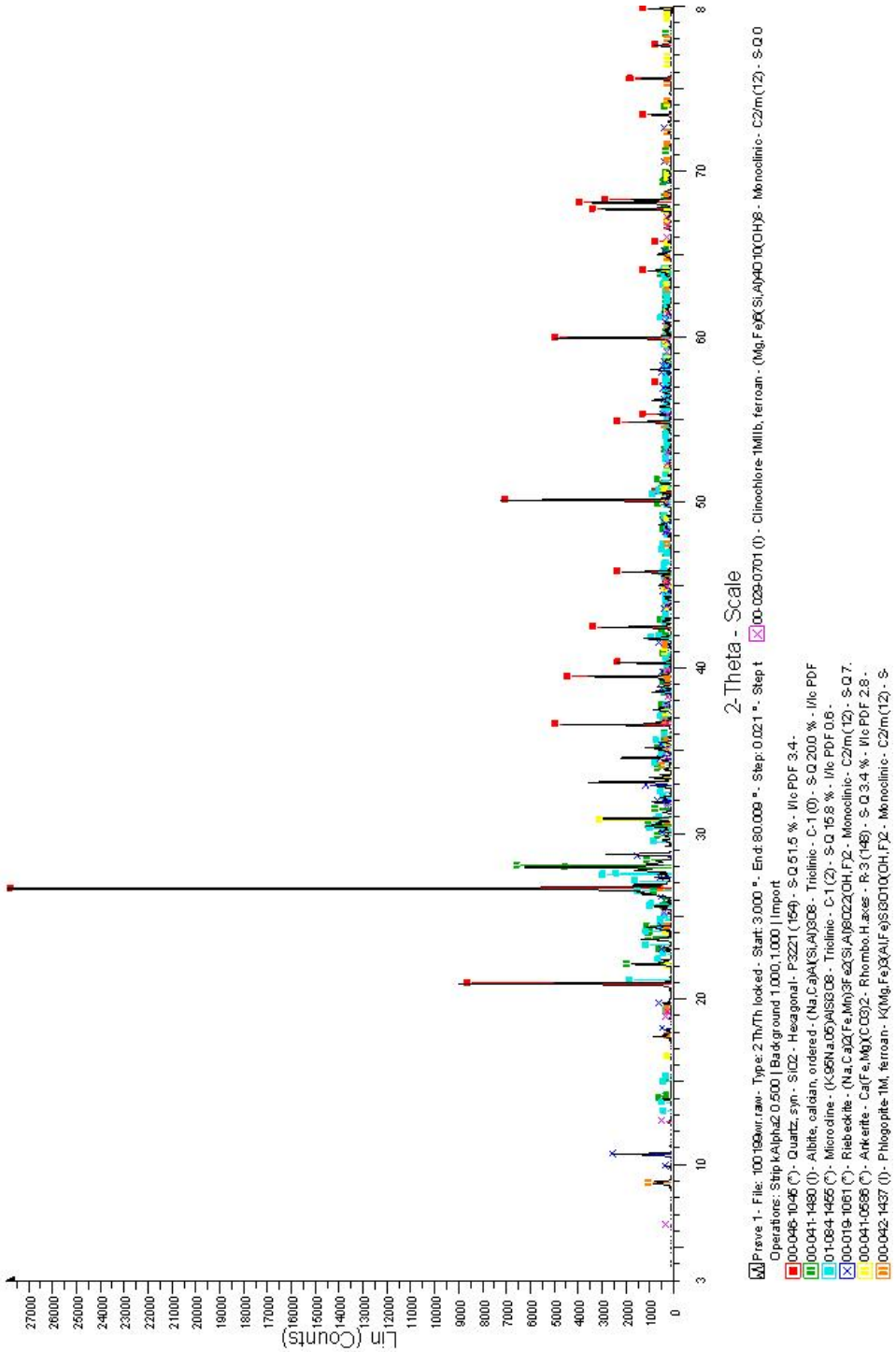

Figure D.3: Results XRD sample 1

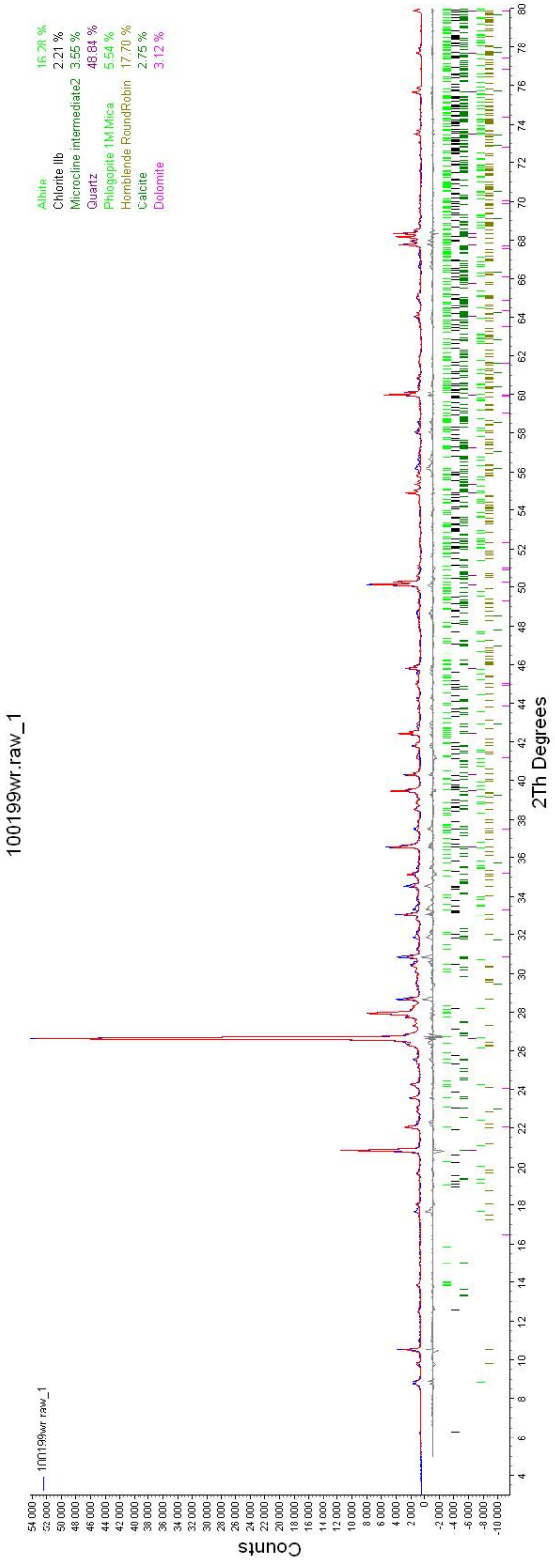

Figure D.4: Results TOPAS quantification sample 1

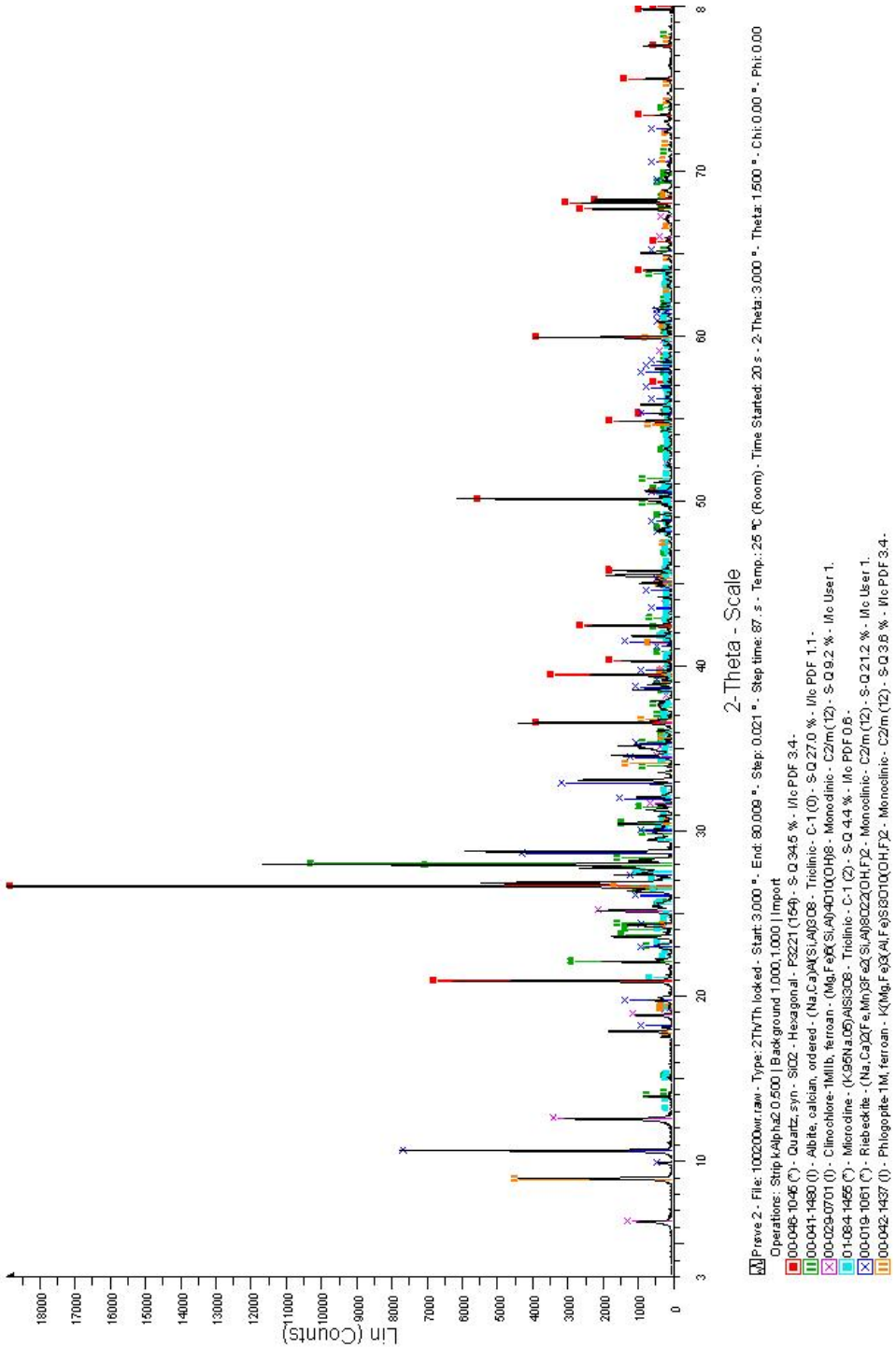

Figure D.5: Results XRD sample 2

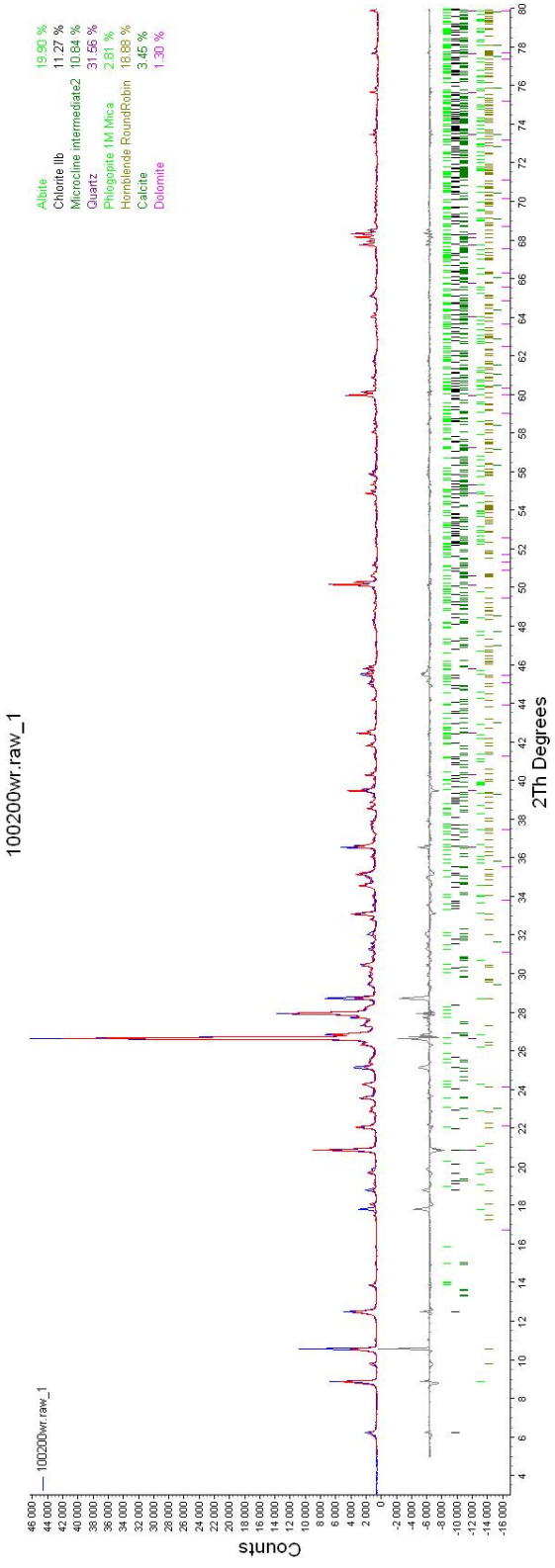

Figure D.6: Results TOPAS quantification sample 2

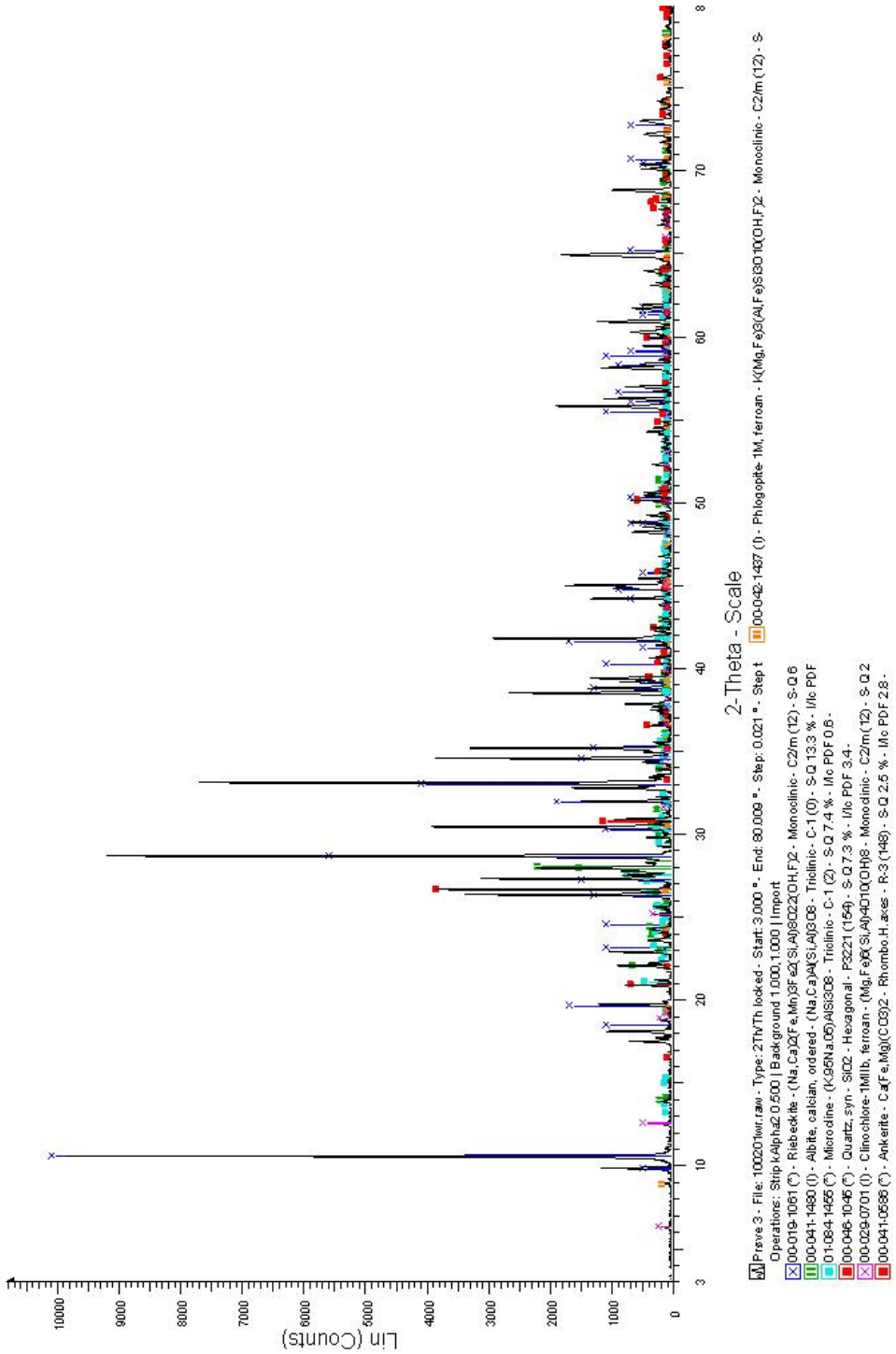

Figure D.7: Results XRD sample 3

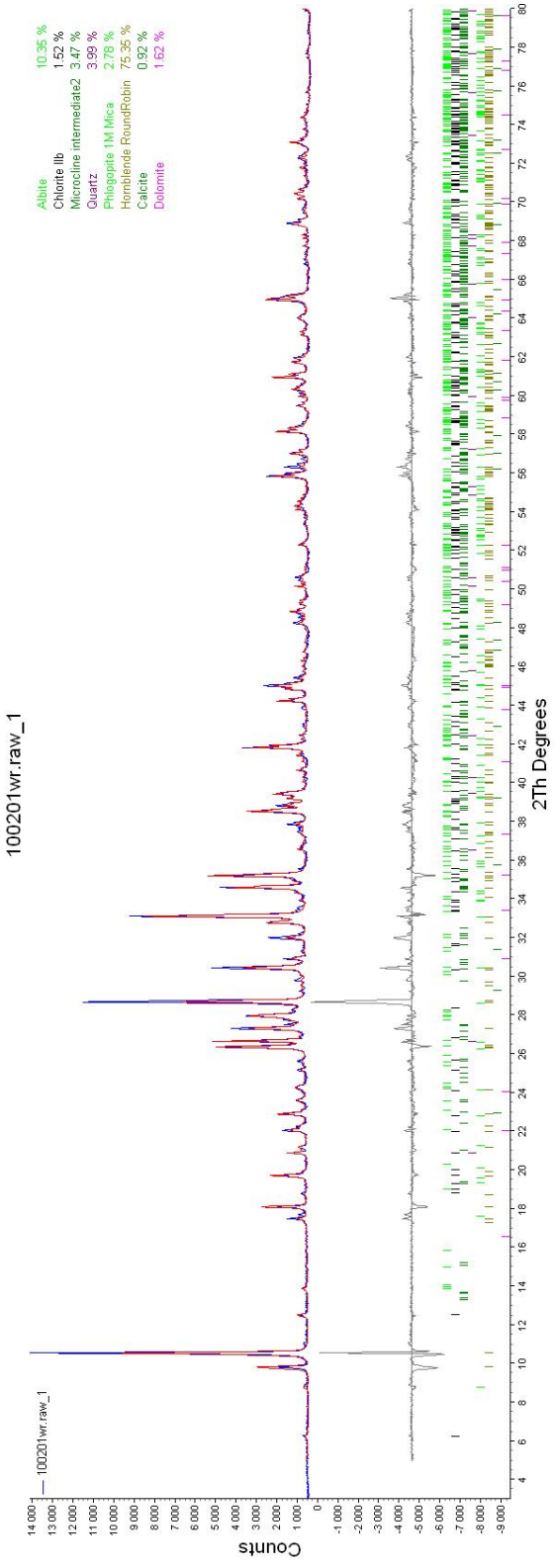

Figure D.8: Results TOPAS quantification sample 3

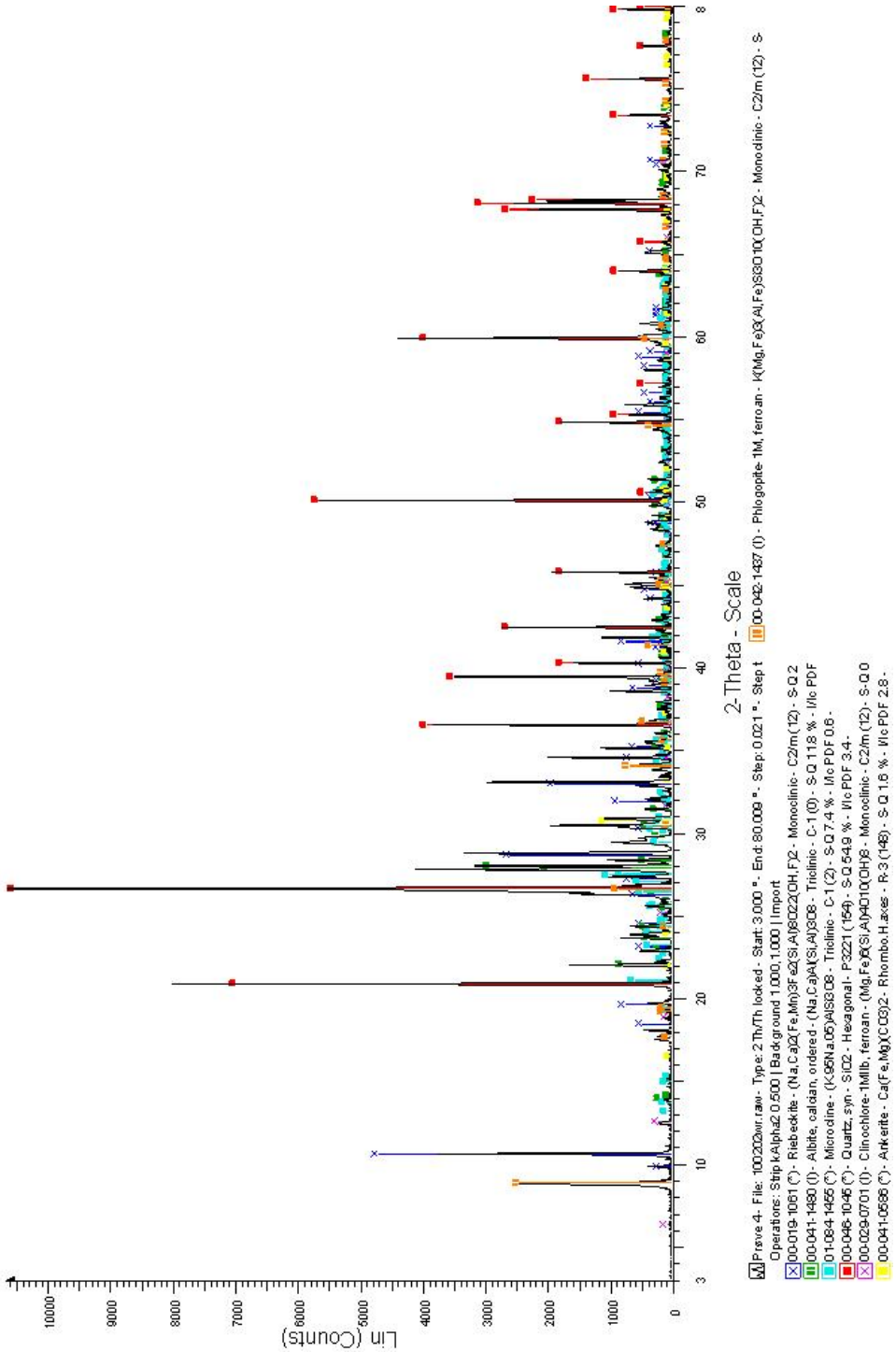

Figure D.9: Results XRD sample 4

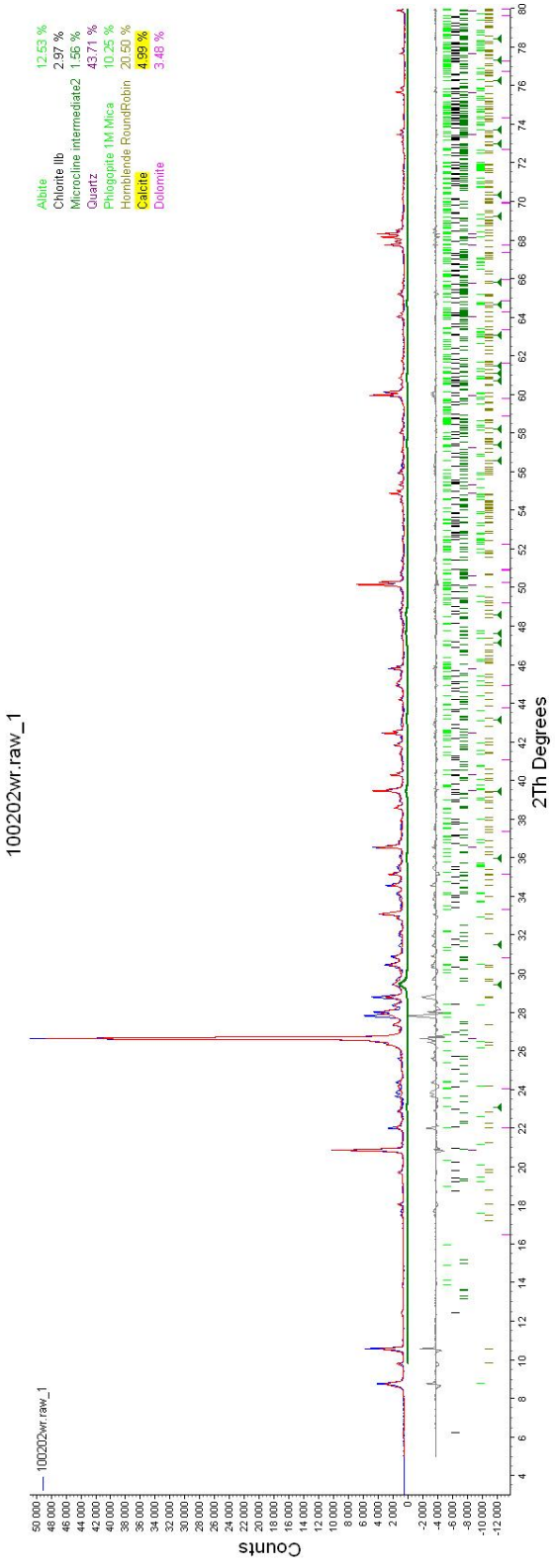

Figure D.10: Results TOPAS quantification sample 4

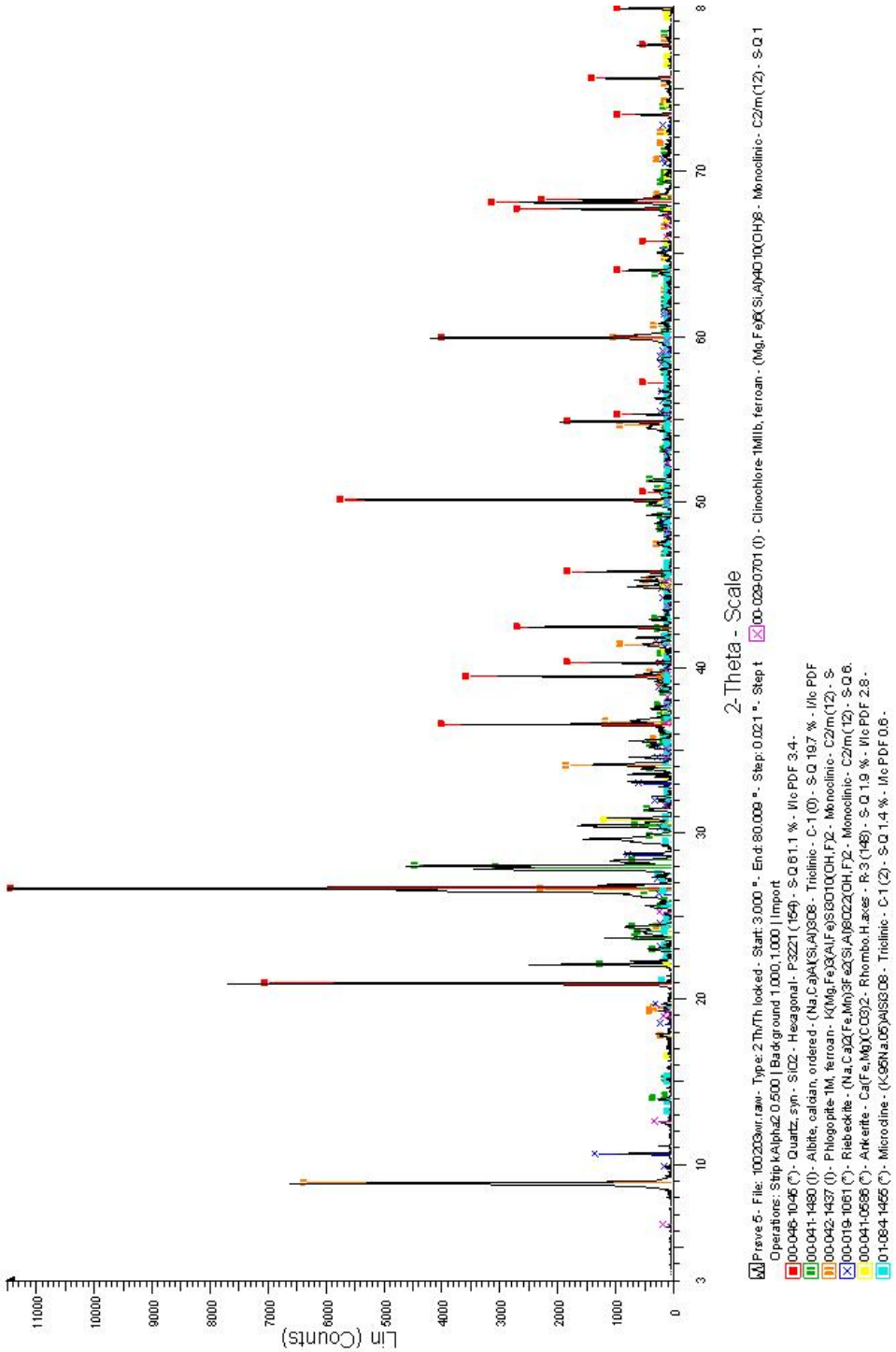

Figure D.11: Results XRD sample 5

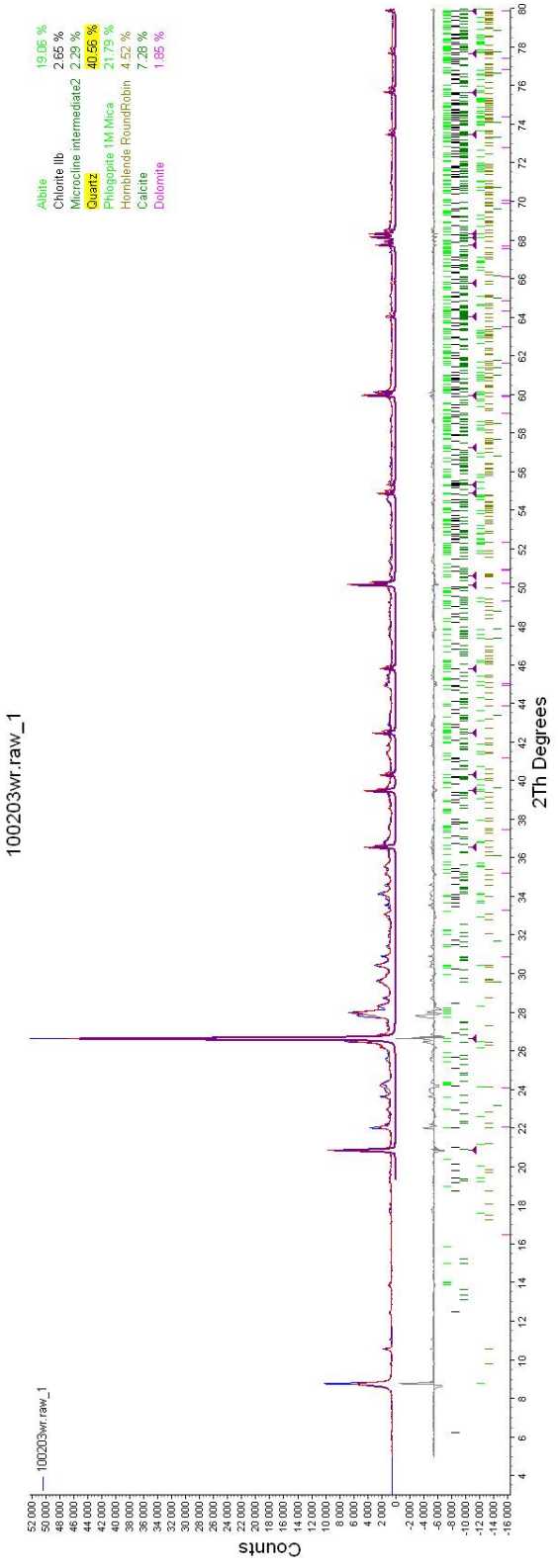

Figure D.12: Results TOPAS quantification sample 5

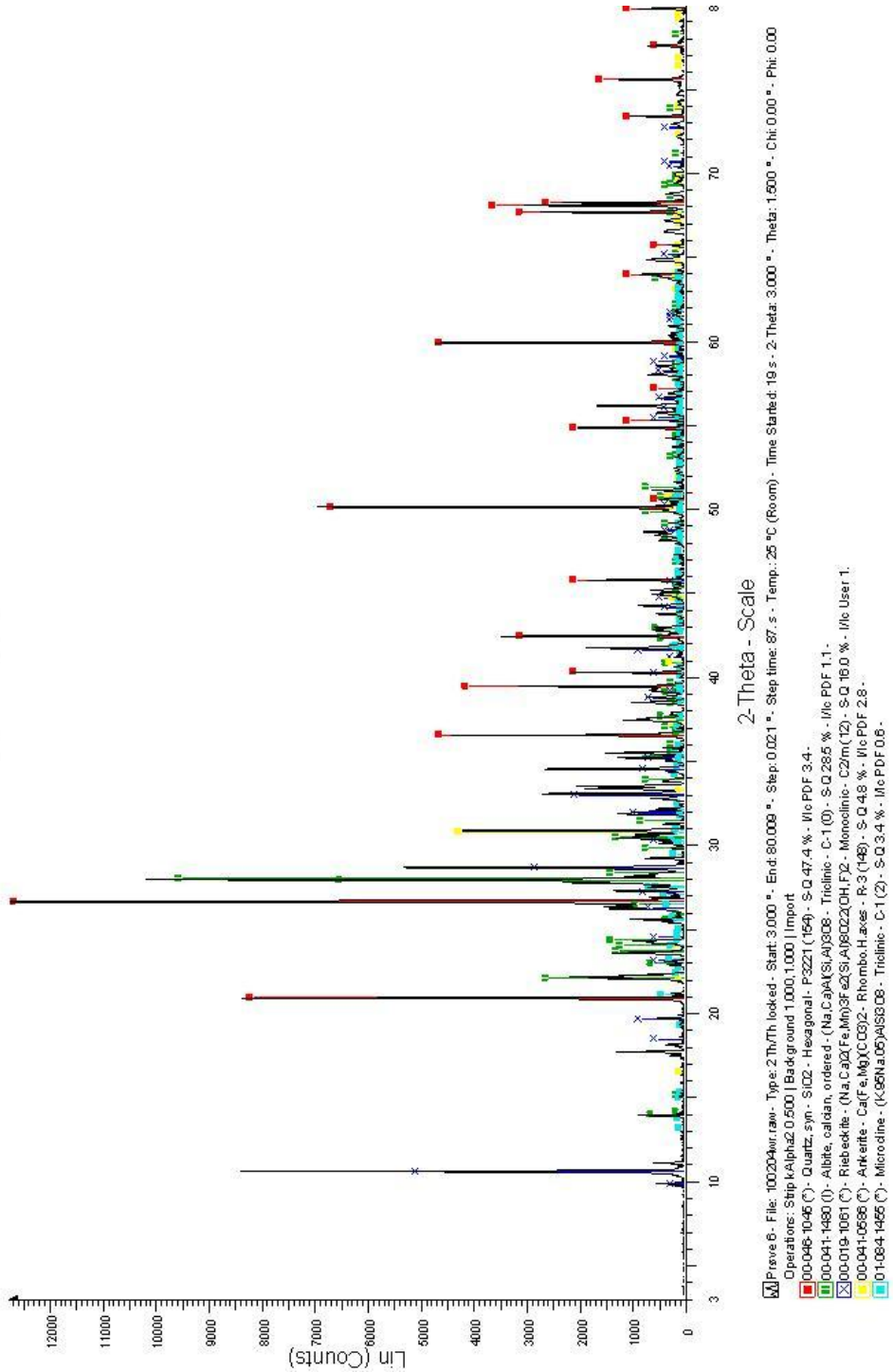

Figure D.13: Results XRD sample 6

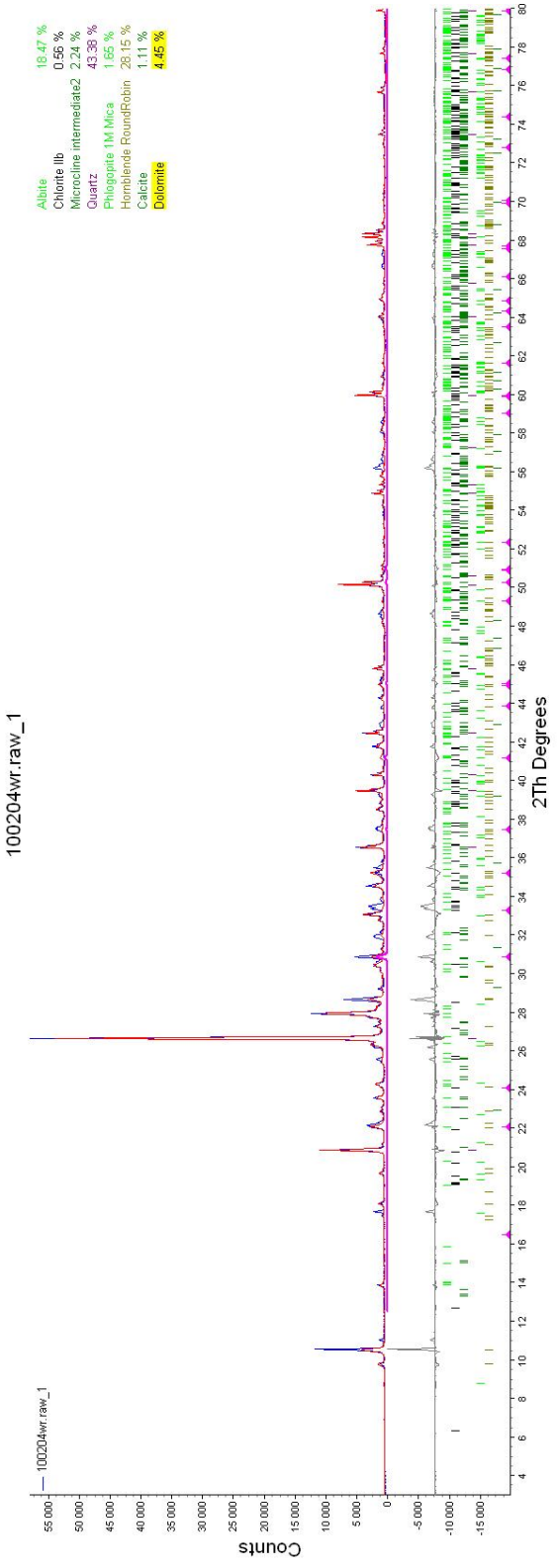

Figure D.14: Results TOPAS quantification sample 6

Appendix E

Laboratory Procedure Thermal Conductivity

The thermal conductivity testing was completed at the laboratories of the Geological Survey of Norway (NGU), under the supervision of Bjørn Willemoes-Wissing. At NGU, a transient method for measuring the thermal conductivity has been developed since 1998 (Ramstad et al., 2008). In this appendix, both the theoretical background, methods and results of the measurements will be presented.

E.1 Theoretical background

This section is mainly based on Middleton (1993). The thermal conductivity is found by using Equation 2.2 as presented in Section 2.1.2. A rock sample is exposed to a heat flow assumed to be constant, and generated by a source which is controlled by a thermostat. The sample is insulated on all surfaces except for the top surface, placed 10 mm from the source. The temperature is being measured at the base of the sample, and the thermal diffusivity is estimated from a plot of temperature *versus* time. Further, the thermal conductivity is calculated from Equation 2.2, assuming a specific heat capacity depending on the rock in question.

The theory behind the transient methods used to measure thermal diffusivity is originally described by Carslaw and Jaeger (1959), and cited by Middleton (1993). They consider a semi-infinite slab of rock which is insulated at its base x=0 and has a constant heat flux introduced at the surface x=a at the time t=0, as evident in Figure E.1. Carslaw and Jaeger showed that there is a specific relation between the temperature at a distance x within the slab at time t , after the introduction of a constant heat flux (F) on the top of the slab (x=a). The temperature *versus* time behavior is linear with time after a certain time, and the intercept t_i on the T=0 axis is used to calculate the thermal diffusivity (α) from Equation E.1:

$$\alpha = \frac{a^2}{6t_i} \tag{E.1}$$

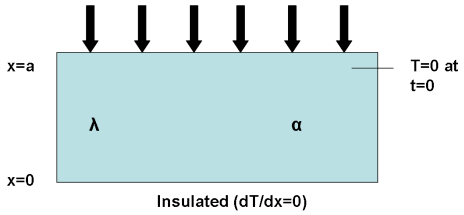

Figure E.1: An illustration of the transient method for measuring thermal conductivity. A semi-infinite slab initially at zero temperature, insulated at the surface x=0, having a constant heat flux introduced at the surface x=a at time t=0. Modified from Ramstad et al. (2008)

E.2 Equipment

The original equipment is described by Middleton (1993), and later versions used by NGU are described by Ramstad et al. (2008). In these experiments, the 2006-version was used, as seen in Figure E.2. It consists of a heat source, a sample holder with a temperature sensor and a personal computer registering the logged temperature at the base of the sample. The heat source, as shown in Figure E.3, consists of a black hotplate originally designed for baking "wafer cones", having a constant temperature of 300 °C ±° C. The temperature sensor configuration consists of a the temperature sensor itself, aluminum foil and a thin pad of foam. The temperature sensor is placed between the foam and the aluminum foil. Copper signal wires lead from the temperature sensor to the logging unit. The interpretation software "Varmeled" is developed at NGU and based on the previously described theory.

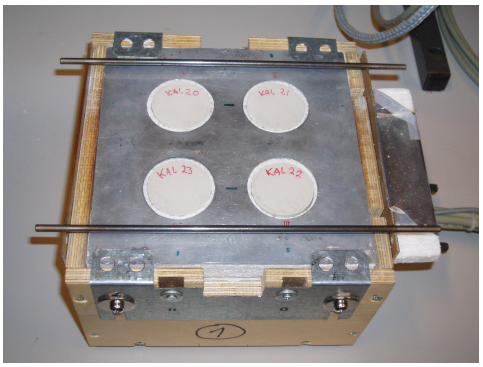

Figure E.2: Sample holder for measuring thermal conductivity. Photo: Marie Stølen

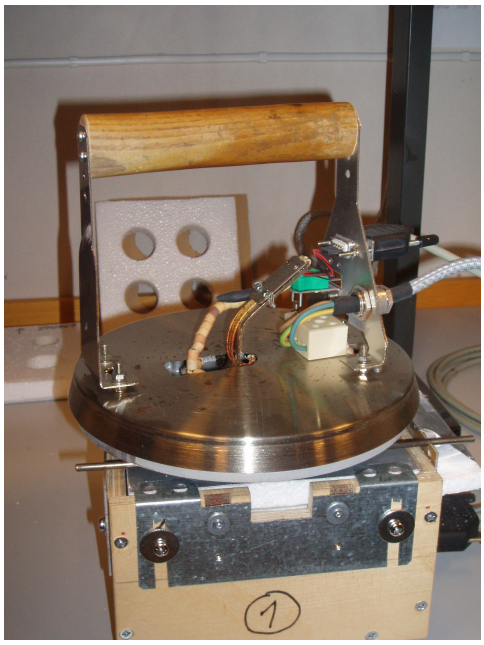

Figure E.3: Sample holder and heat source for measuring thermal conductivity. Photo: Marie Stølen

E.3 Method

First, the physical data of the core samples including diameter, height, thickness, weight, density and UTM-coordinates of the sample location were registered in the sample database. Next, reference samples of the material Pyroceram were tested, and compared to an acceptance criterion of $\pm 2\sigma$. After obtaining acceptable values of the reference material, group selections of three rock samples and one reference sample were measured. Measurements not being compatible with the acceptable values of the reference material were rejected and measured again. The measurements were done for 200 seconds, or at the point when the temperature of the sensor reached 40 °C. A specific heat capacity of 850 $\mathrm{J/(kg \cdot K)}$ was assumed for the calculations.

E.4 Accuracy

Results of a sensitivity analysis by Middleton (1993) indicate that thermal diffusivity can be measured to a best accuracy of about 3 %, and the thermal conductivity of saturated rocks can be determined to a best accuracy of 8 %. At NGU, an accuracy of 10 % is used found to be valid for thermal conductivity measurements (Ramstad et al., 2008).

E.5 Results

Code for description of orientation	The orientation of the measurements in relation to the foliation of the sample
P	Parallel with the foliation
N	Normal to the foliation
S	An angle greater than 10 degreece different from P and N
M	Massive rock without foliation

Colour	Description
1	White
2	Black
3	Light grey
4	Dark grey
5	Light brown
6	Dark brown
7	Light red
8	Dark red
9	Light green
10	Dark green

Texture/structure code	Description
M	Massive
F	Foliated
S	Schistous
L	Stratified
B	Banded
P	Porphyritic
K	Conglomerate

Ores (percentage)	Description
5	5 % of rock
10	10 % of rock
25	25 % of rock
50	50 % of rock

Damage	Description
0	Intact
1	Missing edge
2	Fissure on the long side

Grainsize (mm)	Code	Description
>30	SG	Very course
5-30	G	Course
1-5	M	Medium
<1	F	Fine

Sample name	Rock	ρ [g/cm^3]	S_C[J/(kg·K)]	λ [W/(m·K)]	Orient.	Grain size	Text. /struc.	Defect	Colour	Veins	UTM-zone	UTM E	UTM N
0A	Mica schist	2.85	850	3.3	P						32V	617086	7092947
0B	Mica schist	2.83	850	3.4	P						32V	617086	7092947
0C	Mica schist	2.82	850	2.7	N						32V	617086	7092947
0D	Mica schist	2.80	850	2.4	N						32V	617086	7092947
0E	Mica schist	2.81	850	2.4	N						32V	617086	7092947
0F	Mica schist	2.80	850	3.1	P						32V	617086	7092947
0G	Mica schist	2.78	850	3.3	P						32V	617086	7092947
1A	Mica schist	2.81	850	3.6	P	F	F/S	0	3	5	32V	617611	7092440
1B	Mica schist	2.79	850	3.6	P	F	F/S	0	3	10	32V	617611	7092440
1C	Mica schist	2.82	850	3.7	P	F	F/S	0	3	5	32V	617611	7092440
1D	Mica schist	2.79	850	2.5	N	F	F/S	0	3	5	32V	617611	7092440
1E	Mica schist	2.85	850	2.2	N	F	F/S	0	3	5	32V	617611	7092440
1F	Mica schist	2.82	850	2.3	N	F	F/S	0	3	5	32V	617611	7092440
1G	Mica schist	2.65	850	4.7	N	M	M	0	1	50	32V	617611	7092440
2A	Mica schist	2.77	850	3.4	P	F	F	0	4	0	32V	617 511	7091971
2B	Mica schist	2.73	850	3.6	P	F	F	0	4	0	32V	617 511	7091971
2C	Mica schist	2.77	850	3.5	P	F	F	0	4	0	32V	617 511	7091971
2D	Mica schist	2.77	850	2.4	N	F	F	0	4	5	32V	617 511	7091971
2E	Mica schist	2.77	850	2.6	N	F	F	0	4	5	32V	617 511	7091971
2F	Mica schist	2.80	850	2.5	N	F	F	0	4	5	32V	617 511	7091971
3A	Amphibolite	3.07	850	3.0	P	F	F	0	4	5	32V	617 541	7091969
3B	Amphibolite	3.09	850	3.1	P	F	F	0	4	5	32V	617 541	7091969
3C	Amphibolite	3.06	850	3.1	P	F	F	0	4	5	32V	617 541	7091969
3D	Amphibolite	3.05	850	2.7	N	F	F	0	4	0	32V	617 541	7091969
3E	Amphibolite	3.09	850	2.5	N	F	F	0	4	0	32V	617 541	7091969
3F	Amphibolite	3.06	850	2.7	N	F	F	0	4	0	32V	617 541	7091969
4A	Mica schist	2.82	850	3.0	P	F	F	0	4	0	32V	617 521	7091801
4B	Mica schist	2.85	850	3.0	P	F	F	0	4	0	32V	617 521	7091801
4C	Mica schist	2.83	850	3.0	P	F	F	0	4	0	32V	617 521	7091801
4D	Mica schist	2.85	850	3.3	N	F	F	0	3	0	32V	617 521	7091801
4E	Mica schist	2.85	850	3.5	N	F	F	0	3	0	32V	617 521	7091801
4F	Mica schist	2.84	850	2.3	N	F	F	0	3	0	32V	617 521	7091801
5A	Mica schist	2.79	850	3.6	P	F	S	0	4	10	32V	617 410	7091555
5B	Mica schist	2.80	850	3.6	P	F	S	0	4	10	32V	617 410	7091555
5C	Mica schist	2.79	850	3.5	P	F	S	0	4	10	32V	617 410	7091555
5D	Mica schist	2.80	850	2.4	N	F	S	0	4	10	32V	617 410	7091555
5E	Mica schist	2.81	850	2.4	N	F	S	0	4	10	32V	617 410	7091555
5F	Mica schist	2.80	850	2.2	N	F	S	0	4	10	32V	617 410	7091555
6A	Mica schist	2.90	850	3.9	P	F	S	0	3	5	32V	617 592	7092066
6B	Mica schist	2.90	850	3.9	P	F	S	0	3	5	32V	617 592	7092066
6C	Mica schist	2.91	850	3.9	P	F	S	0	3	5	32V	617 592	7092066
6D	Mica schist	2.90	850	2.4	N	F	S	0	3	5	32V	617 592	7092066
6E	Mica schist	2.92	850	2.3	N	F	S	0	3	5	32V	617 592	7092066
6F	Mica schist	2.91	850	2.3	N	F	S	0	3	5	32V	617 592	7092066

RecID	Group	Sample name	Trial	Celle No.	ρ [g/cm^3]	S_C [J/kg·K]	λ [W/(m·K)]	α [m^2/s]	Φ_q [W/m^2]	Thick. [mm]	Diam. [mm]	Air. W. [g]	Measuring date
2	1	Kal_20	1	1	2.60	870	4.3	1.9E-06	6221	20.78	35	51.36	09.03.2010
15	1	Kal_21	1	2	2.60	870	4.1	1.8E-06	6205	20.99	35	52.23	09.03.2010
25	1	Kal_22	1	3	2.60	870	4.2	1.9E-06	6224	20.06	35	48.64	09.03.2010
36	1	Kal_23	1	4	2.60	870	4.3	1.9E-06	6224	20.71	35	50.8	09.03.2010
3	2	Kal_20	2	1	2.60	870	4.4	1.9E-06	6358	20.78	35	51.36	09.03.2010
16	2	Kal_21	2	2	2.60	870	4.3	1.9E-06	6377	20.99	35	52.23	09.03.2010
26	2	Kal_22	2	3	2.60	870	4.5	2.0E-06	6342	20.06	35	48.64	09.03.2010
37	2	Kal_23	2	4	2.60	870	4.4	1.9E-06	6339	20.71	35	50.8	09.03.2010
4	3	Kal_20	3	1	2.60	870	4.1	1.8E-06	6469	20.78	35	51.36	09.03.2010
45	3	0A	1	2	2.85	850	3.2	1.3E-06	6817	21.9	32	49.23	09.03.2010
48	3	0B	1	3	2.83	850	3.6	1.5E-06	6763	22.09	32	49.28	09.03.2010
50	3	0C	1	4	2.82	850	2.7	1.1E-06	6070	21.89	32	48.69	09.03.2010
17	4	Kal_21	3	1	2.60	870	4.3	1.9E-06	6585	20.99	35	52.23	09.03.2010
52	4	0D	1	2	2.80	850	2.4	1.0E-06	5102	21.91	32	48.74	09.03.2010
54	4	0E	1	3	2.81	850	2.4	1.0E-06	5194	22.17	32	49.26	09.03.2010
56	4	0F	1	4	2.80	850	3.1	1.3E-06	6642	22	32	48.81	09.03.2010
27	5	Kal_22	3	1	2.60	870	4.3	1.9E-06	6426	20.06	35	48.64	09.03.2010
58	5	0G	1	2	2.78	850	3.3	1.4E-06	6831	21.94	32	48.07	09.03.2010
46	5	0A	2	3	2.85	850	3.4	1.4E-06	7005	21.9	32	49.23	09.03.2010
49	5	0B	2	4	2.83	850	3.3	1.4E-06	6872	22.09	32	49.28	09.03.2010
38	6	Kal_23	3	1	2.60	870	3.9	1.7E-06	6859	20.71	35	50.8	09.03.2010
51	6	0C	2	2	2.82	850	2.8	1.2E-06	6352	21.89	32	48.69	09.03.2010
53	6	0D	2	3	2.80	850	2.3	9.8E-07	5095	21.91	32	48.74	09.03.2010
55	6	0E	2	4	2.81	850	2.4	1.0E-06	5190	22.17	32	49.26	09.03.2010
5	7	Kal_20	4	1	2.60	870	2.0	8.8E-07	4611	20.78	35	51.36	09.03.2010
47	7	0A	3	2	2.85	850	3.3	1.4E-06	6653	21.9	32	49.23	09.03.2010
57	7	0F	2	3	2.80	850	3.2	1.3E-06	6432	22	32	48.81	09.03.2010
59	7	0G	2	4	2.78	850	3.3	1.4E-06	6702	21.94	32	48.07	09.03.2010
6	8	Kal_20	5	1	2.60	870	4.0	1.8E-06	6127	20.78	35	51.36	04.05.2010
18	8	Kal_21	4	2	2.60	870	3.9	1.7E-06	5920	20.99	35	52.23	04.05.2010
28	8	Kal_22	4	3	2.60	870	3.9	1.7E-06	5868	20.06	35	48.64	04.05.2010
39	8	Kal_23	4	4	2.60	870	4.0	1.8E-06	6270	20.71	35	50.8	04.05.2010
7	9	Kal_20	6	1	2.60	870	4.1	1.8E-06	6490	20.78	35	51.36	04.05.2010
19	9	Kal_21	5	2	2.60	870	4.0	1.8E-06	6763	20.99	35	52.23	04.05.2010
29	9	Kal_22	5	3	2.60	870	4.0	1.8E-06	6248	20.06	35	48.64	04.05.2010
40	9	Kal_23	5	4	2.60	870	4.1	1.8E-06	6439	20.71	35	50.8	04.05.2010
20	11	Kal_21	6	1	2.60	870	4.2	1.9E-06	6586	20.99	35	52.23	04.05.2010
9	11	Kal_20	8	2	2.60	870	4.1	1.8E-06	6401	20.78	35	51.36	04.05.2010
30	11	Kal_22	6	3	2.60	870	4.1	1.8E-06	6062	20.06	35	48.64	04.05.2010
41	11	Kal_23	6	4	2.60	870	4.2	1.9E-06	6270	20.71	35	50.8	04.05.2010
10	12	Kal_20	9	1	2.60	870	4.1	1.8E-06	6532	20.78	35	51.36	04.05.2010
60	12	1A	1	2	2.81	850	3.6	1.5E-06	6169	20	36	56.26	04.05.2010
61	12	1B	1	3	2.79	850	3.6	1.5E-06	5853	20.13	36	56.38	04.05.2010
62	12	1C	1	4	2.82	850	3.7	1.5E-06	5836	20.06	36	56.57	04.05.2010
31	13	Kal_22	7	1	2.60	870	3.9	1.7E-06	6405	20.06	35	48.64	04.05.2010
63	13	1D	1	2	2.79	850	2.5	1.0E-06	5788	20.47	36	57.31	04.05.2010
65	13	1E	1	3	2.85	850	2.2	9.0E-07	5166	19.95	36	56.74	04.05.2010
67	13	1F	1	4	2.82	850	2.3	9.7E-07	5326	20.5	36	57.74	04.05.2010
21	14	Kal_21	7	1	2.60	870	4.4	2.0E-06	6575	20.99	35	52.23	04.05.2010

RecID	Group	Sample name	Trial	Celle No.	ρ [g/cm³]	S_C [J/kg·K]	λ [W/(m·K)]	α [m²/s]	Φ_q [W/m²]	Thick. [mm]	Diam. [mm]	Air. W. [g]	Measuring date
69	14	1G	1	2	2.65	850	5.0	2.2E-06	6226	20.25	36	53.73	04.05.2010
72	14	2A	1	3	2.77	850	3.7	1.6E-06	5639	20.14	36	55.52	04.05.2010
74	14	2B	1	4	2.73	850	3.8	1.6E-06	5583	20.1	36	54.68	04.05.2010
42	15	Kal_23	7	1	2.60	870	4.2	1.9E-06	6617	20.71	35	50.8	04.05.2010
76	15	2C	1	2	2.77	850	3.5	1.5E-06	5821	19.68	36	54.4	04.05.2010
78	15	2D	1	3	2.77	850	2.4	1.0E-06	5243	20.21	36	55.63	04.05.2010
80	15	2E	1	4	2.77	850	2.6	1.1E-06	5400	20.16	36	55.81	04.05.2010
11	16	Kal_20	10	1	2.60	870	4.0	1.8E-06	6756	20.78	35	51.36	04.05.2010
81	16	2F	1	2	2.80	850	2.5	1.1E-06	5779	20	36	55.79	04.05.2010
82	16	3a	1	3	3.07	850	3.0	1.2E-06	5922	20.13	36	61.75	04.05.2010
83	16	3B	1	4	3.09	850	3.1	1.2E-06	6089	20.23	36	62.2	04.05.2010
32	17	Kal_22	8	1	2.60	870	3.9	1.7E-06	6527	20.06	35	48.64	04.05.2010
84	17	3C	1	2	3.06	850	3.0	1.1E-06	6091	20.11	36	61.12	04.05.2010
86	17	3D	1	3	3.05	850	2.7	1.0E-06	5468	19.8	36	60.06	04.05.2010
88	17	3E	1	4	3.09	850	2.4	9.3E-07	5525	19.9	36	61.11	04.05.2010
22	18	Kal_21	8	1	2.60	870	4.1	1.8E-06	6915	20.99	35	52.23	04.05.2010
90	18	3F	1	2	3.06	850	2.7	1.0E-06	5878	20.11	36	61.69	04.05.2010
91	18	4A	1	3	2.82	850	3.0	1.2E-06	5807	20.1	36	56.39	04.05.2010
92	18	4B	1	4	2.85	850	3.0	1.2E-06	6050	19.96	36	56.21	04.05.2010
12	19	Kal_20	11	1	2.60	870	4.2	1.9E-06	6663	20.78	35	51.36	04.05.2010
93	19	4C	1	2	2.83	850	3.0	1.2E-06	6052	19.98	36	56.07	04.05.2010
94	19	4D	1	3	2.85	850	3.3	1.4E-06	5579	19.89	36	56.38	04.05.2010
95	19	4E	1	4	2.85	850	3.5	1.4E-06	5855	20.18	36	57.04	04.05.2010
33	20	Kal_22	9	1	2.60	870	4.3	1.9E-06	6500	20.06	35	48.64	04.05.2010
96	20	4F	1	2	2.84	850	2.3	9.6E-07	5665	19.58	36	55.27	04.05.2010
97	20	5A	1	3	2.79	850	3.6	1.5E-06	5931	20.32	36	56.37	04.05.2010
99	20	5B	1	4	2.80	850	3.6	1.5E-06	5976	20.02	36	55.46	04.05.2010
23	21	Kal_21	9	1	2.60	870	4.2	1.8E-06	6930	20.99	35	52.23	04.05.2010
100	21	5C	1	2	2.79	850	3.4	1.4E-06	6322	20.48	36	56.86	04.05.2010
102	21	5D	1	3	2.80	850	2.4	1.0E-06	5413	20.26	36	56.38	04.05.2010
103	21	5E	1	4	2.81	850	2.4	9.9E-07	5599	20.38	36	56.73	04.05.2010
43	22	Kal_23	8	1	2.60	870	4.0	1.8E-06	6908	20.71	35	50.8	04.05.2010
104	22	5F	1	2	2.80	850	2.2	9.2E-07	5703	20.24	36	56.4	04.05.2010
105	22	6A	1	3	2.90	850	3.9	1.6E-06	6163	20.16	36	58.25	04.05.2010
106	22	6B	1	4	2.90	850	3.9	1.6E-06	6295	20.38	36	58.87	04.05.2010
13	23	Kal_20	12	1	2.60	870	4.2	1.8E-06	6871	20.78	35	51.36	04.05.2010
107	23	6C	1	2	2.91	850	3.9	1.6E-06	6462	20.34	36	58.91	04.05.2010
108	23	6D	1	3	2.90	850	2.4	9.8E-07	5420	20.37	36	58.84	04.05.2010
109	23	6E	1	4	2.92	850	2.3	9.3E-07	5375	20.24	36	58.77	04.05.2010
34	25	Kal_22	10	1	2.60	870	4.2	1.9E-06	6542	20.06	35	48.64	04.05.2010
110	25	6F	1	2	2.91	850	2.3	9.5E-07	5669	20.37	36	59.21	04.05.2010
64	25	1D	2	3	2.79	850	2.5	1.1E-06	5552	20.47	36	57.31	04.05.2010
66	25	1E	2	4	2.85	850	2.2	9.1E-07	5287	19.95	36	56.74	04.05.2010
24	26	Kal_21	10	1	2.60	870	4.1	1.8E-06	6876	20.99	35	52.23	04.05.2010
68	26	1F	2	2	2.82	850	2.3	9.7E-07	5745	20.5	36	57.74	04.05.2010
70	26	1G	2	3	2.65	850	4.6	2.0E-06	6171	20.25	36	53.73	04.05.2010
73	26	2A	2	4	2.77	850	3.4	1.4E-06	6014	20.14	36	55.52	04.05.2010
44	27	Kal_23	9	1	2.60	870	4.3	1.9E-06	6849	20.71	35	50.8	04.05.2010
75	27	2B	2	2	2.73	850	3.6	1.5E-06	6060	20.1	36	54.68	04.05.2010

RecID	Group	Sample name	Trial	Celle No.	ρ [g/cm^3]	S_C [J/kg·K]	λ [W/(m·K)]	α [m^2/s]	Φ_q [W/m^2]	Thick. [mm]	Diam. [mm]	Air. W. [g]	Measuring date
77	27	2C	2	3	2.77	850	3.5	1.5E-06	5599	19.68	36	54.4	04.05.2010
85	27	3C	2	4	3.06	850	3.1	1.2E-06	5985	20.11	36	61.12	04.05.2010
14	28	Kal_20	13	1	2.60	870	4.2	1.9E-06	6905	20.78	35	51.36	04.05.2010
87	28	3D	2	2	3.05	850	2.7	1.1E-06	5963	19.8	36	60.06	04.05.2010
89	28	3E	2	3	3.09	850	2.5	9.4E-07	5545	19.9	36	61.11	04.05.2010
98	28	5A	2	4	2.79	850	2.5	1.1E-06	5704	20.32	36	56.37	04.05.2010
35	29	Kal_22	11	1	2.60	870	4.2	1.9E-06	6694	20.06	35	48.64	04.05.2010
71	29	1G	3	2	2.65	850	4.8	2.1E-06	6551	20.25	36	53.73	04.05.2010
79	29	2D	2	3	2.77	850	2.4	1.0E-06	5447	20.21	36	55.63	04.05.2010
101	29	5C	2	4	2.79	850	3.5	1.5E-06	6178	20.48	36	56.86	04.05.2010

	ρ[g/cm^3]	λ [W/(m·K)]	α[m^2/s]	Φ_q[W/m^2]
All measurements rock-samples_average	2.84	3.0	1.3E-06	5904
All measurements rock-samples_median	2.82	3.0	1.2E-06	5854
All measurements rock-samples_min	2.65	2.2	9.0E-07	5095
All measurements rock-samples_max	3.09	5.0	2.2E-06	7005
All measurements rock-samples_std	0.10	0.7	3.0E-07	480
All measurements rock-samples_std (%)	3.67	21.6	2.4E+01	8

Calibration samples_average	2.60	4.1	1.8E-06	6446
Calibration_median	2.60	4.2	1.8E-06	6480
Calibration samples_min	2.60	2.0	8.8E-07	4611
Calibration samples_max	2.60	4.5	2.0E-06	6930
Calibration samples_std	0.00	0.4	1.6E-07	400
Calibration samples_std (%)	0.00	8.9	8.9E+00	6

E.6 Photos of sample cores

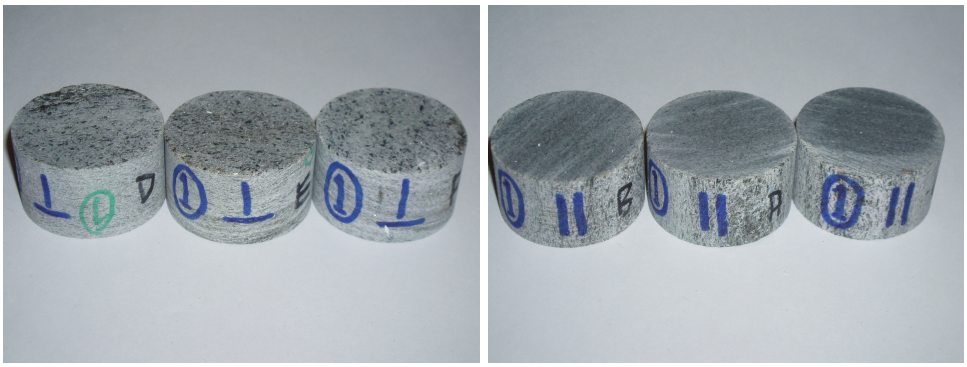

Figure E.4: Core sample 1. Normal orientation on the left and parallel orientation on the right. Photo: Marie Stølen

Figure E.5: Core sample 2. Normal orientation on the left and parallel orientation on the right. Photo: Marie Stølen

Figure E.6: Core sample 3. Normal orientation on the left and parallel orientation on the right. Photo: Marie Stølen

Figure E.7: Core sample 4. Normal orientation on the left and parallel orientation on the right. Photo: Marie Stølen

Figure E.8: Core sample 5. Normal orientation on the left and parallel orientation on the right. Photo: Marie Stølen

Figure E.9: Core sample 6. Normal orientation on the left and parallel orientation on the right. Photo: Marie Stølen

E.7 Conclusion

The standard deviation of the measured calibration samples was acceptable as it is within expected standard deviation found by NGU at 10 %. The results from this laboratory work may therefore be used as valid results.

Appendix F

Differential Thermal Analysis

In differential thermal analysis (DTA), the material being studied undergoes a thermal cycle identical to that of an inert reference. As the temperature changes are being logged by sensors, any exothermic or endothermic reaction will be detected in comparison with the inert reference. The thermal fingerprint is then compared with known features, and the identity of certain minerals and elements can be found.

The DTA was performed by Simon Hagen for SINTEF at the department of Infrastructure. According to SINTEF (Hagen, 2010), the lower detection limit for quartz is 1 % and the accuracy of the values within ±5%.

SINTEF 1

DIFFERENSIALTERMISK ANALYSE (DTA) MED BESTEMMELSE AV KVARTSINNHOLD

Saksbehandler: *SAHA*
Dato: *12.05.2010*

Det er foretatt følgende analyser:

- Differensialtermisk analyse (DTA)

RESULTAT

Prøve merking	Kvarts (vekt %)
Prøve 1	47
Prøve 2	27
Prøve 3	3
Prøve 4	37
Prøve 5	33
Prøve 6	40

Appendix G

Vibrational Analysis

,

Table G.1: Vibration measurements - standard collector, pipe in

	Acceleration [m^2/s] for each test								
Frq[Hz]	1	3	5	7	9	11	13	15	17
1	0.398	0.385	0.525	0.343	0.275	0.214	0.335	0.339	0.143
1.25	0.153	0.240	0.195	0.245	0.117	0.120	0.282	0.115	0.095
1.6	0.083	0.117	0.100	0.077	0.136	0.074	0.191	0.075	0.065
2	0.072	0.105	0.077	0.048	0.086	0.047	0.047	0.063	0.032
2.5	0.055	0.051	0.039	0.039	0.056	0.030	0.033	0.048	0.039
3.15	0.041	0.034	0.032	0.031	0.054	0.044	0.039	0.038	0.032
4	0.036	0.035	0.029	0.041	0.031	0.051	0.045	0.038	0.035
5	0.035	0.029	0.045	0.035	0.033	0.043	0.039	0.035	0.032
6.3	0.045	0.033	0.040	0.030	0.035	0.034	0.035	0.038	0.033
8	0.036	0.037	0.041	0.034	0.039	0.041	0.035	0.048	0.036
10	0.033	0.041	0.045	0.035	0.038	0.046	0.041	0.046	0.033
12.5	0.040	0.041	0.040	0.041	0.042	0.040	0.043	0.045	0.040
16	0.048	0.047	0.042	0.045	0.048	0.043	0.043	0.039	0.050
20	0.051	0.046	0.051	0.042	0.056	0.051	0.056	0.050	0.050
25	0.056	0.052	0.055	0.052	0.055	0.050	0.054	0.048	0.048
31.5	0.055	0.061	0.058	0.056	0.053	0.058	0.060	0.073	0.064
40	0.066	0.062	0.060	0.056	0.062	0.070	0.065	0.083	0.063
50	0.072	0.066	0.073	0.071	0.065	0.077	0.074	0.095	0.062
63	0.078	0.080	0.078	0.072	0.076	0.077	0.090	0.082	0.072
80	0.083	0.082	0.081	0.087	0.081	0.083	0.091	0.092	0.080
100	0.093	0.088	0.092	0.091	0.091	0.091	0.101	0.099	0.088
125	0.098	0.098	0.105	0.101	0.099	0.099	0.110	0.099	0.100
160	0.106	0.104	0.110	0.105	0.110	0.106	0.117	0.108	0.105
200	0.117	0.115	0.115	0.114	0.119	0.117	0.133	0.115	0.112
250	0.124	0.123	0.124	0.116	0.130	0.129	0.141	0.129	0.115
315	0.130	0.132	0.132	0.129	0.138	0.136	0.143	0.136	0.124
400	0.146	0.143	0.140	0.140	0.141	0.148	0.151	0.141	0.141
500	0.158	0.157	0.155	0.148	0.157	0.157	0.157	0.155	0.148
630	0.172	0.170	0.170	0.162	0.172	0.170	0.172	0.170	0.164
800	0.188	0.182	0.178	0.172	0.191	0.191	0.193	0.188	0.172
1000	0.202	0.200	0.195	0.197	0.200	0.207	0.202	0.200	0.193
1250	0.221	0.221	0.216	0.211	0.226	0.226	0.219	0.219	0.211
1600	0.234	0.234	0.243	0.245	0.248	0.248	0.234	0.232	0.251
2000	0.254	0.260	0.260	0.257	0.257	0.272	0.257	0.254	0.254
2500	0.282	0.285	0.282	0.292	0.279	0.299	0.279	0.282	0.282
3150	0.309	0.313	0.316	0.309	0.309	0.327	0.305	0.313	0.316
4000	0.347	0.351	0.351	0.343	0.347	0.359	0.343	0.347	0.347
5000	0.389	0.394	0.389	0.385	0.380	0.385	0.380	0.389	0.389
6300	0.427	0.432	0.437	0.437	0.427	0.427	0.427	0.437	0.437
8000	0.484	0.490	0.484	0.495	0.479	0.473	0.479	0.490	0.484
10000	0.543	0.543	0.556	0.562	0.550	0.531	0.543	0.550	0.569
12500	0.624	0.624	0.631	0.638	0.638	0.603	0.624	0.624	0.653
16000	0.733	0.724	0.741	0.776	0.724	0.692	0.724	0.724	0.767
20000	0.861	0.861	0.851	0.977	0.832	0.794	0.851	0.871	0.871

Table G.2: Vibration measurements - turbo collector, pipe in

	Acceleration [m^2/s] for each test									
Frq[Hz]	21	23	25	27	29	32	34	36	38	40
1	1.413	0.955	0.944	1.288	0.603	0.776	0.794	0.776	0.385	0.422
1.25	1.189	0.556	0.596	1.035	0.841	0.437	0.525	0.804	0.282	0.257
1.6	0.603	0.363	0.266	0.394	0.200	0.282	0.251	0.320	0.232	0.148
2	0.490	0.132	0.157	0.188	0.160	0.111	0.168	0.266	0.079	0.099
2.5	0.184	0.099	0.082	0.127	0.066	0.107	0.111	0.095	0.064	0.041
3.15	0.100	0.054	0.057	0.079	0.038	0.039	0.064	0.065	0.046	0.029
4	0.066	0.043	0.037	0.037	0.039	0.047	0.047	0.054	0.040	0.033
5	0.048	0.031	0.040	0.036	0.031	0.040	0.037	0.033	0.040	0.032
6.3	0.042	0.041	0.040	0.032	0.036	0.036	0.036	0.045	0.028	0.037
8	0.051	0.051	0.034	0.042	0.037	0.035	0.050	0.030	0.030	0.044
10	0.056	0.047	0.039	0.042	0.038	0.038	0.042	0.038	0.036	0.044
12.5	0.046	0.040	0.039	0.046	0.042	0.045	0.046	0.042	0.040	0.043
16	0.052	0.048	0.045	0.046	0.048	0.045	0.048	0.040	0.044	0.040
20	0.054	0.056	0.048	0.047	0.049	0.051	0.047	0.041	0.045	0.051
25	0.054	0.056	0.055	0.054	0.056	0.054	0.051	0.058	0.049	0.056
31.5	0.060	0.064	0.063	0.063	0.058	0.054	0.057	0.060	0.057	0.063
40	0.072	0.062	0.073	0.066	0.064	0.065	0.065	0.062	0.065	0.065
50	0.085	0.073	0.075	0.074	0.074	0.080	0.077	0.071	0.063	0.068
63	0.086	0.089	0.082	0.080	0.082	0.085	0.079	0.079	0.075	0.075
80	0.099	0.092	0.088	0.087	0.088	0.090	0.087	0.087	0.079	0.084
100	0.101	0.101	0.097	0.097	0.097	0.092	0.104	0.093	0.097	0.094
125	0.110	0.110	0.101	0.105	0.098	0.094	0.112	0.105	0.101	0.099
160	0.120	0.120	0.116	0.108	0.110	0.110	0.115	0.130	0.115	0.105
200	0.129	0.130	0.127	0.122	0.117	0.114	0.119	0.145	0.114	0.114
250	0.135	0.135	0.140	0.122	0.124	0.130	0.136	0.132	0.123	0.120
315	0.153	0.155	0.146	0.135	0.135	0.136	0.157	0.150	0.138	0.129
400	0.162	0.160	0.162	0.143	0.143	0.150	0.153	0.155	0.140	0.136
500	0.168	0.168	0.164	0.157	0.160	0.158	0.166	0.176	0.157	0.150
630	0.174	0.195	0.182	0.176	0.176	0.174	0.172	0.180	0.174	0.158
800	0.186	0.197	0.207	0.191	0.188	0.184	0.184	0.186	0.182	0.176
1000	0.202	0.221	0.226	0.209	0.209	0.209	0.211	0.209	0.202	0.188
1250	0.211	0.232	0.237	0.224	0.232	0.226	0.229	0.229	0.257	0.226
1600	0.234	0.254	0.254	0.248	0.260	0.254	0.254	0.257	0.266	0.248
2000	0.257	0.288	0.272	0.282	0.275	0.263	0.257	0.260	0.285	0.275
2500	0.292	0.309	0.299	0.299	0.295	0.279	0.275	0.282	0.282	0.316
3150	0.339	0.380	0.343	0.343	0.316	0.320	0.313	0.313	0.313	0.335
4000	0.355	0.385	0.355	0.347	0.351	0.347	0.343	0.347	0.351	0.347
5000	0.422	0.398	0.385	0.389	0.385	0.380	0.385	0.380	0.389	0.385
6300	0.501	0.452	0.437	0.442	0.432	0.427	0.427	0.427	0.427	0.432
8000	0.531	0.490	0.490	0.484	0.490	0.484	0.484	0.484	0.484	0.484
10000	0.646	0.569	0.556	0.556	0.562	0.556	0.550	0.556	0.569	0.556
12500	0.724	0.638	0.646	0.653	0.668	0.653	0.631	0.638	0.676	0.646
16000	0.871	0.804	0.804	0.804	0.776	0.776	0.741	0.741	0.785	0.794
20000	1.230	1.230	1.084	1.216	0.955	0.989	0.861	0.841	0.891	1.318

Table G.3: Vibration measurements - standard collector, pipe out

	Acceleration [m^2/s] for each test								
Frq[Hz]	2	4	6	8	10	12	14	16	18
1	9.333	7.943	12.882	1.905	3.055	8.511	7.674	7.244	4.571
1.25	5.433	4.786	5.495	0.394	1.641	2.818	4.217	4.027	2.917
1.6	3.020	2.786	5.888	0.432	1.000	1.549	2.600	2.600	1.641
2	1.718	1.758	1.718	0.389	0.912	0.794	1.334	1.567	0.966
2.5	0.716	0.933	1.413	0.331	0.462	0.432	0.624	0.933	0.531
3.15	0.462	0.543	0.759	0.363	0.422	0.468	0.447	0.668	0.484
4	0.569	0.343	0.582	0.537	0.427	0.484	0.389	0.372	0.550
5	0.389	0.700	0.525	0.437	0.380	0.412	0.479	0.484	0.537
6.3	0.412	0.507	0.525	0.389	0.432	0.452	0.473	0.468	0.582
8	0.422	0.741	0.589	0.519	0.513	0.537	0.537	0.543	0.562
10	0.519	0.700	0.556	0.589	0.525	0.519	0.569	0.556	0.603
12.5	0.575	0.724	0.525	0.589	0.550	0.550	0.596	0.582	0.638
16	0.617	0.785	0.767	0.638	0.653	0.653	0.631	0.596	0.646
20	0.741	0.692	0.767	0.676	0.575	0.741	0.684	0.785	0.661
25	0.776	0.733	0.785	0.785	0.708	0.708	0.661	0.750	0.716
31.5	0.776	0.881	0.832	0.822	0.822	0.891	0.861	0.851	0.813
40	0.944	1.059	0.912	0.861	0.832	0.923	0.966	0.912	0.933
50	1.012	1.047	1.000	0.989	0.933	1.059	0.977	1.012	1.012
63	1.148	1.189	1.109	1.059	1.109	1.135	1.072	1.059	1.096
80	1.189	1.259	1.230	1.148	1.216	1.202	1.175	1.259	1.230
100	1.349	1.334	1.318	1.274	1.303	1.303	1.396	1.303	1.288
125	1.396	1.479	1.396	1.462	1.396	1.365	1.445	1.462	1.413
160	1.531	1.641	1.549	1.549	1.567	1.496	1.603	1.603	1.567
200	1.679	1.778	1.679	1.679	1.603	1.679	1.679	1.660	1.641
250	1.679	1.884	1.738	1.718	1.758	1.738	1.718	1.679	1.718
315	1.841	2.018	1.799	1.799	1.758	1.820	1.778	1.820	1.778
400	1.995	2.163	1.950	1.905	1.862	1.905	1.862	1.884	1.928
500	2.089	2.291	2.089	1.995	1.995	2.065	1.995	1.995	2.042
630	2.265	2.512	2.213	2.138	2.213	2.239	2.239	2.213	2.213
800	2.483	2.754	2.427	2.344	2.483	2.399	2.600	2.455	2.399
1000	2.786	3.055	2.661	2.600	2.692	2.600	2.754	2.600	2.600
1250	2.884	3.350	3.020	2.951	3.273	2.951	3.236	2.917	3.055
1600	3.236	3.846	3.273	3.388	3.846	3.236	4.677	3.311	3.388
2000	3.981	3.981	3.758	3.890	4.571	3.758	4.786	3.589	3.673
2500	4.786	4.519	4.365	4.519	5.370	4.732	5.559	4.315	5.012
3150	5.129	6.166	4.955	6.457	6.026	5.248	6.310	5.495	6.310
4000	5.754	5.888	6.457	6.761	6.761	5.689	6.531	5.821	6.607
5000	7.328	7.328	7.244	6.918	6.761	6.761	6.683	6.839	7.079
6300	7.943	7.413	7.674	7.943	7.852	8.035	7.852	8.128	7.852
8000	8.511	8.414	8.511	8.511	8.511	8.128	8.414	8.222	8.414
10000	9.772	9.550	9.550	10.233	9.886	9.886	9.661	9.550	10.116
12500	10.839	11.482	10.715	12.023	11.885	11.092	11.220	11.614	12.445
16000	14.622	13.335	14.289	13.646	13.032	16.218	12.589	14.962	13.335
20000	28.840	19.498	26.303	16.982	15.136	26.915	15.668	26.303	17.179

Table G.4: Vibration measurements - turbo collector, pipe out

	Acceleration [m^2/s] for each test									
Frq[Hz]	22	24	26	28	31	33	35	37	39	41
1	24.266	21.627	24.547	27.542	13.964	17.378	17.179	17.579	19.953	10.715
1.25	17.179	14.454	11.885	23.988	5.821	11.885	7.328	5.957	5.623	8.035
1.6	10.116	5.957	7.943	14.454	6.095	5.559	7.586	5.070	6.918	3.126
2	8.511	2.985	5.012	11.614	4.467	4.365	3.936	2.570	3.890	1.318
2.5	3.428	2.692	2.371	4.624	2.213	2.917	2.042	2.541	2.213	0.912
3.15	2.344	1.274	1.884	1.950	1.758	1.622	1.245	1.862	1.047	0.537
4	1.318	0.966	1.230	3.548	1.318	1.445	1.096	1.175	0.813	0.531
5	1.059	0.562	0.733	1.479	1.288	0.851	0.871	0.759	0.479	0.484
6.3	0.832	0.550	0.596	1.216	1.245	0.668	0.638	0.603	0.473	0.575
8	1.035	0.582	0.631	0.822	1.109	0.776	0.484	0.661	0.484	0.543
10	1.012	0.603	0.519	0.733	0.923	0.923	0.484	0.589	0.575	0.582
12.5	0.966	0.661	0.569	0.804	1.035	1.047	0.617	0.668	0.550	0.610
16	1.059	0.684	0.646	0.692	0.923	0.989	0.700	0.724	0.724	0.653
20	0.944	0.684	0.668	0.832	0.861	0.923	0.610	0.759	0.638	0.822
25	1.000	0.794	0.794	0.861	0.902	0.891	0.638	0.724	0.851	0.684
31.5	1.000	0.822	0.871	0.871	1.109	0.933	0.750	0.881	0.785	0.841
40	1.023	0.933	0.944	1.072	1.230	0.955	0.902	0.923	0.923	0.923
50	1.109	0.966	1.012	1.161	1.230	1.135	0.944	0.966	0.977	0.966
63	1.161	1.072	1.148	1.274	1.259	1.259	1.216	1.135	1.189	1.096
80	1.318	1.135	1.245	1.245	1.365	1.259	1.245	1.175	1.216	1.175
100	1.514	1.288	1.303	1.413	1.549	1.334	1.303	1.274	1.413	1.303
125	1.514	1.413	1.413	1.531	1.641	1.514	1.396	1.365	1.479	1.445
160	1.820	1.603	1.622	1.718	1.928	1.718	1.622	1.603	1.603	1.660
200	1.905	1.641	1.603	1.820	2.089	1.799	1.641	1.679	1.862	1.567
250	1.972	1.799	1.698	1.884	2.188	1.862	1.738	1.679	1.928	1.718
315	2.188	1.862	1.841	2.089	2.317	2.018	1.841	1.778	1.995	1.862
400	2.344	1.972	1.972	2.188	2.661	2.213	1.972	1.905	2.399	1.928
500	2.884	2.113	2.113	2.483	2.786	2.512	2.089	2.089	2.630	2.089
630	3.758	2.239	2.188	2.723	3.126	2.692	2.239	2.213	2.917	2.213
800	3.802	2.483	2.483	2.851	3.236	2.951	2.455	2.455	3.126	2.371
1000	3.631	2.723	2.692	3.055	3.631	3.428	2.661	2.600	3.350	2.692
1250	4.624	3.020	3.311	3.467	4.217	3.890	2.951	2.985	3.673	2.985
1600	5.248	3.890	3.673	3.758	4.677	4.519	3.350	3.981	4.467	4.315
2000	5.248	4.315	4.027	4.217	4.955	4.786	4.169	4.027	5.012	4.121
2500	6.383	4.677	5.070	4.467	5.309	5.070	4.677	4.467	5.370	5.129
3150	6.383	5.248	5.370	5.309	6.457	5.821	5.495	5.821	6.095	6.607
4000	6.310	7.161	6.095	5.957	6.531	6.310	6.383	6.095	6.531	6.237
5000	7.674	6.683	7.328	6.607	6.998	6.998	6.683	6.839	7.328	7.943
6300	8.414	7.586	7.499	7.762	7.674	7.674	8.222	7.852	7.943	8.128
8000	9.441	10.000	9.333	8.810	8.222	8.511	8.913	8.710	8.511	8.610
10000	10.471	10.233	11.350	11.749	9.333	9.550	9.772	10.715	9.550	10.351
12500	12.023	15.311	13.804	12.882	10.839	11.749	11.092	13.032	11.092	11.482
16000	15.136	21.380	19.275	17.579	12.735	14.622	16.596	18.408	13.490	14.125
20000	23.442	22.909	23.714	20.654	15.488	19.275	27.227	21.878	20.893	22.131

Table G.5: Vibrations from pump

Frq[Hz]	Acceleration [m^2/s]
1	13.646
1.25	6.918
1.6	3.802
2	2.917
2.5	1.841
3.15	0.966
4	0.881
5	0.543
6.3	0.596
8	0.490
10	0.603
12.5	0.881
16	2.951
20	0.692
25	0.804
31.5	1.380
40	0.989
50	1.047
63	1.072
80	1.175
100	1.334
125	1.380
160	1.718
200	1.660
250	1.698
315	1.862
400	1.972
500	2.089
630	2.399
800	3.055
1000	2.951
1250	3.311
1600	3.846
2000	4.519
2500	5.188
3150	5.070
4000	6.531
5000	8.035
6300	7.762
8000	44.157
10000	56.885
12500	25.119
16000	41.687
20000	66.069

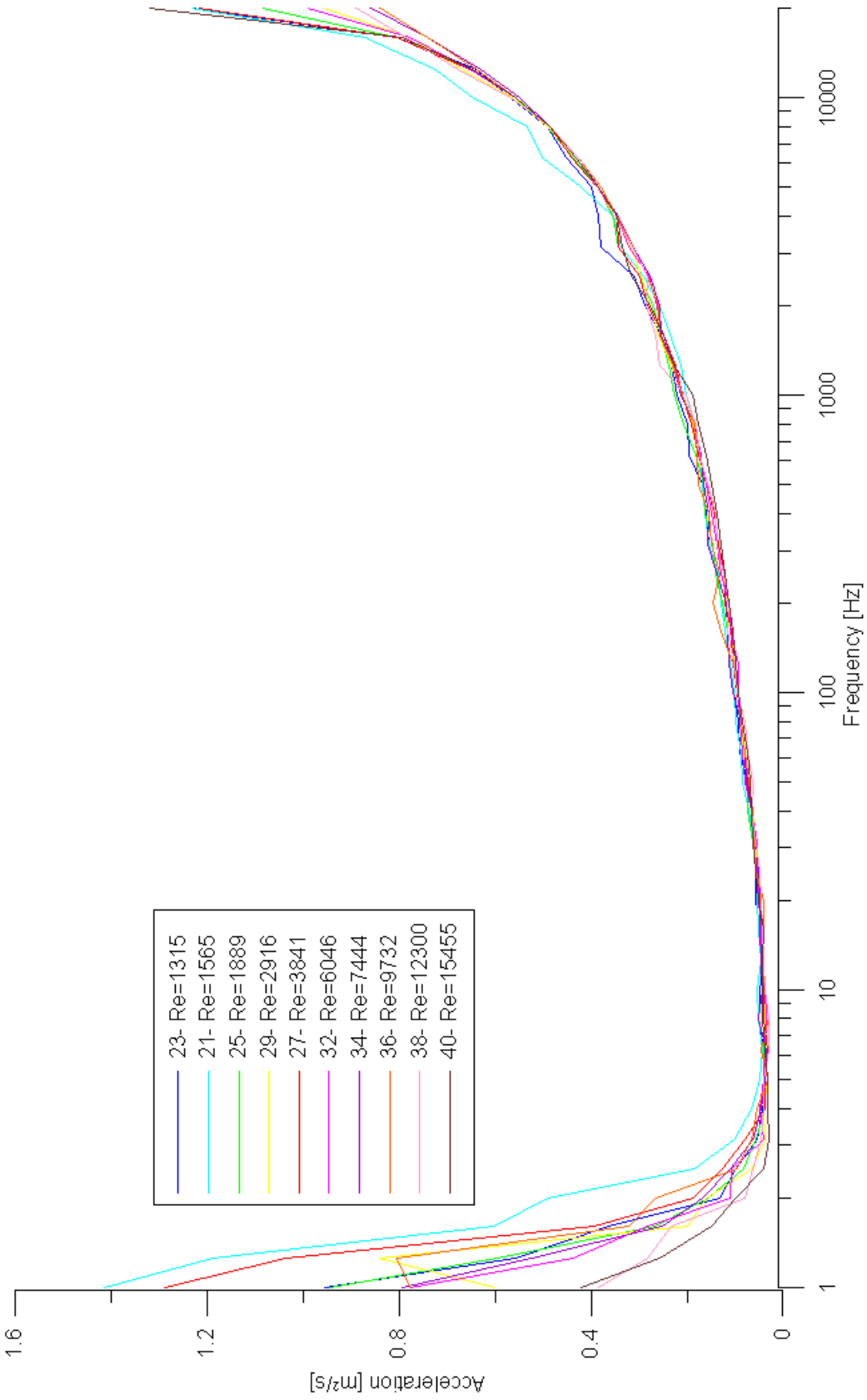

Figure G.1: Vibration measurements - turbo collector, pipe in

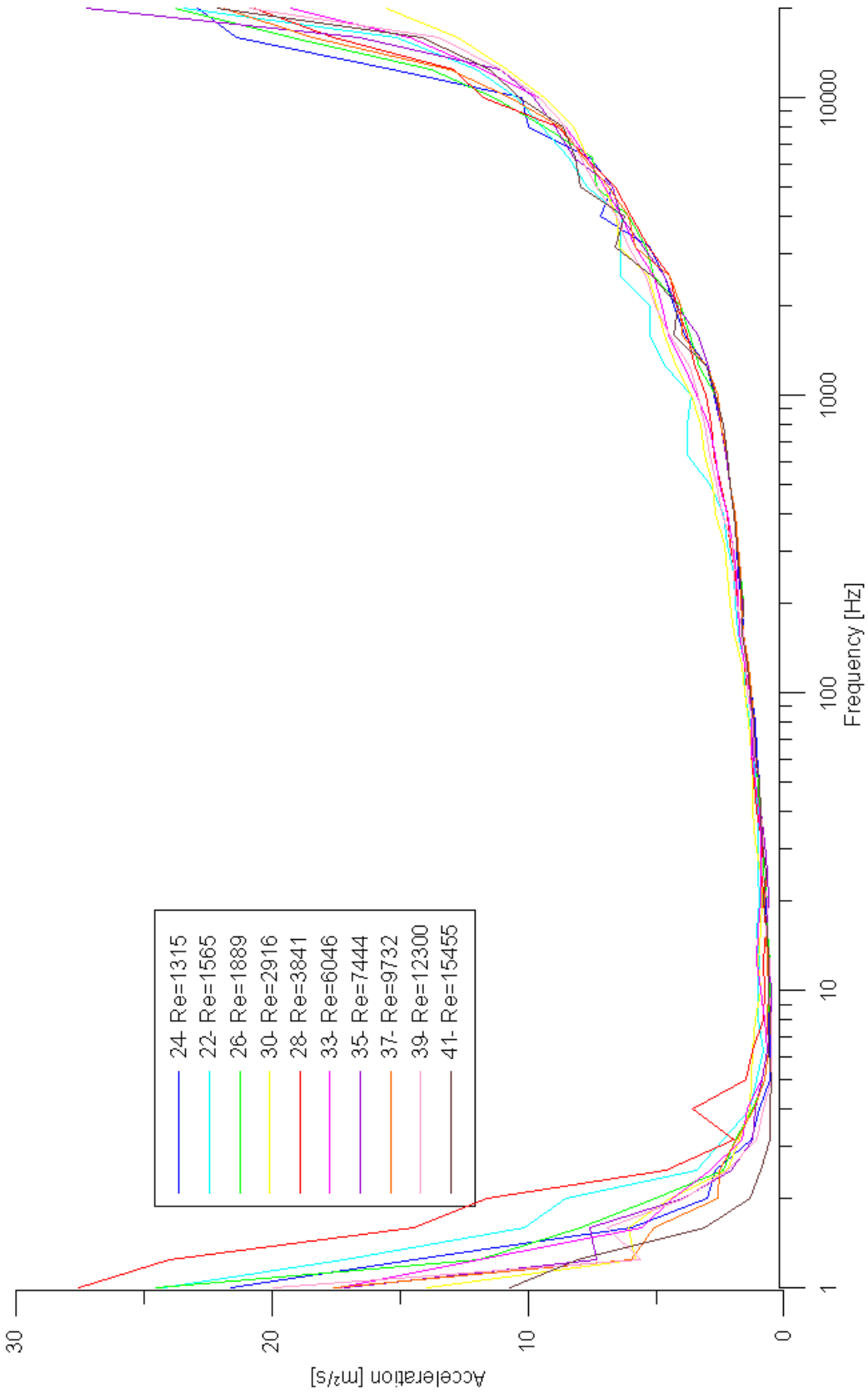

Figure G.2: Vibration measurements - turbo collector, pipe out

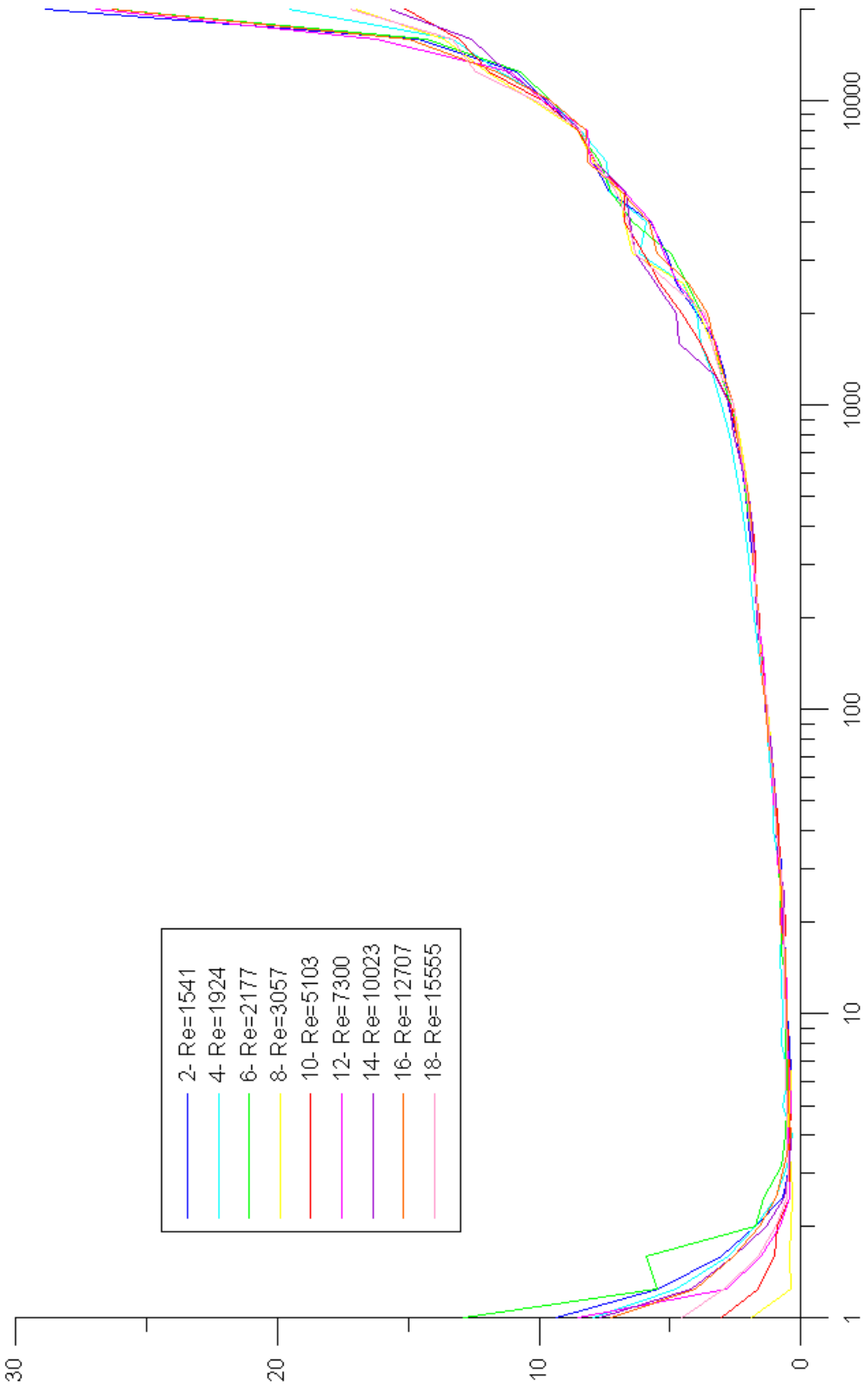

Figure G.3: Vibration measurements - standard collector, pipe out

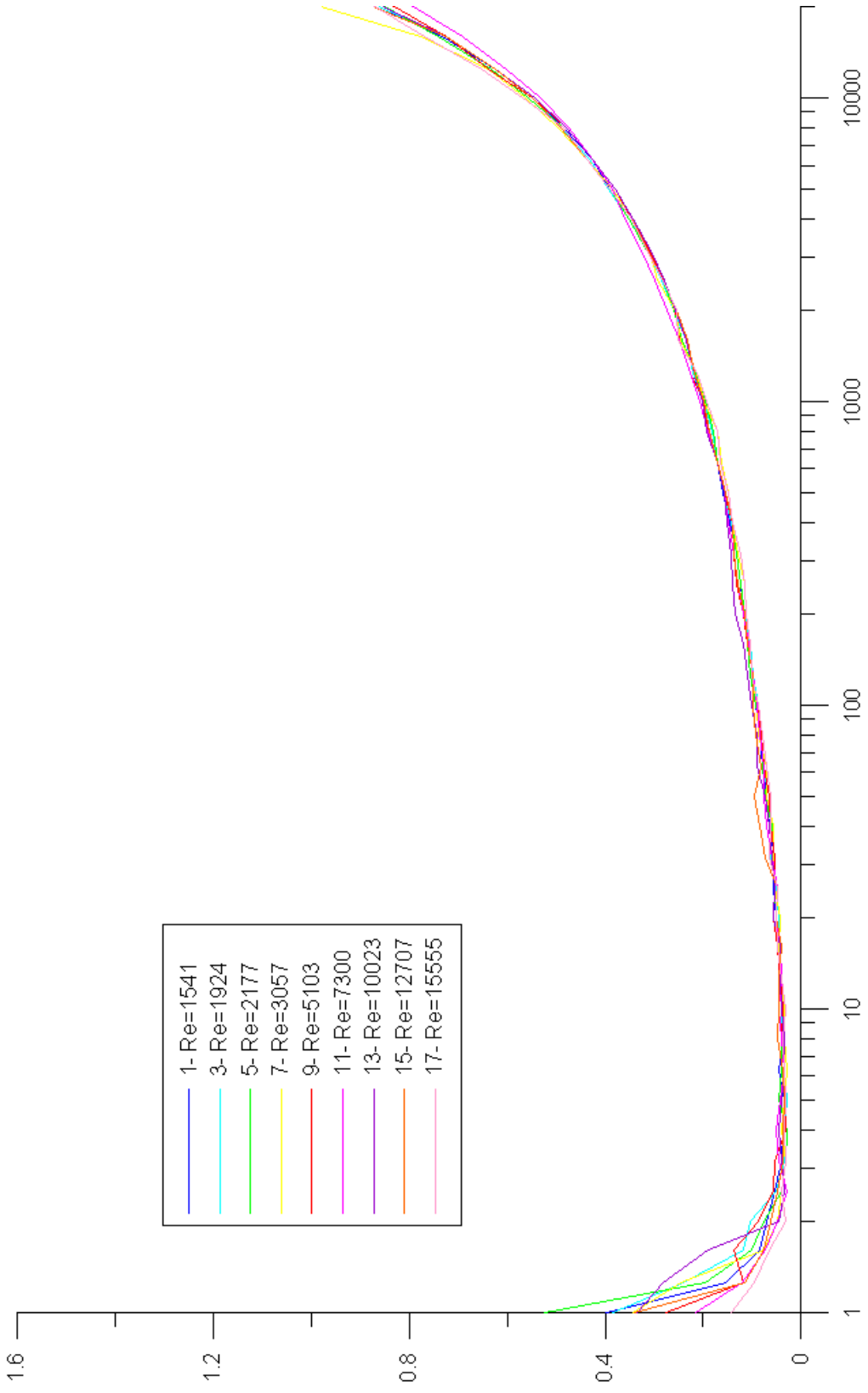

Figure G.4: Vibration measurements - standard collector, pipe in

Appendix H

Simulation Data

EED Version 2.0 (October 15, 2000), license for Hellström
P. Eskilson, G. Hellstrom, J. Claesson, T. Blomberg, B. Sanner
Input file: C:\Documents and Settings\mariesig\Skrivebord\Master\EED\Mære\Mære.dat
This output file: MæRE.OUT Date: 25.05.2010 Time: 18:42:50

MEMORY NOTES FOR PROJECT
-(no notes)

D E S I G N D A T A
==========

GROUND

Ground thermal conductivity	3.000 W/m,K
Ground heat capacity	2200000 J/m³,K
Ground surface temperature	7.02 °C
Geothermal heat flux	0.0500 W/m²

BOREHOLE

Configuration: 12 : 3 x 4, rectangle	
- g-function No.	249
Borehole depth	142.88 m
Borehole spacing	7.00 m
Borehole installation	SINGLE-U
Borehole diameter	0.115 m
U-pipe diameter	0.040 m
U-pipe thickness	0.0024 m
U-pipe thermal conductivity	0.420 W/m,K
U-pipe shank spacing	0.0500 m
Filling thermal conductivity	0.600 W/m,K
Contact resistance pipe/filling	0.0200 K/(W/m)

THERMAL RESISTANCES

Borehole therm. res. fluid/ground	0.0700 K/(W/m)
Borehole therm. res. internal	0.0000 K/(W/m)

HEAT CARRIER FLUID

Thermal conductivity	0.453 W/m,K
Specific heat capacity	3565 J/kg,K
Density	1068 kg/m³
Viscosity	0.007600 kg/m,s
Freezing point	-21.0 °C
Flow rate per borehole	0.000500 m³/s

BASE LOAD

Seasonal performance factor (heating)	4.00
Seasonal performance factor (cooling)	10000.00

Monthly energy values

Month	Heat load	Cool load	(MWh)
JAN	21.75	0.02	
FEB	28.75	0.00	
MAR	26.02	0.00	
APR	12.76	7.99	
MAY	4.88	23.90	
JUN	3.26	27.88	
JUL	0.00	23.94	
AUG	0.17	26.97	
SEP	2.98	21.97	
OCT	21.25	0.00	
NOV	21.50	0.04	
DEC	29.65	0.00	
Total	172.97	132.72	

PEAK LOAD

Monthly peak powers (kW)

Month	Peak heat	Duration	Peak cool	Duration
JAN	0.00	0.0	0.00	0.0
FEB	0.00	0.0	0.00	0.0
MAR	0.00	0.0	0.00	0.0
APR	0.00	0.0	0.00	0.0
MAY	0.00	0.0	0.00	0.0
JUN	0.00	0.0	0.00	0.0
JUL	0.00	0.0	0.00	0.0
AUG	0.00	0.0	0.00	0.0
SEP	0.00	0.0	0.00	0.0
OCT	0.00	0.0	0.00	0.0
NOV	0.00	0.0	0.00	0.0
DEC	0.00	0.0	0.00	0.0

Number of simulation years 25
First month of operation SEP